Xing, Cheng (2011) *Modelling multimode dynamics of semiconductor ring lasers.* PhD thesis.

http://theses.gla.ac.uk/2427/

To: Dr. Timothy Drysdale
        Department of Electronic and Electrical Engineering
        University of Glasgow, Glasgow, G12 8BLT

Ref.   Post-oral report on Mr. Cheng Xing's PhD thesis

Dear Dr. Drysdale:

two main revisions were requested to Mr. Xing's thesis after the VIVA on 8 February 2010:
(1) Additional chapters on multimode dynamics of semiconductor ring lasers
(2) Clarification of specific issues in the examiners copies of the thesis (including the issue of the absence of detunings in the analysis of semiconductor ring lasers).

With regard to point (1), Mr. Xing was provided with a copy of Reference [120] where modal expansions of the populations in bi-directional ring lasers are discussed in detail. It is disappointing to see that revision (1) and a large part of (2) (in particular the issue of detunings) have not been done. The newly added material in the thesis ignores population modes and reduces to a repetition of results that have been known in the literature for more than 20 years. The issue of detunings and the inclusion of appropriate boundary conditions in the models in chapter 3 have also being ignored. This has confirmed my opinion that although Mr. Xing is competent and well acquainted with the theory and simulation of semiconductor ring lasers, basic requirements for the development and attainment of research results are not met in Mr. Xing's thesis. This is further supported by the fact that no material in the thesis is worth publishing in research journals.

At this time it would be pointless to ask for further reviews of the research material in the thesis and I support that a PhD degree is awarded on the basis that Mr. Xing's thesis is a competent review of the literature on semiconductor ring lasers, that Mr. Xing has competently defended his review work during the VIVA and that no further improvement in the compilation of the review of the literature on semiconductor ring lasers is necessary. It has to be clear, however, that my support for a PhD award is not based on any assessment of the research content, if any, of the thesis. This report should become an integral part of the thesis evaluation and be presented in all occasions where a view of the thesis is requested.

Yours sincerely,

Prof. Gian-Luca Oppo
Director of the Institute of Complex Systems at Strathclyde
Department of Physics, University of Strathclyde
Glasgow, G4 0NG, Scotland, U.K.
Email: g.l.oppo@strath.ac.uk

Modelling Multimode Dynamics of Semiconductor Ring Lasers

by

Cheng Xing

Submitted in fulfillment of the requirements for
the Degree of Doctor of Philosophy

Department of Electronics and Electrical Engineering
Faculty of Engineering
University of Glasgow

UNIVERSITY OF GLASGOW

Abstract

Faculty of Engineering

Department of Electronics and Electrical Engineering

Doctor of Philosophy

by Cheng Xing

In this thesis, a modal decomposition method and a time-frequency-domain formalism for the analysis of multimode dynamics of semiconductor ring laser are developed. The diffusion coefficient is suggested as a crucial parameter to take into account. The directional switching dynamics and dependence on the operation parameters has been studied. The lasing wavelength switching accompanied by directional flipping have also been studied. In this framework, a prior selection of the lasing mode is seen as a key factor for the numerical results.

Acknowledgements

Last but not least, the author wishes to express his gratitude to his parents; for their understanding and endless support, especially through the difficult times during his studies.

Contents

List of Figures

Chapter 1

Introduction

1.1 Historical Review

1.1.1 General Lasers

The original idea of lasers has to be traced back to Einstein's emission theory, according to which energy in the form of a photon can be absorbed or emitted through carrier transitions between different energy levels. A monochromatic light wave travelling through the atoms with two energy levels with the difference equal to the energy of the photon could induce the transition of atoms from a higher level to a lower energy level accompanied by emission of photons of exactly the same energy as the injected ones, assuming that the atoms in the upper lever outnumber those in the lower level. This is illustrated in Fig. 1.1.

Classified by the amplifying material, lasers could be classified into gas lasers, dye lasers, solid state lasers and semiconductor lasers, etc[1, 2].

The first laser to work in continuous wave operation was the helium-neon gas laser working at wavelengths corresponding to the infrared region[3]. The helium atoms are excited by a DC or RF discharge and excited to a variety of higher levels. Those atoms relaxed into one of the two metastable 2^1S_0 and 2^3S_1 energy levels with long decay time. By collisions with neon atoms, energy transfer between helium and neon atoms takes place. Part of the energy contributes to excitation of ground state neon atoms to excited energy levels, another transfers to the form of kinetic energy. It is the relaxation of the excited neon atom that provides lasing. Although first demonstrated in infrared region, the He-Ne lasers could also emit red light. Actually, all of the noble gases have
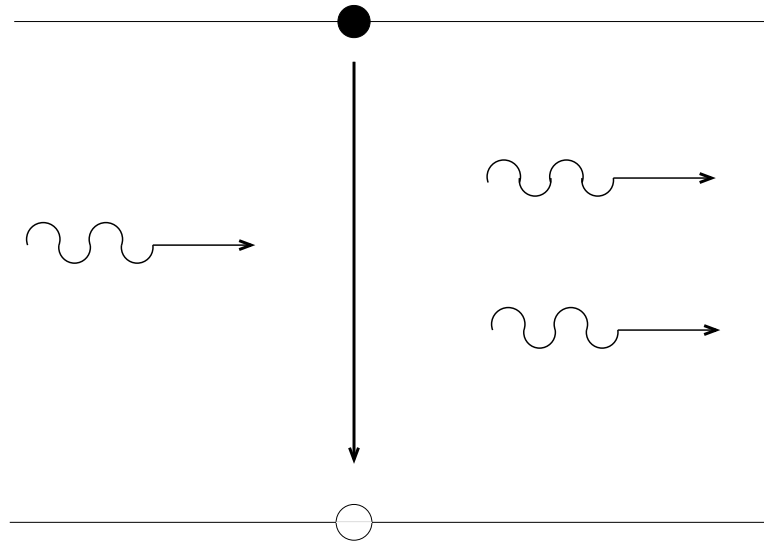
FIGURE 1.1: Stimulated emission in a two level atom. A photon with energy equal
to the energy difference induces a downward transition in energy and a new photon is
generated coherent to the injected one

been used as active media for gas lasers. Lasers made from normal molecular gases like
carbon dioxide have been demonstrated as well. However, unlike in the case of He-Ne
lasers where lasing occurs between electron transitions between excited energy levels,
CO_2 lasers emit light when transitions between internal vibration modes occurs.

Although gas lasers have been demonstrated for a long time, they are still widely used
as light sources with high output power which are easy to construct and relatively inex-
pensive.

Solid state lasers, as the name suggests, are lasers using crystals as the amplifying
medium. Flashlamps are commonly placed inside the laser cavity and provide pump-
ing. Therefore this kind of laser is sometimes called the optically pumped laser. Ruby
lasers, as an example of solid state lasers, are the first functional lasers in the history
and widely studied after that[4]. As in gas lasers, ions are excited into the absorption
bands by the trigger of the flashlamp. They decay to a metastable upper energy level
and further relax to a lower energy level with photons emitted. For systems referred as
a four-level system, the ions at lower energy level finally drain to the ground level and
wait for another flash to excite. They are called four-level system as it is formed by
absorption bands, two metastable levels and the ground state. However, for the case of
ruby lasers, the lower energy level is the ground level. The name three-level system is
used to denote such lasers.

Apart from ruby, rare earth ions in an oxide host has been widely used for the lasing materials. Among them, YAG is one of the most popular. As excited by flashlamps, solid state lasers usually work in pulsed operation. Output power is usually quite high for such kinds of lasers. Even the ruby system could reach the level of gigawatts. Flashlamps are not the only pumps for such lasers, flashlamps being sometimes substituted by laser diodes.

1.1.2 Semiconductor Lasers

The idea of semiconductor lasers goes back to the 1960s when Basov first published the negative temperature theory, i.e. population inversion in a semiconductor and consequent lasing by injecting carriers into a semiconductor PN junction[5]. Subsequent researches were conducted and lasing of semiconductor PN junctions in lab conditions have been reported by different groups [6, 7, 8, 9]. In so called homostructure junctions, as the carrier emission occurs in a relatively broad area around the junction, a large number of carriers is needed to reach lasing conditions. Therefore a very high current density, which is in the range of $4 \times 10^4 \mathrm{A/cm^2}$ - $1 \times 10^5 \mathrm{A/cm^2}$ is needed. It is hard to dissipate the heat efficiently by the limited techniques at that time. However, as the threshold current density is highly temperature sensitive, lasing could start by injection below the room temperature threshold by working in a low temperature environment. Actually these lasers only worked below liquid Nitrogen temperature. Even in such condition, only pulsed operation was demonstrated. This severely limited the application of these lasers at that time. The band structure, refractive index and light intensity of PN junction lasers as a function of lateral position is illustrated in Fig. 1.2(a). Low carrier and photon densities are the main drawbacks of such lasers.

The improvement was made to lower the lasing threshold current density by introducing the idea of the heterojunction which confines carriers in a small area to boost their local densities and enhance the possibility of stimulated recombination.

The normal heterojunctions are made by placing a layer with p-type wide bandgap material next to the p-side of a PN junction. The abrupt bandgap change works as an energy barrier to prevent further carrier diffusion in one side of the PN junction, and restricts the carriers inside it. Also, wide bandgap material has lower refractive index which could confine optical field in the low bandgap side by total internal reflection. By such effects, the room temperature threshold current density has been made as low as
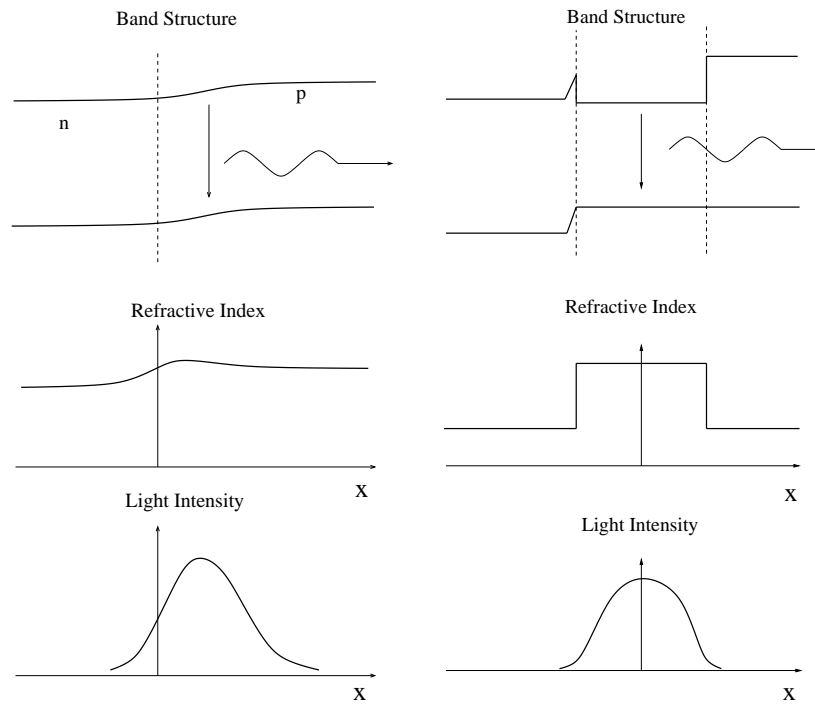
(a) Homostrucure lasers. No energy barrier and refractive index abrupt change at the junction. No carrier and photon confinement is provided

(b) Double heterostructure lasers. Energy barrier is provided in the two layers of the surface of the sandwich structure to confine carriers in between. Refractive index in the active layer is higher than that in the outer layers to form a waveguide structure to confine photons.

FIGURE 1.2: Schematic diagram of band structure, refractive index and light intensity along the lateral direction for (a)homostructure lasers and (b)double heterostructure lasers.

$2.3 \times 10^2 \mathrm{A/cm^2}$, a value 3 magnitudes smaller than the homojunction semiconductor lasers. With lower threshold, room temperature pulsed lasing has been demonstrated. However, the current density is still high, excess heat is generated and room temperature CW lasing is not possible in such lasers.

By a further sandwich, a PN junction forms an active layer between two layers with wide band-gap material. Carrier and photon confinement are obtained within the middle layer of the sandwich structure, as displayed in Fig/ 1.2(b). This gives the stimulated emission a further efficiency boost. By doing this, the first room temperature CW semiconductor laser was experimentally demonstrated and the new era of optoelectronics started[10].
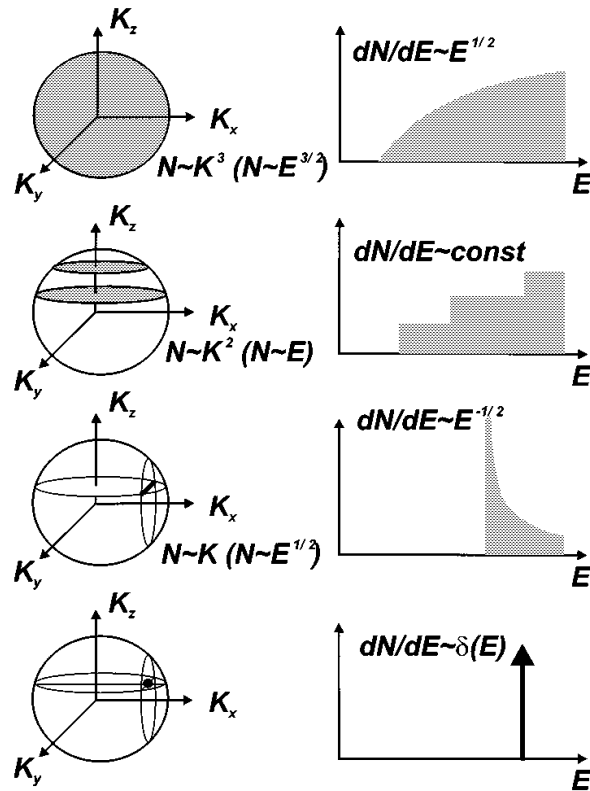
FIGURE 1.3: Carrier confinement and its density of states with different dimensionalities. The confinement of bulk, quantum well, quantum wire and quantum dot structure are illustrated from top to bottom respectively[11]. ©2000 IEEE.

From 1970, semiconductor lasers experienced great progress, thanks to the new fabrication technologies like Molecular Beam Epitaxy(MBE), Metalorganic Vapour Phase Epitaxy(MOCVD), etc. Their possibility to precisely control the growth of the material layers gave birth to so called bandgap engineering, by which artificial structures called quantum-confined structures such as quantum well, quantum wire and quantum dot with size confined below de Broglie wavelength in 1-D, 2-D and 3-D have been fabricated. In such structures, the carriers are localized and consequently, the shape of the density of states is modified.

The carrier confinement in $k-$space and the corresponding density of states is shown in Fig. 1.3. From top to bottom, the situations of bulk, quantum well, quantum wire and quantum dot have been illustrated respectively. It is seen that in a bulk semiconductor there is no confinement while in a quantum well there is confinement in the k_z direction but carriers can make free movement in the $k_x k_y$ plane. Carriers in quantum wires are confined in k_x and k_z direction but free on k_y direction. Quantum dot carriers are confined in all three directions and localised to discrete points in $k-$space. The corresponding densities of states are discrete δ functions. Those lasers show superior characters like low threshold current, temperature insensitivity, etc. The evolution of
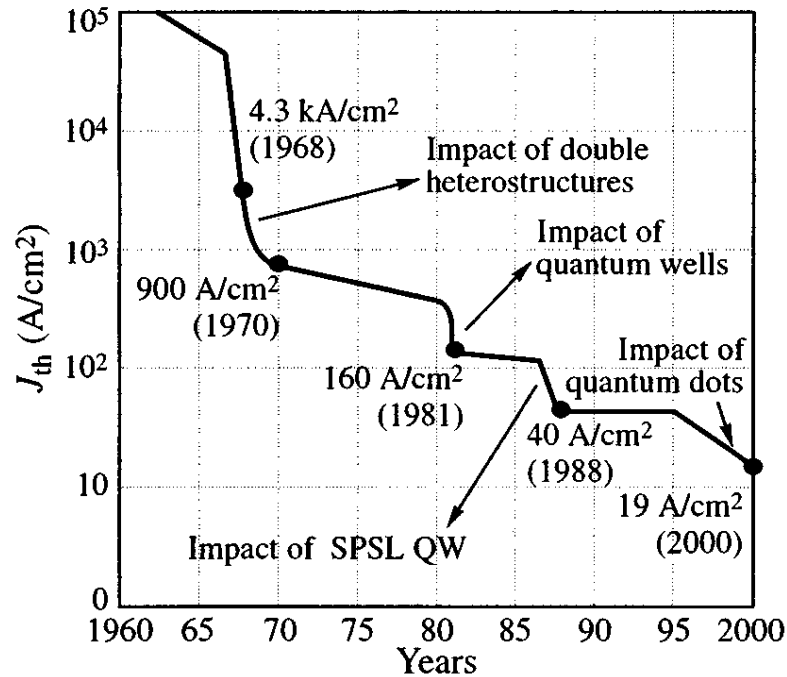
FIGURE 1.4: Evolution of the threshold current density of semiconductor lasers with time. Each new structure roughly decreases the threshold current density one order of magnitude[12]. ©2000 IEEE.
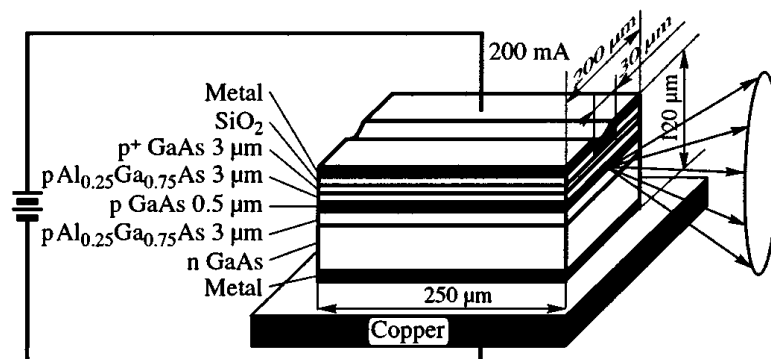
FIGURE 1.5: The schematic diagram of the first CW double heterostructure semiconductor laser at room temperature as an example of edge-emitting lasers. Laser output is in the heterojunction plane[12]. ©2000 IEEE.

the threshold current density of semiconductor lasers with time is shown in Fig. 1.4. The introduction of double heterostructure lasers, quantum well lasers and quantum dot lasers each lower the laser threshold respectively. The introduction of quantum dot lasers is promising for mode locking operations due to the wide output spectrum by inhomogeneous broadening[13]
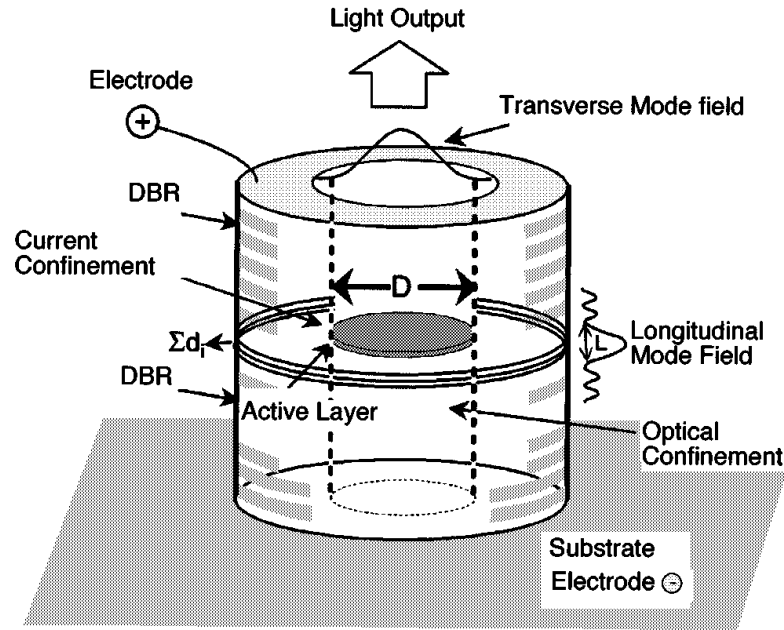
FIGURE 1.6: The schematic diagram of a VCSEL. Light output direction is perpendicular to the substrate. DBRs are fabricated ion both sides of the active layer to increase reflection[15]. ©2000 IEEE.

1.2 Edge-emitting Lasers and Surface-emitting Lasers

Semiconductor lasers were first proposed in in-line or edge-emitting cavity configuration. In terms of semiconductor lasers, two facets perpendicular to the heterostructure junction plane are cleaved to provide feedback as end mirrors in conventional lasers. As mentioned before, both carriers and photons are confined in the heterostructure junction plane. Photons are amplified by iterations of travelling between cleaved facets. Further confinement has been made by various lateral patterns, such as ridge structure, etched mesa buried heterostructure, impurity induced discorded buried heterostructure, etc[14]. A typical edge-emitting laser is illustrated in Fig. 1.5

The surface-emitting lasers, especially the Vertical-Cavity Surface-Emitting Lasers (VC-SELs) have been intensively studied recently. As shown in Fig 1.6, the active layer is sandwiched between two distributed Bragg reflectors (DBRs). A DBR is a reflector with wavelength-dependent reflectivity. It is usually formed by varying effective index periodically in the waveguide. The laser direction is perpendicular to the substrate, hence it has the word vertical in its name. The light is not amplified much after each traverse of the single active medium layer due to its small thickness. Therefore the DBRs have to be carefully designed to be highly reflective to make sure most light is reflected back at the mirror and travels as any circuits possible inside the cavity to obtain sufficient

gain. Usually the reflectivity has to be at least as high as 99.9%.

VCSELs provide some unique advantages over edge-emitting lasers because of the cavity configuration. For example, *in situ* monitoring during fabrication, far field profile with Gaussian shape good for coupling to fibers and two-dimensional arrays, high frequency insensitivity against temperature and low threshold current[15, 16]. The cavity length is relatively short, thus it has a large free spectral range. Therefore good quality single longitudinal mode operation is anticipated.

1.3 Semiconductor Ring Lasers

Semiconductor ring lasers (SRLs) have recently drawn great interest due to their unique directional bistability properties: ideal ring lasers present perfect degeneracy between waves travelling in clockwise (CW) and counter-clockwise (CCW) directions. A micrograph of the ring laser is Fig. 1.7. A schematic diagram of the laser with similar structure to Fig. 1.7 is displayed in Fig. 1.8. Strong gain competition between the light in the two directions should therefore lead to bistable, unidirectional operation of the device [17]. According to Hill et al. [18], fast switching time is possible. Such a characteristic has potential applications in optical memory.

At the early stage, research on SRL was carried out on unidirectional operation by various approaches to introducing anisotropy between two lasing directions, for example by fabricating a crossover waveguide[21], optical diode, tapered waveguide[22] or by feedback from external cavities[23]. The applications of such lasers are taking advantage of its unique property by which no cleaved facets are needed for optical feedback[24]. Desirable lasing properties like CW operation with the enhanced mode purity or higher single beam power are achieved.

The report on observations of directional bistability in triangular semiconductor ring lasers and large diameter semiconductor ring lasers[20, 25] opened new applications such as optical memory [18] and optical switching[26, 27]. Unlike in the unidirectional lasers mentioned before, of which the lasing direction is pre-determined by the asymmetry in the cavity, the lasing direction for these devices is reproducible but unpredictable[25].
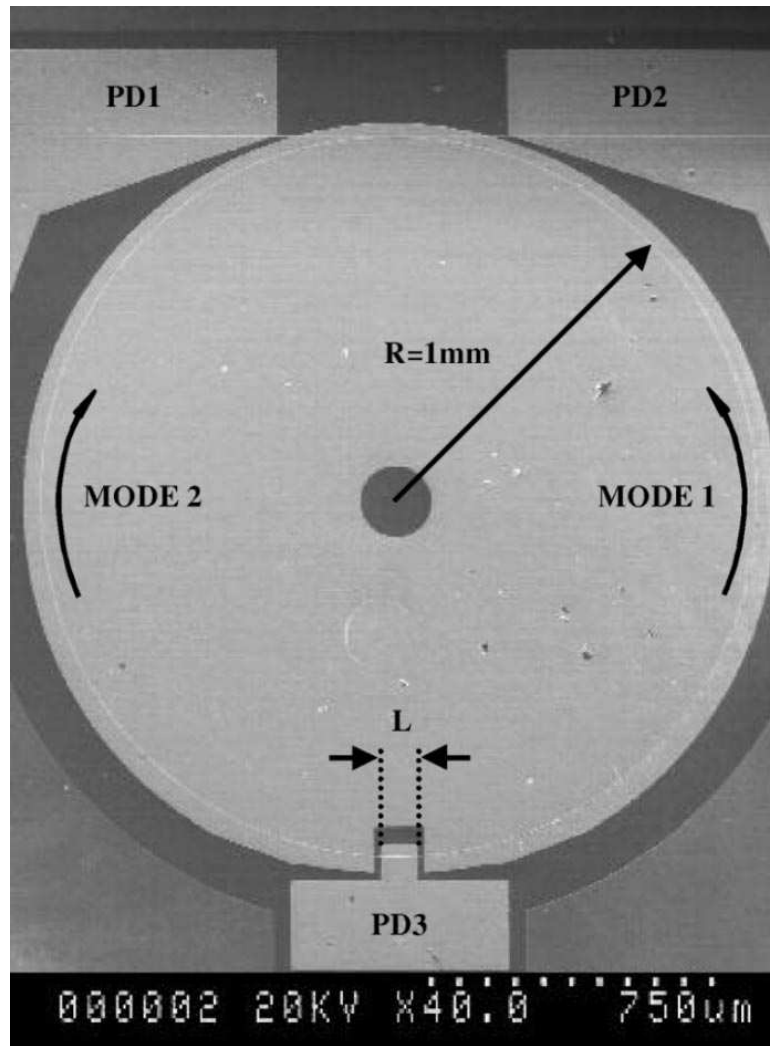
FIGURE 1.7: SEM of a semiconductor ring laser. Three photon detectors are marked as PD1, PD2 and PD3[19]. ©2003 IEEE.

Switching between the two directions could happen even after the laser has been stabilised. Close to the lasing threshold these devices usually exhibit a regime of bidirectional operation that arises from imperfections in the laser cavity due, e.g., to the light-extraction sections. At higher currents, the bidirectional regime becomes unstable and leads to bistable operation between unidirectional CW and CCW states. Often, the bifurcation occurs through an intermediate regime called Alternate Oscillation (AO) where the laser works bidirectionally but the power emitted in both directions oscillates in antiphase at frequencies of the order of tens of MHz (Sorel et al. [28]).

A careful examination of the region above lasing threshold revealed that in the unidirectional regime, as the bias current is further increased the dominant direction of emission is observed to switch at almost regular current intervals (Sorel et al. [20]), the flips in lasing direction being accompanied by abrupt increases in the emission wavelength which
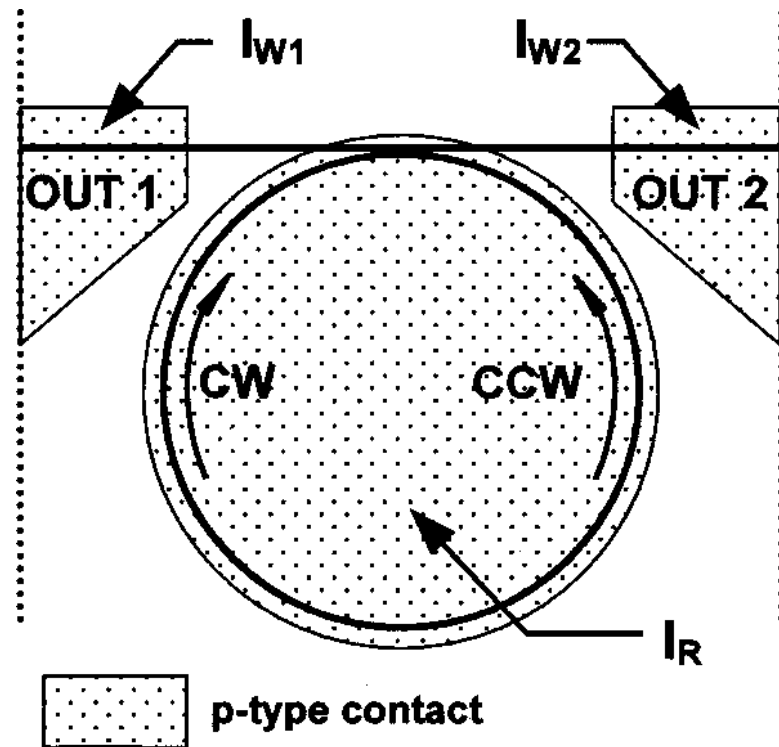
FIGURE 1.8: The schematic diagram of a semiconductor ring laser. Current is injected into the ring cavity. OUT1 and OUT2 is used to detect the output. Reversed bias could be applied there to extinguish the feedback from facets. Reprinted with permission from[20]. Copyright 2002, American Institute of Physics.

correspond to several mode spacings of the SRL [29]. The points of flip are quite sensitive to the device and the details of the working conditions, but for fixed parameters this behaviour is robust and reproducible. Interestingly, the lasing direction remains stable when the current is decreased, and although the wavelength blue-shifts in the process, in this case the wavelength jumps correspond essentially to single mode spacings of the SRL cavity. The backscattering from the coupler was thought to be the reason for bi-direction operation and further study was carried out on this factor[19]. It was found that the dissipative part of the backscattering favours the CW operation, and it is the conservative part of the backscattering which drives the lasers to alternative oscillations.

Since the carrier lifetime is much longer than the photon lifetime, the fact that a certain amount of carrier density corresponds to two distinct lasing directions provides the possibility of fast switching of the lasing direction without involving slow carrier density fluctuation. This is promising for applications like optical memory[18] and all-optical regeneration[27]. Switching triggered by optical pulses injected into the nonlasing directions has been studied theoretically in [30, 31, 32]. Surprisingly, the lasing direction could also be changed by optical injection co-propagating with the lasing mode[33, 34]. This is called backfire. Although believed not to boost the switching character, it has

practical advantages in circuit integration as control of lasing direction could simply be done by light injection into one end of the output waveguide.

Small cavity size has the advantage of fast switching time which is governed by photon lifetime[35]. Small-sized SRLs with retro-reflector cavities which used parabolic mirrors are reported[35, 36, 37, 38]. The parabolic mirrors harness the problem of usual high current leakage of closed loop bend waveguides along with strong mirror loss and the technical difficulty to downscale them in the triangular and rectangular shaped SLRs.

The other branch of research of semiconductor ring lasers is the attempt to generate short pulses with high repetition rate by mode locking them. Both active, passive and hybrid mode locked SRLs are reported[39, 40, 41]. Counter propagating pulses collide inside either gain modulator or saturable absorber as in the case of colliding pulse mode-locking. High repetition frequency and almost transform limited pulses are reported. Those promising behaviours are probably inherited from colliding pulse mode-locked inline lasers as they have similar structure in terms of mode locking configuration[42].

One thing to be noted is that, although in the first demonstration, the semiconductor ring lasers were fabricated in a circular cavity[43], different cavity geometries have been utilised, such as racetrack [38, 44], square and triangular[22, 25, 45].

1.4 Review of Modelling Approaches

1.4.1 Maxwell-Bloch Equations

The theory of modelling lasers has been long established by Maxwell-Bloch equations, for example in [46, 47, 48, 49]. In such a theoretical framework, the so-called semiclassical approach has been taken, in which light is treated as a classical electromagnetic wave and the lasing material is seen as a collection of individual particles subject to quantum mechanical principles. The light travelling inside the cavity interacts with the lasing medium which induces a macroscopic polarization made up from microscopic dipole resonances. The polarization on the other hand behaves as a source of emission after being stimulated by the laser field. The optical field reproduces itself after such iteration. This is called the self-consistent approach[17, 46]. As the Maxwell equation is used to express the field and the active material equations have a Bloch form (first used for nuclear magnetization), this approach is called Maxwell-Bloch equations.

This approach has been successfully applied to laser systems with various amplification materials like gas lasers and solid-state lasers of which the active medium can be described as an ensemble of atoms with two distinct energy levels, e.g. two level atoms. Emission takes part at energy equal to the energy difference between those levels. In this case, only population inversion between those two levels and atomic polarization is relevant to the dynamics which could be described by Bloch equations. However, this is not the case in semiconductor lasers as will be discussed in the following section. Carrier transition happens between energy bands which are governed by Fermi distributions and unique occupation of electronic states. This gives semiconductor lasers an asymmetrical gain curve around the peak, while for gas and narrow bandwidth solid-state lasers the gain curve is symmetrical. Also, a strong amplitude-phase coupling is presented in semiconductor lasers[50]. To make such peculiarities fit into the framework of Maxwell-Bloch equations, either second quantization[48] or using a susceptibility to represent the dynamics of fast macroscopic polarization are required[29].

1.4.1.1 Time Domain Modelling

The Maxwell-Bloch equations as a set of partial differential equation with both time and spatial dependence can be numerically solved by the Finite-Difference-Time-Domain(FDTD) method. This is a quite straightforward approach. In laser device modelling, further assumption have been made that the solution of the equations are waves travelling in certain directions. This is called travelling-wave model. Both of them are sometimes referred as time-domain model.

Examples of the time domain approach could be found in 2-level atoms[51], semiconductor lasers[52, 53, 54, 55, 56, 57], Semiconductor amplifiers[58, 59] and mode-locking semiconductor lasers[60, 61, 62]. Some of them have polarization equation adiabatically eliminated and a more phenomenological gain term in the model, like [58, 59, 60, 61, 62]. Others have full Maxwell-Bloch equations like [52, 53, 54, 55, 56, 57].

1.4.1.2 Rate Equation Approach

Another approach called rate equation has been presented since the 1960s to provide a simple way to model the lasing dynamics[63, 64]. The interaction between photons and carriers via stimulated emission has been described by such an approach. Phase dynamics are not considered in the early rate equation approaches.

The approach is generalized to the multimode case by taking into account gain saturation[63]. However on the argument that phase-sensitive interactions might be critical to dynamics in certain cases[65], several attempts have been made to take this effect into account, for example[66].

The lasing light in the cavity is defined as $E(t,z) = \sum_k E_k(t)U_k(z)$ to separate the spatial and temporal variables, where E_k and U_k are complex valued functions defined as the kth mode amplitude and spatial profile. The idea is to decompose the total field into a set of components which have the properties of self-reproducing after each round-trip. They are called eigenmodes. Early works usually take U_k as a sin or cos function in the Fabry-Perot lasers or complex exponential in the ring lasers[67]. The above approach is based on the assumption of ideal closed cavity. In Fabry-Perot lasers that means end mirrors or cleaved facets with 100% reflectivity while in the case of ring lasers, it means no output coupler is incorporated in the cavity. In[68], wave equations can be represented in matrix form. In such cases, the wave equations of the cavity fields are Hermitian. It has real eigen values which corresponds to the lossless cavity. Furthermore, the eigenmodes are energy-orthogonal and form a complete set. Any form of field travelling inside the cavity could be expanded on a combination of them.

However, in real life, all cavities are open due to the finite reflectivity at facets and cavity configuration complexity is introduced by components like a coupler, which leaves the above assumption untrue. In such cases, the operators corresponding to the wave equations are not Hermitian any more. The eigenvalues are complex having both real part corresponding to the phase shift and imaginary part corresponding to the gain/loss. Furthermore, the eigenmodes are neither orthogonal nor guaranteed complete. However, a biorthogonal relation of such eigenmodes is fulfilled. This can be seen as a generalised orthogonal relation on to counterpropagating eigenmodes. Such biorthogonality is based on the observation of more than one photon spontaneously emitted for each transverse mode [69] and hence the transverse eigenmodes are not energy orthogonal and complete due to the non-Hermitian nature of the system[70, 71]. The same analysis has been later generalised and applied to the longitudinal modes in standing-wave lasers[72].

Based on the above discussion, a real eigenmode decomposition and instantaneous mode calculation is needed for accurately modeling lasers with fast dynamics[73, 74] or complex cavity construction[75]. In such approach, the travelling waves inside the cavity and longitudinal eigenmode follows a Schrodinger equation[68]. A redefined inner product has been used to separate the rate equations of each longitudinal mode from the

travelling wave equation[73, 74]. A real mode with profile and frequency changing from time to time has been identified and its dynamics have been studied.

The above approach, although providing a more accurate description of laser dynamics, is computationally demanding. This contradicts the purpose of utilizing rate equations which is easy and fast yet accurate. Therefore they have been only used to model DFB lasers[73] in the limit of the single mode approximation and DBR lasers[74] with only two modes taken into consideration.

To overcome this drawback and provide a computationally efficient multimode model, an intermediate approach between calculating real instantaneous frequency and using simple functions to represent eigenmode has been developed[67]. It is appealing to use in the study of fast dynamics of mode-locked semiconductor lasers, where a large number of equations are need for the broad spectrum width.

The rate equation approach could be reduced from the Maxwell-Bloch approach with adiabatic elimination of the atomic polarization[65]. Therefore the rate equation approach is only applicable to dynamics slower than the polarization dephasing time, an ultrafast dynamics cannot be reproduced in rate equations. Also, as mentioned above, the spatial dependence is hidden in the rate equation approach. As spatial electron and hole occupation variation might be nonneglegible in cases like mode-locking, the travelling wave approach is thought to be more favourable in certain applications. However, by representing the problem with less degrees of freedom, far less computational complexity is needed than that for a time domain approach. In certain problems, this advantage is obtained without obvious losing accuracy of the result. A comparison between results from rate equation and time domain models on a mode locked semiconductor laser with saturable absorber is seen in Fig. 1.9 and Fig. 1.10. From the figures, there is no big discrepancy for the rate equation from the time-domain approach. However, as a simplified version of time domain approach, its usage has to be strictly restrained to certain problems and it should not be used without evaluating the error it might introduce into the system.

1.4.2 Gain

In laser physics, gain as a measure of the amplifying of the light by laser medium is critical. Strictly speaking, a microscopic calculation has to be performed to get an accurate description of gain [76]. However, such an approach needs extensive computation which
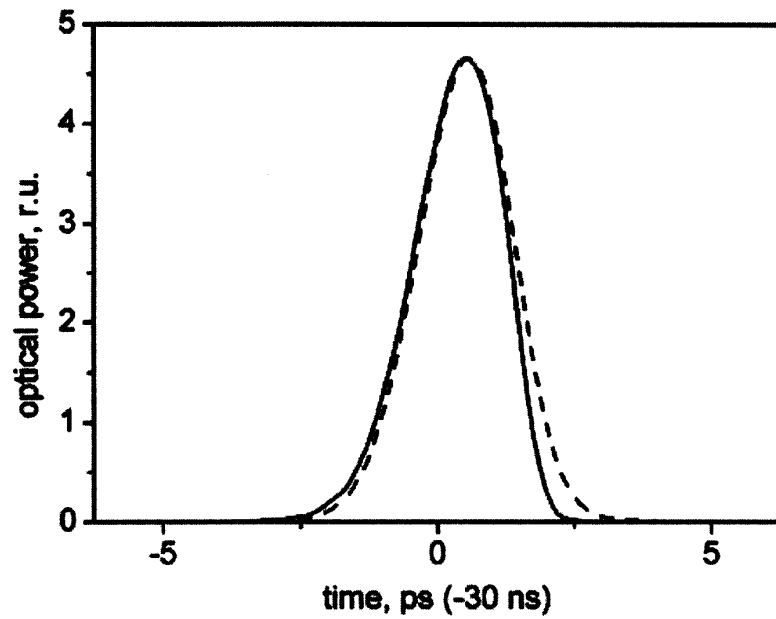
FIGURE 1.9: Temporal pulse profile for a laser with single saturable absorber. Solid line is for a rate equation approach while the dashed line is for time-domain simulation[67]. ©2003 IEEE.
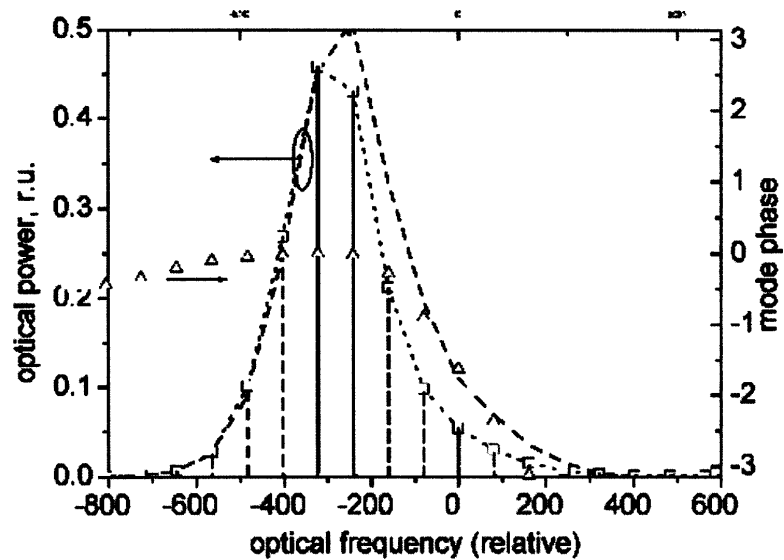
FIGURE 1.10: Steady state spectrum profile for a laser with single saturable absorber. Solid line is for a rate equation approach while the dashed line is for time-domain simulation[67]. ©2003 IEEE.

is not desirable for device modelling. For this reason, phenomenological gain is widely used.

To fit in the early rate equation approach, linear gain independent of lasing frequency has been used in the form $g(N) = a(N - N_0)$ where a is differential gain $\frac{\partial g}{\partial N}$ and N_0 is transparency electron density[14]. However, this approximation is only accurate within a small range just above the lasing threshold. Gain starts to be nonlinear with carrier density at high injection current. To obtain a closer agreement with experiments, further corrections to the gain form have been made such as a power law gain dependence.

A gain nonlinearity is inherited in the rate equation model via the '-' sign in front of gain terms. The interpretation is carrier depletion at higher photon density, and thus smaller modal gain, is expected in semiconductor lasers. This nonlinearity is confirmed by a logarithmic gain relation with current for quantum wells[77]. However, [78, 79, 80] shows a further nonlinear gain suppression that photon density dependence has to be added into the model to accurately obtain agreement with experiments, especially to compare the discrepancy with the experimentally observed relaxation oscillation frequency. This can be done by a nonlinear saturation term ε in the modal gain expression as $G = G_L(1 - \varepsilon I)$ where G_L is the linear gain[81, 82]. Another approach is to write gain as $G = \frac{G_L}{1 + I/I_s}$ where I_s is called saturation energy[80, 83]. By doing this, the gain saturation of semiconductor lasers has the same form as that of a two-level one[17]. Different nonlinear gain like $G = \frac{G_l}{\sqrt{1 + I/I_s}}$ has also been used by some author[84].

This nonlinear gain saturation is crucial in dynamics of semiconductor lasers as it affects modulation response and modulation bandwidth[78, 80, 85]. Asymmetric gain curve has also been shown to result[86, 87]. Carrier heating and spectral hole burning are seen as mechanisms behind this nonlinearity and have been studied numerically[88]. Both spectral-hole burning and carrier heating are fast intraband dynamics happening below the picosecond time scale. The name spectral hole burning is used for the process that a 'hole' is burnt in the spectrum because of the local gain depletion and the intraband carrier-carrier scattering mediation of it within finite time, while carrier heating denotes the process of carrier distribution deviating from the quasi-Fermi one inside each energy band and the relaxation by carrier-phonon scattering. These effects are usually studied by a density matrix[85, 86, 88, 89]. Third order perturbative method has been used to solve the density matrix equations. A priori assumption has to be made that the optical field is small to make the above method justified.
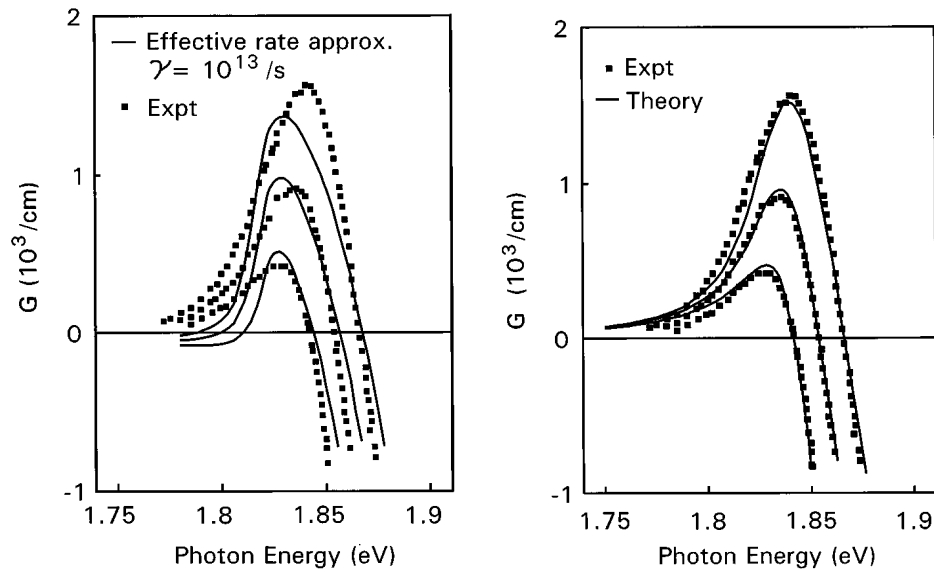
(a) Experimental versus theoretical result of gain spectrum. No many body calculation was carried on. A dephasing time is used here

(b) Experimental versus theoretical result of gain spectrum. A many body calculation is done here

FIGURE 1.11: Comparison of the gain curve calculated with models with and without many body effect with the experimental result. Reprinted with permission from [90]. Copyright 1997, American Institute of Physics.

On the other hand, microscopic theories which calculate the gain from the electronic structure have been developed[91, 92, 93]. The optical field is quantized to model the annihilation and creation of it, and consequently the carrier occupation change. This approach uses a many body Hamiltonian which is consistent with summation of the kinetic energies for single particles over all particles, stimulated emission and absorption, and Coulomb interactions. The correction introduced by many body effects could be seen in Fig. 1.11(a) and Fig. 1.11(b). Although a better fit to experiment can be obtained, intensive numerical calculation is needed in this approach. This makes its use difficult in device modelling and studying of laser dynamics. Works to simplify the microscopic theory have been done by Balle[94, 95]. In this works, an analytical yet quite accurate approximation including gain nonlinearity has been developed. Both spectral hole burning and four wave mixing are taken into account.

1.4.3 Modelling the Semiconductor Ring Lasers

The rate equation form of two mode bi-directional model for semiconductor ring lasers has been derived in [66]. The gain material is seen as an ensemble of two-level atoms and the atomic polarizations are adiabatically eliminated. The fields and carrier density

are expanded into Fourier series. By doing that, a system with four complex valued ordinary differential equations or seven real equations is obtained[65]. A similar study has been conducted on Fabry-Perot configurations and an almost identical set of equations except for a real carrier grating has been derived[65]. The backscattering is not considered in this work and the dynamics are attributed to the phase coupling via the carrier grating although it is small. It has been shown that this phase effect can even trigger the quasiperiodic and periodic two-mode solutions which fall out of the framework of this two-mode bi-directional model.

The study shows that, apart from the uni-directional operation favoured by nonlinear gain saturation[96], the system might work in steady-state bi-directional lasing operation because of the phase interaction between modes established via a carrier grating. The influence of diffusion and linewidth enhancement factor on the carrier grating and in turn the dynamics are studied in [97]. Furthermore, the behaviour of the relaxation oscillation are influenced by carrier diffusion smoothing out of the spatial inhomogeneity of the carrier density.

To model realistic semiconductor ring lasers, the output coupler has to be taken into account to extract the light out from inside the ring cavity. The backscattering from end mirrors in gas ring lasers has been studied in [98, 99]. An oscillatory instability has been identified and explained as the interplay between the conservative part of the backscattering and nonlinear gain saturation. In semiconductor ring lasers, backscattering is usually added in the same way by introducing a phenomenological complex backscattering constant[19, 28]. The value of the backscattering term and its real and imaginary parts have been studied to identify the different lasing regimes, and bifurcations between them. The origin of alternative oscillation is explained with such a model. Although similar effects were found in He-Ne ring lasers[98] and dye ones[100], the origin is not exactly the same as in semiconductor ring lasers. In semiconductor lasers, the cross-saturation c is stronger than the self-saturation s in semiconductor material. Therefore the condition for the oscillation in He-Ne, which is $c/s < 1$, has to be relaxed.

As an application, the model has been extensively used to study the switching between two bi-stable lasing directions in[30, 31, 32, 101, 102]. The optical injection used to trigger the directional switching is seen as a fast injection locking, therefore the Lang-Kobayashi model is used to model them[103]. In [30], the relaxation oscillation after the trigger pulse has been studied while the injection locking property has been studied in [102]. The switching time dependence on the trigger pulse energy and width have been

studied in [32].

The model presented previously can be further simplified for the semiconductor lasers and other class-B lasers which have a large ratio of photon lifetime to carrier lifetime and consequently small carrier density at time scales longer than the relaxation oscillation time[104]. The equations can be asymptotically reduced to two-dimensional model plus a conservation law of total photon intensity on the slow time scale. By doing this, the slow dynamics can be presented in a two-dimensional phase space. This model presented a way to illustrate boundaries of operation regimes and bifurcations between them. It has thus been used further on study of the directional bi-stabilities[33, 105, 106, 107, 108].

In order to analyse the wavelength jumps that occur, a multimode rate-equation approach has been used in Stamataki et al. [109] with the modal interaction terms being determined from a χ_3-description of the response of the active material based on [110] followed the theory in[111, 112, 113]. The gain asymmetry due to spectral hole burning and carrier density pulsation have not been included in the model. The four-wave mixing effect is not included in this model as the authors believe the radius they used is too small for this effect to happen.

However, the four-wave mixing term has been added into the model by carrier density pulsation, carrier heating and spectral hole burning[114, 115, 116]. The neglected carrier diffusion has been recovered in [116]. In [115], the experimental results were used to fit the parameters like the strength of the nonlinear interactions.

More recently, a Travelling-Wave Model has been applied to study the directional properties of the emission of SRLs [29]. Numerical simulations of this model allowed to successfully reproduce the observed phenomenology, and they indicate that the modulation of the cavity losses imposed by the residual reflectivities in the light extraction sections (output coupler and output waveguides), the thermal shift of the gain spectrum and the spatial hole burning in the carrier density play a crucial role in the directionality of the emission and its changes with operation current. The simulations also indicated that parameters have to be finely tuned in order to reproduce the observations, but the complexity of the model did not allow one to have a clear-cut picture of the underlying dynamical mechanisms.

1.5   Thesis Objective

In this thesis, multimode dynamics of semiconductor ring lasers, specifically the switching between different operations has been studied. Generally one finds wavelength switching in the conventional in-line lasers, eg the lasing frequency shift with certain operation parameter. With the unique symmetrical geometry, which provides the possibility of bidirectional lasing, a ring laser offers the possibility of novel directional switching in addition to the conventional wavelength one[19]. This two fold switching makes the ring lasers promising candidate for future optical networks while presents richer and more complicated dynamics to study[20].

The problem of knowing the initial states and searching for the final states after a certain process falls into the scope of the dynamical systems theory. When study dynamical systems, identifying steady states and the possible trajectories among them in the phase space are more relevant than the actual time traces of the transitions. Qualitative understanding of the system is always approached geometrically[117]. This philosophy serves the study of switching dynamics well in the device modelling, as in such circumstances, where the device finally settles down after tuning the control parameter given a initial state is more significant in practical[105].

Generally, static analysis has to be done to one's best effort to identify steady states and their stabilities before numerically solving the dynamical systems. The numerical results without knowing any steady states by simply running simulations might be misleading as one might encounter hysteresis in case of bistable states and have unpredictable behaviours by numerical simulations.

As stated in previous section, travelling wave approach and rate equation model are two main methods to study the transient of laser devices. Although the travelling wave models is believed to introduce least simplifications and been widely used, rate equations could offer a solution with less computation and good accuracy in certain circumstances. The problem to be studied in this thesis, as the author believes, is especially appealing to solve in multimode rate equations.

First of all, the unique geometry of the ring laser cavity, supplements the Maxwell-Bloch equations, as light travelling inside it reproduces itself after one round trip which can be modelled as a system of differential equations with a periodic boundary condition. Without output coupler, the fields inside the ring are expected to be smooth everywhere.

All these aspects make the usage of a spectral method, rate equations approach specifically in this thesis, appealing in this specific cavity configuration.

Comparing with popular numerical algorithms such as the Finite-Difference-Time-Domain or Finite-Element-Method, the spectral method is a global method using high-order orthogonal basis elements for the whole domain while other methods chop the domain into small subdomains and use piecewise functions within each of them. Given a regular domain, as studied in this thesis, ring cavity with periodic boundary condition, the spectral method offers high accuracy with minimum memory demands and possibly faster calculation time.

The thesis is focused on single transverse/lateral mode lasing. By restricting the problem in two-dimension, the field can be written into a series expansion with infinite terms.

$$E(t,z) = \sum_{N=0}^{N=\infty} f_N(t)u_N(z) \tag{1.1}$$

In this, the spatial and time coordinates are treated spectrally. In the case of periodic boundary condition, the base function $u_N(z)$ is chosen to be Fourier series under the Galerkin method.

Although the time coordinate could be treated spectrally as well as the spatial coordinate, the spectral method is only applied to the spatial dependence in this thesis as marching forward in time is much cheaper than a full spectral approach. In this case, the partial differential equations with respect to both time and space have been reduced to a set of ordinary differential equations with respect to time. Each ordinary differential equation corresponds to a distinct mode, in terms of spatial frequency, evolving with time. Therefore this approach is a spatial frequency domain method in contrast to a travelling wave one. After such a discretization, the ODEs could be solved for example by Runge-Kutta method or any other stable method.

Secondly, truncation of the series in Eq (1.1) further decreases the demand of computation. A pure mathematics transformation from spectral method to time domain approach as in Eq (1.1) shows that the discretization of the coordinates leads to an infinite series. This is inappropriate for numerical analysis, as the limited capacity of computers, not only in terms of computation time, but also in the size of storage, requires a method of truncation to make the computation in a manageable time while

keeps the discretization error in charge. Only a limited number of modes have to be selected. There are some physics considerations to make such truncation, as in the case of lasers, the finite bandwidth of the gain curve of the lasing medium selects a limited number of spectral components by providing the gain in excess of the loss for those whose frequencies are within the gain bandwidth. Components falling far outside that range die away after a few round-trips. However, the problem is not so simple. The coherent nature of inter-mode interaction allows modes with negligible amplitudes to influence lasing modes dramatically. Therefore, the way to identify modes which are to be considered in the simulation becomes important, and a sensible selection rule should be adapted.

Actually the truncation remains an open question after years of development of lasing physics theories. Although models with limited number of modes genuinely exclude the possibility of representing certain effects, for example gain cross saturation and four wave mixing are not expected to be found in single mode modelling, a general believe of using limited number of modes around the gain peak is widely adopted and correctly represented the experiments in certain problems[118]. Discussions also held in [119, 120] of using truncated rate equations to represent the full travelling wave approach when the ratio of time constants in the system is negligibly small. In the following chapter, a comparison between travelling wave and multimode model has been made and using very small number of modes to model the lasing behaviours around the bifurcation point at low pump current has been justified numerically.

The thesis is organised as following. In Chapter 1, the history of semiconductor ring lasers has been briefly reviewed. Popular modelling approaches are compared. In this thesis, a spectral method is used to discretize the Maxwell-Bloch equations. In Chapter 2, a multimode rate equation approach is derived. The multimode rate equations approach and the justification of the truncation to model the bifurcation has been made. The directional switching has been studied in Chapter 3 with two modes involved. Then in the Chapter 4, frequency switching is considered in addition to the directional once and the asymmetrical dynamics with frequency red shift and blue shift have been tried to explain.

Chapter 2

Fundamental Mathematical Model

This section covers the detailed aspects of the modelling of a semiconductor ring lasers from the light-material interaction and cavity configuration to the numerical method to solve the equations of the system.

The derivation follows a semiclassical approach with field self-consistency[17]. In this framework, the lasing material is seen as an ensemble of discrete particles which obeys quantum mechanics for energy emission/absorption while the optical field is treated as a classical continuous electromagnetic field. The restrictions imposed by the cavity geometry are discussed. The material response of both two level atoms and semiconductor are discussed in this chapter. A phenomenological susceptibility to describe the interaction between light and semiconductor is presented to assist the complicated numerical calculation. Numerical implementations of time domain and rate equation models are compared and the finally equations are presented in the form of frequency-time domain.

2.1 Light Field Consideration–Maxwell's Equation

2.1.1 Maxwell's Equations in Vacuum

The derivation starts from Maxwell's equations of a field E travelling in a general cavity regardless of its configuration. The plane wave approximation is used here. The laser field is considered to be travelling only in the z direction. The transverse profile is defined in the $x - y$ plane. In this thesis, the laser is considered to work in the lowest

transverse mode. Therefore the x and y dependence of the field are neglected from now on.

The Maxwell's equations is seen as

$$\bigtriangledown^2 E - \frac{1}{c^2}\frac{\partial^2 E}{\partial t^2} = \frac{1}{\varepsilon_0 c^2}\frac{\partial^2 P}{\partial t^2} \tag{2.1}$$

where c is the speed of light in vacuum and ε_0 is the vacuum permittivity. P on the right hand side of Eq(2.1) is the response of the medium to the electromagnetic field, eg polarization. E and P depend on both time and position.

The polarization is macroscopic here which is defined as the summation of dipole moments in the medium. In vacuum, as there is no medium, no dipole moment is found, therefore there is no macroscopic polarization so the right hand side of Eq(2.1) has to be 0. The equation in this case becomes homogeneous and admits simple plane wave solutions

$$E(z,t) = E_0 e^{-i(\omega t - kz)} \tag{2.2}$$

where wave number k and angular frequency ω meet the following requirement

$$k^2 = \frac{\omega^2}{c^2} \tag{2.3}$$

and k has the meaning of spatial frequency. Eq(2.3) is called a dispersion relation. It is two straight lines where the light frequency and wave vector has a constant ratio. The reason for each ω corresponds to two ks with opposite signs lay in the fact that two beams counterpropagating have the same dispersion relation. This is illustrated in Fig. 2.1

2.1.2 Maxwell's Equations in Linear Material

When the cavity is filled with material, the right hand side of Eq (2.1) is not zero any longer. Microscopic dipoles are induced and resonate with the optical field. This oscillation of dipole moments in turn emits light. The polarization P is used to illustrated
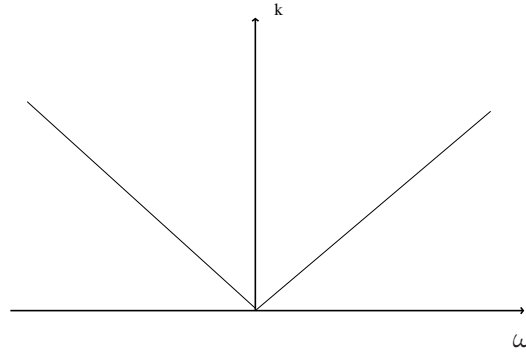
FIGURE 2.1: Dispersion relation of the laser in the vacuum. Two straight lines with same amplitude of gradient but opposite signs indicate that two waves travelling in opposite directions are supported by the same dispersion relation.

the macroscopic effect of this dipole moment resonance. In general, the polarization is not instantaneous with the field but a convolution of susceptibility χ and the field as following[121]

$$P(t) = \varepsilon_0 \int_0^\infty \chi(\tau)E(t-\tau)d\tau. \tag{2.4}$$

There is no spatial dependence in this equation. It is for the polarization at any arbitrary position inside the cavity. It is worth noting here that the polarization responds to the field instantaneously only in the lossless medium. From Kramers-Kronig relation, this kind of medium is dispersionless.

In the case of strong light intensity, polarization could show explicit nonlinear response to the induction field. However, only the linear regime is considered in this section. Here $\chi(t)$ is the susceptibility of the medium. The product in Eq (2.4) is integrated from 0, coming from the implication of casualty that past events can not be influenced by future ones.

Eq (2.4) is a convolution of susceptibility and field. Its Fourier transform gives the response of the material following a chromatic optical field.

$$P(\omega) = \varepsilon_0 \chi(\omega)E(\omega). \tag{2.5}$$

In general lasers, the polarization P could be broken into two parts

$$P = P_b + P_t \tag{2.6}$$

where P_b is the background polarization of the waveguide structure and P_t is the polarization related with the lasing transition. Generally speaking P_b is linear with the respect of field and P_t is nonlinear in this term.

The corresponding susceptibility is written as a summation accordingly

$$\chi = \chi_b + \chi_t. \tag{2.7}$$

For the time being, the passive cavity is considered in which case no transition occurs and thus $P_t = 0$. The Maxwell's equation Eq (2.1) undergoes a two dimensional Fourier transform with the respect of time and space reads,

$$k^2 E(k, \omega) = \frac{\omega^2}{c^2}[1 + \chi_b(k, \omega)]E(k, \omega). \tag{2.8}$$

The new dispersion relation is hence obtained

$$k^2 = \frac{\omega^2}{c^2}[1 + \chi_b(k, \omega)]. \tag{2.9}$$

By performing a Taylor expansion around certain frequency Eq (2.9) is

$$k(\omega) = k(\omega_0) + (\omega - \omega_0)\frac{dk}{d\omega} + \frac{1}{2}(\omega - \omega_0)^2\frac{d^2k}{d\omega^2}. \tag{2.10}$$

Group velocity is defined as the reciprocal of the first order coefficient in Eq (2.10) $v_g = (\frac{dk}{d\omega})^{-1}$. This is the generalization of the definition of velocity to the so-called wave packet or envelope of the amplitude. The coefficient of the second order term in the above equation is called group velocity dispersion $GVD = \frac{d^2k}{d\omega^2}$.

As group velocity is dispersive, the dispersion relations are no longer straight lines now. As shown in Fig. 2.2 a divergence from the straight line occurs around a certain frequency ω_m which is the resonance frequency of the background material.

2.1.3 Maxwell's Equations with nonlinear polarization

As illustrated in Chapter 1, the active layer of semiconductor lasers are usually sandwiched between waveguides. Therefore the total polarization is the summation of both
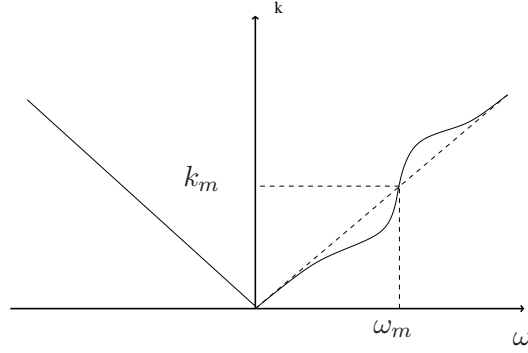
FIGURE 2.2: Dispersion relation for the medium. Near its natural resonance, the curve is not a straight line any longer. A divergence is seen around the material's nature resonance frequency.

waveguide polarization and polarization from lasing transitions in the active layer as in Eq (2.6), and so does the susceptibility χ.

Usually, the lasing frequency is far from the resonance frequency of the background waveguides. It is discussed in the next section that the susceptibility far away from the peak is relatively flat. Therefore the frequency dependence of the background susceptibility χ_b is neglected in the following discussion. A schematic diagram of the frequency dependence of susceptibility in the limit of two level system is displayed later in Fig. 2.3.

In this case, a group velocity without frequency is obtained from Eq (2.9)

$$v_g = \frac{d\omega}{dk} = \frac{c}{\sqrt{1 + \chi_b}} \tag{2.11}$$

and the full Maxwell equation with both linear and nonlinear polarization on the right hand side of Eq (2.1) which carried out this postulation reads

$$\bigtriangledown^2 E - \frac{1}{v_g^2} \frac{\partial^2 E}{\partial t^2} = \frac{1}{\epsilon_0 c^2} \frac{\partial^2 P_t}{\partial t^2}. \tag{2.12}$$

Within the laser cavity, the waveguide and active medium provide the microscopic dipole moments which buildup the macroscopic polarization. The optical field acts on the dipole moments and pushes them following it by rapid altering their alignments constantly. Each of such fast alternation can be seen as a form of an oscillation which on the other hand emits an electromagnetic wave. As the microscopic dipoles are induced by the same incoming wave, they tend to oscillate identically with each other. Therefore the frequencies and phases of the waves radiated by each of them not only equal to each

other but also are the same as that of the induction wave's. In the other word, the total optical wave will be reinforced.

2.1.4 Slowly Varying Envelope Approximation

As source with high purity, the laser is seen emitting a bunch of different frequencies within a narrow spectral width. In the time domain, such waveform could be treated as a fast carrier with slow modulation on it. The fast component could be cancelled in the Eq (2.12) and only the slow part kept. This is called the slowly-varying envelope approximation.

In such an approach, the slow and fast component are separated such that

$$E(z,t) = E_T(z,t)e^{-i\omega_c t} + c.c \tag{2.13}$$

where ω_c is central frequency which is the fast carrier frequency. The nonlinear polarization to follow the optical field has the same form

$$P_t(z,t) = P_T(z,t)e^{-i\omega_c t} + c.c. \tag{2.14}$$

Here E_T and P_T are slow in time but fast spatially. The usual ω_c is about 10^{15}Hz; however, the spectral bandwidth is of the order of 10^{13}Hz which is much smaller. Therefore

$$|\frac{\partial E_T}{\partial t}| \ll \omega_c|E_T| \tag{2.15}$$

and hence

$$|\frac{\partial^2 E_T}{\partial t^2}| \ll \omega_c^2|E_T|. \tag{2.16}$$

Also one has

$$|\frac{\partial P_T}{\partial t}| \ll \omega_c|P_T| \tag{2.17}$$

$$|\frac{\partial^2 P_T}{\partial t^2}| \ll \omega_c^2|P_T|. \tag{2.18}$$

By substituting Eq (2.13) and Eq (2.14) into Eq (2.12)

$$\bigtriangledown^2 E_T + \frac{1}{v_g^2}\left(2i\omega_c \frac{\partial E_T}{\partial t} + \omega_c^2 E_T\right) = \frac{1}{\epsilon c^2}(-\omega_c^2 P_T). \tag{2.19}$$

The second derivatives on left hand side of Eq(2.19) and all the derivatives on right hand side are neglected according to Eq (2.15)-(2.18). Now the field $E_T(z,t)$ and polarization $P_T(z,t)$ can be written as the composition of two counter propagating waves

$$E_T(z,t) = F(z,t)e^{ik_c z} + B(z,t)e^{-ik_c z} \tag{2.20}$$

$$P_T(z,t) = P_F(z,t)e^{ik_c z} + P_B(z,t)e^{-ik_c z}. \tag{2.21}$$

By substituting Eq(2.20) and Eq(2.21) into Eq(2.19),

$$
\begin{aligned}
& \left[\left(\frac{\partial^2 F}{\partial z^2} + 2i\frac{\partial F}{\partial z}k_c - k_c^2 F\right) + \frac{1}{v_g^2}\left(2i\omega_c\frac{\partial F}{\partial t} + \omega_c^2 F\right)\right]e^{ik_c z} \\
+ & \left[\left(\frac{\partial^2 B}{\partial z^2} - 2i\frac{\partial B}{\partial z}k_c - k_c^2 B\right) + \frac{1}{v_g^2}\left(2i\omega_c\frac{\partial B}{\partial t} + \omega_c^2 B\right)\right]e^{-ik_c z} \\
= & -\frac{\omega_c^2}{\varepsilon c^2}\left(P_F e^{ik_c z} + P_B e^{-ik_c z}\right).
\end{aligned}
\tag{2.22}
$$

Eq (2.22) are multiplied by $e^{-ik_c z}$ and averaged over a wavelength, one has

$$
\begin{aligned}
& \left[\left(\frac{\partial^2 F}{\partial z^2} + 2i\frac{\partial F}{\partial z}k_c - k_c^2 F\right) + \frac{1}{v_g^2}\left(2i\omega_c\frac{\partial F}{\partial t} + \omega_c^2 F\right)\right] \\
= & -\frac{\omega_c^2}{\varepsilon c^2}P_F e^{ik_c z} - \langle\left[\left(\frac{\partial^2 B}{\partial z^2} - 2i\frac{\partial B}{\partial z}k_c - k_c^2 B\right) + \frac{1}{v_g^2}\left(2i\omega_c\frac{\partial B}{\partial t} + \omega_c^2 B\right) + \frac{\omega_c^2}{\varepsilon c^2}P_B\right]e^{-2ik_c z}\rangle
\end{aligned}
\tag{2.23}
$$

where expressions between $\langle$ and $\rangle$ are spatially averaged in a couple of wavelengths as in [56] and [122].

Multiply Eq (2.22) by $e^{ik_c z}$, a similar equation reads

$$\left[\left(\frac{\partial^2 F}{\partial z^2} + 2i\frac{\partial F}{\partial z}k_c - k_c^2 F\right) + \frac{1}{v_g^2}\left(2i\omega_c\frac{\partial F}{\partial t} + \omega_c^2 F\right)\right] \tag{2.24}$$

$$= -\frac{\omega_c^2}{\varepsilon c^2}P_F e^{ik_c z} - \langle\left[\left(\frac{\partial^2 B}{\partial z^2} - 2i\frac{\partial B}{\partial z}k_c - k_c^2 B\right) + \frac{1}{v_g^2}\left(2i\omega_c\frac{\partial B}{\partial t} + \omega_c^2 B\right) + \frac{\omega_c^2}{\varepsilon c^2}P_B\right]e^{-2ik_c z}\rangle.$$

By using $\omega_c = k_c v_g$, neglecting the second order spatial derivative of F and B, and realising that spatial average over a couple of wavelengths gives 0, Eq (2.23) and Eq (2.24) reads

$$\frac{\partial F}{\partial z} + \frac{1}{v_g}\frac{\partial F}{\partial t} = \frac{i\omega_c}{2\eta_g c\epsilon_0}P_F \tag{2.25}$$

$$-\frac{\partial B}{\partial z} + \frac{1}{v_g}\frac{\partial B}{\partial t} = \frac{i\omega_c}{2\eta_g c\epsilon_0}P_B. \tag{2.26}$$

2.2 Active Medium Consideration–Two Level System

The reduced Maxwell equations Eq (2.25) and (2.26) provide a general description of the interaction between light and matter. The left hand sides of those equations indicate waves advect along the cavity considering both time and space. In the semiclassical approach, dipole moments vibrate following the induction field and emit electromagnetic waves in the form of light. The induced emission has to be coherent to the inducing wave.

Those two equations are universal to all kinds of lasers with different active material. The difference is represented from the form of polarization on the right hand sides of them.

A two-level system, as implied by its name, is a system with only two energy levels, corresponding to two distinct eigen states. The system stays in either of them with certain possibility. This could be perturbed by introducing a varying potential into the system, such as an electromagnetic wave. After the injection of light, the system starts to oscillate between the two eigen states and absorbs/emits energy accordingly.

This is not only the simplest laser model but is always representation of some laser in the reality. For simple two-level homogeneous broadening lasers, such a model is enough

to model the device. Even in the more complicated lasers, this approach is still a building-block in the whole picture. For example in semiconductor lasers, a popular way for modelling is to treat the active medium as a summation of a large number of two-level atoms with certain distributions with respect to the transition energy and interaction between each other.

2.2.1 Density Matrix

The pure-case density matrix is introduced to modelling of light interaction with a bunch of identical two-level atoms[17, 123]. Here a and b are used to indicate the upper and lower energy levels $\mid a \rangle$ and $\mid b \rangle$. ρ_{aa} and ρ_{bb} are probabilities of an atom sitting on high/low energy state. ρ_{ab} is the complex dipole moment, which by summation over all the electrons gives the macroscopic polarization P. The density matrix is written as $\rho = \begin{pmatrix} \rho_{aa} & \rho_{ab} \\ \rho_{ab} & \rho_{bb} \end{pmatrix}$. The Hamiltonian is written as $H = H_0 + V$. Here H_0 is for eigenstates and does not contain time explicitly. It is the time-dependent potential V that causes transitions between upper and lower states. H_0 is a diagonal matrix while only off-diagonal elements of V are non-zero.

The off-diagonal elements of V read

$$V_{ab} = -er_{ab}E = -\mu_{ab}E \tag{2.27}$$

$\mu_{ab} = er_{ab}$ is the electric-dipole matrix element.

$$r_{ab} = \langle a \mid r \mid b \rangle = r_{ba} \tag{2.28}$$

so $\mu_{ab} = \mu_{ba}$ and $V_{ab} = V_{ba}$.

The dynamics of the density matrix follows the Schrödinger equation

$$\dot{\rho} = \frac{i}{\hbar} [\rho, H]. \tag{2.29}$$

Therefore a breakdown of the Eq (2.29) gives three equations governing the response of two-level system to induction electromagnetic waves corresponding to each matrix

component[17]

$$\frac{d\rho_{aa}}{dt} = -\frac{i}{\hbar}[V_{ab}\rho_{ba} - c.c] \tag{2.30}$$

$$\frac{d\rho_{bb}}{dt} = \frac{i}{\hbar}[V_{ab}\rho_{ba} - c.c] \tag{2.31}$$

$$\frac{d\rho_{ab}}{dt} = -i\omega_A\rho_{ab} + \frac{i}{\hbar}V_{ab}(\rho_{aa} - \rho_{bb}) \tag{2.32}$$

where ω_A is the angular frequency corresponding to the atomic transition.

As it is always desirable to measure macroscopic quantities rather than probabilities, the above equations Eq (2.30)-Eq (2.31) are converted to equations for corresponding macroscopic quantities, which are population inversion and polarization.

$$D = \frac{N(\rho_{aa} - \rho_{bb})}{V} \tag{2.33}$$

and

$$P = \frac{N\mu(\rho_{ab} + \rho_{ba})}{2V}. \tag{2.34}$$

The P in Eq (2.34) is fast but it is the slow-varying amplitude which is more relevant. Therefore, the slow envelope P_T from Eq (2.21) is used to measure the polarization

$$P_T = \frac{N\mu\rho_{ab}}{2V}e^{i\omega_c t}. \tag{2.35}$$

Eq(2.30), (2.31) and (2.32) can be transferred into equations with those two quantities by substituting Eq (2.33) and Eq (2.35) into them. To be more physical, the incoherent decay has to be taken into account. They are added phenomenologically as in following

$$\frac{dD}{dt} = -\frac{D - D_0}{T_1} + \frac{2i}{\hbar}E(P_T^*e^{i\omega_c t} - P_T e^{-i\omega_c t}) \tag{2.36}$$

$$\frac{dP_T e^{-i\omega_c t}}{dt} = -(i\omega_A + \frac{1}{T_2})P_T e^{-i\omega_c t} - \frac{i\mu^2}{\hbar}ED. \tag{2.37}$$

T_1 and T_2 are time constant for decay of population inversion and atomic polarization respectively. The corresponding decay rates $\gamma_{\parallel}$ and $\gamma_{\perp}$, which are inversion of T_1 and T_2, are sometimes used. D_0 is the population inversion at steady state. A careful look at Eq (2.36)and (2.37) shows the right hand sides of both of them contain product which could generate both slow components and fast components rotate as fast as $2\omega_c$. Those fast terms will become small comparing with the slow once after integration, as they will have large denominators. Under the so called rotating-wave approximation[17], those fast terms are neglected. It is called the rotating-wave approximation as only terms corresponding to the atomic and field waves rotating together are kept under this approximation.

The final equations read

$$\frac{dD}{dt} = -\gamma_{\parallel}(D - D_0) + \frac{2i}{\hbar}(E_T P_T^* - c.c) \tag{2.38}$$

$$\frac{dP_T}{dt} = -(i\omega_{AC} + \gamma_{\perp})P_T - \frac{i\mu^2}{\hbar}E_T D \tag{2.39}$$

where $\omega_{AC} = \omega_A - \omega_c$ is the detuning of the carrier from atomic transition frequency. They form the basic equations of two-level atoms supplied by field equations Eq (2.25) and Eq (2.26)

2.2.2 Susceptibility

As an application of the two level system modelling, the susceptibility of the medium can be obtained from the steady state of Eq (2.38) and Eq (2.39). By setting the derivatives equal to 0, the polarization is

$$P_T = -\frac{\mu^2 E_T D_0}{(\omega_{AC}^2 + \gamma_{\perp}^2)\hbar}(\omega_{AC} + i\gamma_{\perp}) \tag{2.40}$$

Therefore, from Eq (2.5), the susceptibility as a function of detuning reads

$$\chi(\omega_{AC}) = -\frac{\mu^2 E_T D_0}{(\omega_{AC}^2 + \gamma_{\perp}^2)\hbar}(\omega_{AC} + i\gamma_{\perp}) \tag{2.41}$$
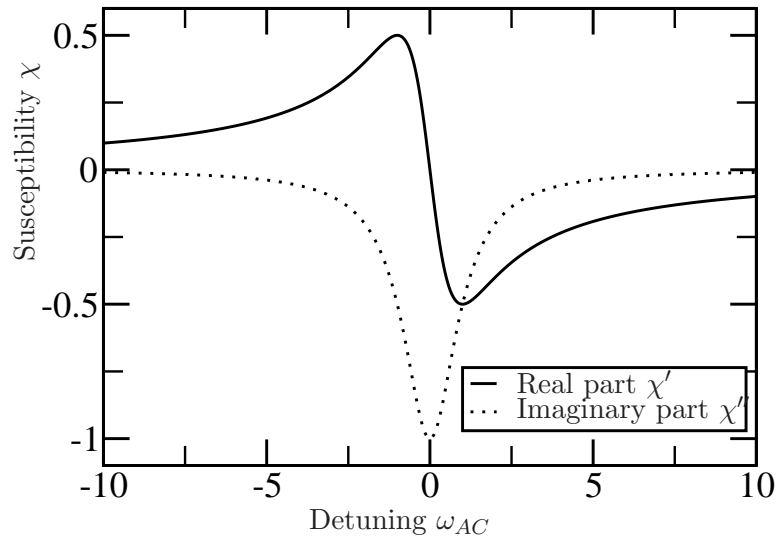
FIGURE 2.3: Diagram of real and imaginary part of susceptibility of the two level system. χ' and χ'' are real and imaginary part respectively.

The Fig. 2.3 shows the diagram of the real and imaginary part of the susceptibility dependence on detuning. χ' and χ'' are real and imaginary part of the susceptibility χ. The curve is normalised for the purpose of illustration. Two properties applicable to all two-level lasers are shown in this figure. Firstly, the real part has a Lorentzian shape and decays faster than the imaginary part at large detuning. Secondly, the refractive index is zero at gain peak.

As mentioned in the previous chapter, the two-level system is used to model homogeneous broadening ring lasers under unidirectional single-mode plane waves which is the conceptually simplest laser. Reference could be found in [124]

2.3 Cavity Design Consideration–Boundary Conditions

The mathematics behind the physics of the laser dynamics is actually a boundary condition problem of partial differential equations. Generic equations for field and active medium with their interaction regardless of the actual cavity design are obtained in previous sections in Eq (2.25), (2.26), (2.38) and (2.39). Boundary conditions have to be supplied to make this problem solvable in terms of specific solutions.

The schematic diagram of a practical ring laser configuration is shown in Fig (2.4). The light inside the ring cavity is extricated by the evanescent coupler. Optical injection and feedback from the end of the output waveguide can be sent into the cavity by the
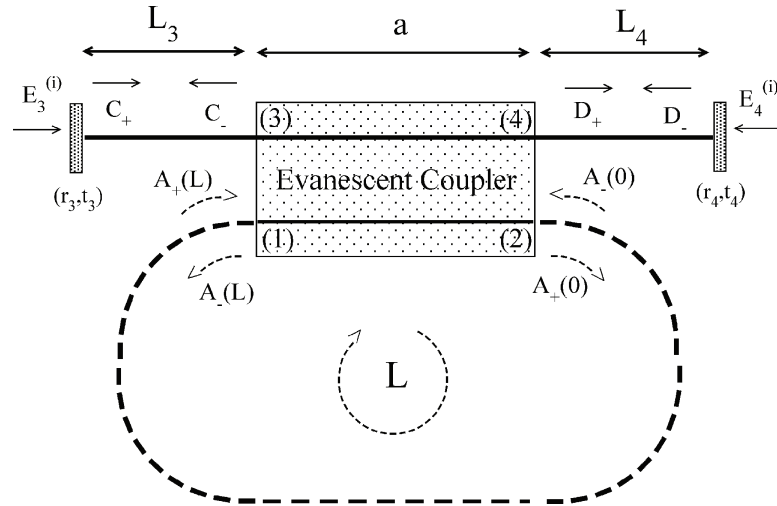
FIGURE 2.4: Schematic diagram of ring laser structure with evanescent coupler. A certain portion of light transfers between coupler and the inside of the ring cavity[29]. ©2009 IEEE

coupler as well. To model such a device in the travelling wave approach, four sets of boundary conditions have to be provided at both ends of the coupler and facets of the output waveguide[29].

In this thesis where the system is decomposed based on the spatial modes, the boundary condition imposes the restriction that modes have to be periodic. That is to say, any two modes corresponding to the distance of a cavity length has to be the same. This leads to a series of equally spaced wave number ks.

Three circumstances are studied in this thesis, which are closed ring, ring with an output coupler and ring with coupler and mirrors on both sides of the output waveguide. In the closed ring case, the cavity is symmetric without any spatial discontinuity introduced by losses. This is the ideal case to apply the Fourier expansion on the system. No additional measures have to be taken. In the case of ring with output coupler, a local loss variation has been introduced. In the modal domain loss is therefore modelled as being distributed evenly for each mode. In the final circumstances where reflectivities from the mirrors on both sides of the output waveguide are considered, a linear mode coupling term has been added to each of the rate equation. By the phase matching condition, only counterpropagating modes with the same frequency are coupled by this effect.
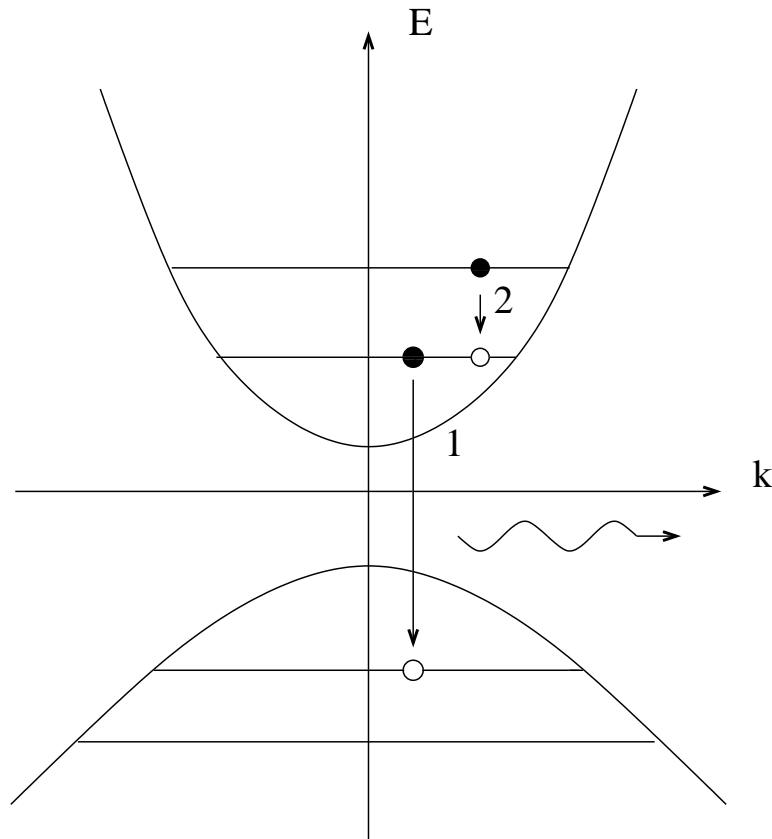
FIGURE 2.5: Schematic diagram of transitions in semiconductor. Interband transition from conduction band to valence band with photon emission is marked as 1. Intraband transition inside the conduction band by collisions is marked as 2.

2.4   Susceptibility–Semiconductor Material

In semiconductors, large numbers of carriers are confined in bands of energy. The upper and lower bands are called the conduction band and the valence band respectively. The energy between the extrema of those two bands is called the energy gap, or band gap. Carriers are not supposed to exist in the energy gap. At room temperature, electrons at the top of the valence band are excited into the conduction band, leaving empty sites which are called holes. The conduction electrons could fall into holes and emit energy as photons. As the transition involves carriers in two different bands, this is called an interband transition. A schematic diagram of transitions in a semiconductor is displayed in Fig. 2.5. An interband transition is marked as 1 in this figure.

One natural way to model semiconductor lasers is to see each electron-hole pair a two-level subsystem and the whole semiconductor as a reservoir of such subsystems. However, such approach leads to unrealistically large numbers of equations as the carrier density is as high as the order of 10^{12}m^{-2}[76]. Also, electrons and holes are created and annihilated during the lasing process, thus a second quantization is required and the number

of two-level subsystems is not constant[125].

The electrons in the conduction band and holes in the valence band reach thermal equilibrium in a Fermi-Dirac distribution in time longer than 1ns. However, the electrons in the conduction band and holes in the valence band reach their own so called quasi-equilibrium in time scales shorter than 1ps by carrier-carrier scattering (eg 50fs for example[126]). This is called intraband relaxation because collisions occur within each band. Intraband transition is illustrated at transition 2 in Fig. 2.5. As intraband relaxations have shorter decay times, when considering dynamics not shorter than 1ps, one may think the conduction band and valence band always stay in their quasi-equilibrium[125]. As mentioned in the last chapter, the dynamics could be hidden behind a phenomenological susceptibility χ which describes polarization as the response of optical field.

The analytical susceptibility from [95] has been used in this thesis. The frequency and carrier dependence along with the spectral hole burning have been taken into account by it, as it is based on the adiabatical elimination and the characteristic intraband relaxation time is around 0.1ps. Using such susceptibility on the dynamics slower than the picosecond timescale is justified.

To make the argument clear, the susceptibility from [95] is copied here

$$\chi(t) = \left[\frac{\Lambda(t)+1}{2\Lambda(t)} f(t) + \frac{\Lambda(t)-1}{2\Lambda(t)} f^*(t) \right] \tag{2.42}$$

where

$$\Lambda(t) = \sqrt{1 + \varepsilon |E(t)|^2} \tag{2.43}$$

is the saturation, $E(t)$ is the optical field, and $f(t)$ is the susceptibility without spectral hole burning given by

$$f(t) = \frac{m\mu^2}{\pi W \hbar^2} \left\{ -2\ln\left[1 - \frac{D}{u + i\Lambda(t)} \right] + \ln[1 - \frac{b}{u + i\Lambda(t)}] \right\} \tag{2.44}$$

The meanings of parameters in Eq (2.44) are the same as in [95] and [94] where m is the reduced mass of the electron-hole pair, D is normalized carrier density $D = \frac{N}{N_t}$, b
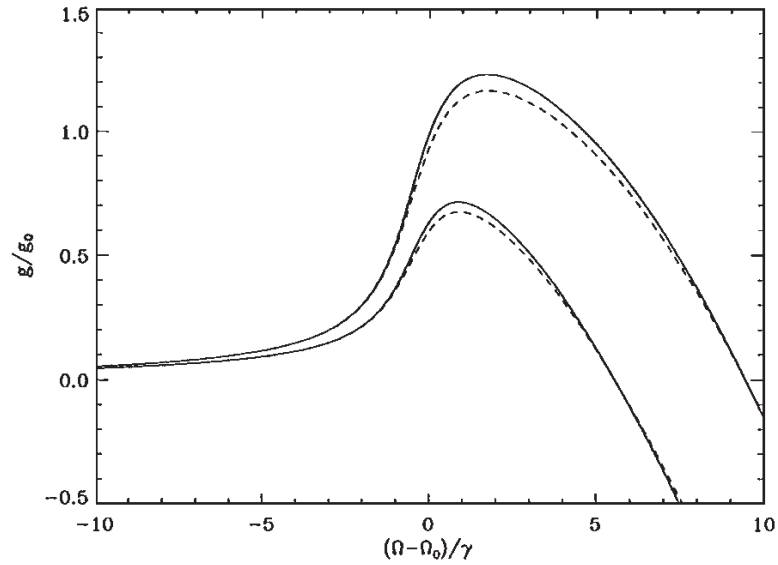
FIGURE 2.6: Comparison of gain curves calculated with and without the spectral hole burning correction. The solid curves are gain without spectral hole burning while the dashed curves are calculated with spectral hole burning. The two sets of curves are calculated with different amount of carriers[95].

is a measure of the transition energy where $b = \frac{\hbar k_m^2}{2m\gamma}$. u is a measure of the difference between the photon energy and the renormalized bandgap energy $u = \frac{\omega - E_t/\hbar}{\gamma}$. However, it is worth noting that f is dependent on carrier density as it is a function of the scaled carrier density D. Therefore $\chi(t)$ is dependent on carrier density as well. Also, wave mixing is represented in $\Lambda(t)$ as shown in Eq (2.43). The Fourier transform of $\chi(t)$ will be a carrier density and frequency dependent susceptibility $\chi(\omega, N)$.

The gain suppression from this susceptibility is shown in Fig. 2.6. A slight gain decrease can be seen from the curve. Higher gain values are shown with large amount of carriers injected.

The dephasing time in semiconductor are usually less than $0.1ps$ while the carrier decay time is about $1ns$. This leads to a polarization decay rate $\gamma_\perp$ three orders of magnitude larger than the carrier decay rate $\gamma_\parallel$. It is therefore usually regard the polarization dynamics happen instantly and safe to use the susceptibility instead of the rate equation for polarization when study the dynamics slower than picosecond. This leaves the Bloch part of the Maxwell-Bloch equations only carrier density equation. As for the carrier density, the equation should look the same except for a diffusion term which does not appear in two level systems.

$$\gamma_\parallel^{-1} \frac{dN}{dt} = J - N + D\frac{\partial^2}{\partial z^2}N + \frac{1}{\hbar}(iP_T^* E_T + c.c.). \tag{2.45}$$

2.5 Numerical Aspects–Discretization

The system is modelled by a set of differential equations according to the above sections. Differential equations, by their continuous nature, can not be processed directly by computer to simulate infinite small time and space interval, one needs infinite large storage[127]. Therefore certain numerical implementations to discretize the problem for numerical solutions are invented, eg finite difference, Monte Carlo method, spectral method etc[128]. In the field of laser physics, finite difference and spectral methods are two most usual ways to tackle the differential equations.

One dimensional finite difference approach, referred as to the travelling wave method, time domain approach, is widely used in modelling laser dynamics as generally speaking, only dynamics along the lasing axis is important and needs to be studied carefully. The basic idea is that, after discretizing time and space, one could obtain the values of each point by initial conditions. The value of each point is updated by advance in time.

Time and spatial coordinates can be discretized as follows

$$t_n = t_0 + n\Delta t \tag{2.46}$$

$$z_j = z_0 + j\Delta z \tag{2.47}$$

where t_n is the time after n time steps, z_j is the jth spatial coordinate j. Δt is the time step and Δz is the grid sized.

Then the continuous unknowns, say field $E(z,t)$ for example, can be sampled at discrete points both in time and space to represent the original function. This is written as $E(z_j, t_n)$, and then further simplified by E_j^n. In the simplest case, the time and spatial derivatives of $E(z_j, t_n)$ are written as

$$\frac{\partial E_j^n}{\partial t} = \frac{E_j^{n+1} - E_j^n}{\Delta t} \tag{2.48}$$

$$\frac{\partial E_j^n}{\partial z} = \frac{E_{j+1}^n - E_j^n}{\Delta z}. \tag{2.49}$$

However, such discretization scheme can only be seen for the sake of demonstration as it is numerically unstable[128].

Time domain model is a genuinely good approach in the sense that it solves the discretized equations directly without any simplifications made by analysis. However, the trade-off is obvious. The numerical stability requires a finely meshed set of points to be used to represent the original equations which is storage demanding. Bad numerical schemes always lead the dispersion relation of the discrete sets to diverge from the one for the original equations. To compute such a large amount of equations is time consuming although in most cases the equations are sparse. For partial differential equations, by introducing one more dimension in the solution space, the computation time required increases in a polynomial order.

On the contrary, the spectral approach could be partially applied to the spatial coordinate and decompose the problem into a set of ordinary differential equations with respect to time. Under periodic boundary conditions, as in the case of ring lasers, the spatial method tends to be faster than time domain models.

Runge-Kutta method is used to solve the ODEs from spectral decomposition. To solve the following equation

$$\frac{dy}{dt} = f(t, y) \tag{2.50}$$

by a fourth-order Runge-Kutta method, the following formula is adapted to get the solution at n+th step from the nth result[128]

$$
\begin{aligned}
k_1 &= hf(t_n, y_n) & (2.51) \\
k_2 &= hf(t_n + \frac{h}{2}, y_n + \frac{k_1}{2}) & (2.52) \\
k_1 &= hf(t_n + \frac{h}{2}, y_n + \frac{k_2}{2}) & (2.53) \\
k_1 &= hf(t_n + h, y_n + k_3) & (2.54) \\
y_{n+1} &= y_n + \frac{k_1}{6} + \frac{k_2}{3} + \frac{k_3}{3} + \frac{k_4}{6} & (2.55)
\end{aligned}
$$

where k_1, k_2, k_3, k_4 are intermediate coefficients and h is the time step.

2.6 Truncation on The Mode Number

As mentioned in the previous chapter, a multimode modelling rate equation with limited number of modes is less computationally intensive. For specific problems it is a favourable approach, for instance the example above. However it might not work for all the times. The error introduced by truncation is one of the major drawbacks. It is therefore most important to clearly define the specification of the problem on which the multimode modelling could be applied with the best accuracy beforehand. And strictly restrictions on its usage to such problems has to be applied. By doing these, one can safely claim that, for those certain problems, multimode modelling gives results in moderate accurate and high efficiency far superior than the time domain approaches.

In fact, rate equations have been used to study bistabilities for long times[129]. As argued by Lugiato *et al*[118], the multimode approach is good in the case of a very limited number of modes lasing simultaneously. For example, the chaotic behaviour in the unstable regime has been studied by considering only one mode in the model. The paper also argued that a severe truncation of the mode number should work in most of the cases with mode spacing sufficiently larger than the gain bandwidth.

In this section, the author would like to demonstrate the justification of the rate equations at moderate pump current with a small number of modes when studying the switching dynamics, and show its superior efficiency which makes it more favourable than the travelling wave approach.

To illustrate this point, bifurcation of two-level uni-directional ring lasers is studied by both of the two approaches in this section. The effect of the truncation on the rate equation model has been studied by varying the number of modes involved in the calculation. The results have been compared with those obtained from the travelling wave model.

To begin with, Perez-Serrano *et al*'s model[130] has been taken as the travelling wave model used in this section. The model is written here for the sake of convenience

$$\pm \frac{\partial F_\pm}{\partial z} + \frac{\partial F_\pm}{\partial t} = P_\pm - \alpha F_\pm \tag{2.56}$$

$$\frac{1}{\gamma}\frac{\partial P_\pm}{\partial t} = -(1 + i\tilde{\delta})P_\pm + g(D_0 F_\pm + D_{\pm 2}F_\mp) + \sqrt{\beta D_0}\xi_\pm(x,t) \tag{2.57}$$

$$\frac{1}{\varepsilon}\frac{\partial D_0}{\partial t} = J - D_0 + \triangle\frac{\partial^2 D_0}{\partial x^2} - (F_+ P_+^* + F_- P_-^* + c.c.) \tag{2.58}$$

$$\frac{1}{\eta}\frac{\partial D_{\pm 2}}{\partial t} = -D_{\pm 2} - \frac{\varepsilon}{\eta}(F_\pm P_\mp^* + F_\mp^* P_\pm). \tag{2.59}$$

It is a travelling wave one made for the bi-directional ring lasers. The $F_\pm$ and $P_\pm$ are slowly varying envelopes of the forward and backward moving waves and corresponding polarizations. D_0 and $D_{\pm 2}$ are quasi-stationary population inversion and the one induced by copropagating waves. α is the internal losses. $\tilde{\delta}$ and $\triangle$ are detuning and diffusion coefficient respectively. ε and η are dimensionless parameters denoting the lifetimes of D_0 and $D_{\pm 2}$. γ corresponds to the gain bandwidth.

As only unidirectional lasing is studied in this section, the Eq (2.56) - Eq (2.59) could be reduced accordingly. As no standing wave pattern would be generated by counter-propagating interference, no $D_{\pm 2}$ exist in the uni-directional lasing. Assuming the lasing is forward, the full set of equations for a bi-directional ring laser, as Eq (2.56) - Eq (2.59) is reduced to a uni-directional one

$$\frac{\partial F_+}{\partial z} + \frac{\partial F_+}{\partial t} = P_+ - \alpha F_+ \tag{2.60}$$

$$\frac{1}{\gamma}\frac{\partial P_+}{\partial t} = -(1 + i\tilde{\delta})P_+ + gD_0 F_+ + \sqrt{\beta D_0}\xi_+(x,t) \tag{2.61}$$

$$\frac{1}{\varepsilon}\frac{\partial D_0}{\partial t} = J - D_0 + \triangle\frac{\partial^2 D_0}{\partial x^2} - (F_+ P_+^* + c.c.). \tag{2.62}$$

This is the travelling wave approach which will be used in the later analysis. The boundary condition reads

$$F_+(0) = TF_+(1) \tag{2.63}$$

where T is the transmission from the ring to the coupler. A rate equation approach is derived form this point.

Although varying slowly, the field F_+ might consist of spectral components in case of multimode lasing. So do the polarizations P_+ and the population inversions D_0. To make this point, the fields and polarizations are written as

$$F_+ = \sum_{n=-\frac{N}{2}}^{\frac{N}{2}} F_n e^{-i\omega_n t + iq_n x} \tag{2.64}$$

$$P_+ = \sum_{n=-\frac{N}{2}}^{\frac{N}{2}} P_n e^{-i\omega_n t + iq_n x}. \tag{2.65}$$

The "0" mode is selected to be the closest one to the gain peak. The population inversion D_0 could correspondingly be written as

$$D_0 = d_0 + (\sum_{n=1}^{N} d_n e^{-i\omega_n t + iq_n x} + c.c.). \tag{2.66}$$

By substituting Eq (2.64) - Eq(2.66) into Eq (2.60) - Eq (2.62), and grouping up terms with the same spatial frequency, one has the final form of modified rate equations as

$$\dot{F}_n = P_n - \alpha F_n + i(\omega_n - q_n)F_n \tag{2.67}$$

$$\dot{P}_n = P_n[i\omega_n - \gamma(1 + i\dot{\delta})] + \gamma g(d_0 F_n + \sum_{m=1}^{\frac{N}{2}+n} d_{om}F_{n-m} + \sum_{m=1}^{\frac{N}{2}-n} d_{om}^* F_{n+m}) \tag{2.68}$$

$$\dot{d}_o = \varepsilon[J - d_0 - \sum_{n=-\frac{N}{2}}^{\frac{N}{2}} (F_n P_n^* + c.c.)] \tag{2.69}$$

$$\dot{d}_{on} = d_{on}[i\omega_n - (1 + q_n^2 \triangle)\epsilon] - \varepsilon \sum_{m=-\frac{N}{2}}^{\frac{N}{2}-n} (F_{n+m}P_m^* + F_m^* P_{n+m}). \tag{2.70}$$

To compare the above two approaches, simulations based on the travelling wave one of Eq(2.60) - Eq(2.62) have been conducted at first as this is made with less assumptions and is believed more rigorous. Rate equations approach Eq(2.67) - Eq(2.70) with truncation on mode number is done later in comparison with the travelling wave one.

The Fig 2.7 displays the bifurcation of light-current diagram to show the different steady states and the transitions among them. As in this section, only unidirectional operation

is considered, transmission and reflectivity from the output coupler are set to $T = 1$ and $r = 0$ respectively. The detuning δ is 0, gain $g = 2$, internal loss $\alpha = 1.58$, spontaneous emission $\beta = 0$. two dimensionless parameters ε and η are 0.1 and 10 respectively. γ is selected to be 10 to represent a moderate gain bandwidth.

To get the bifurcation diagrams, the laser is set for each current for 2000 round-trip times then perturbed by a small current increase or decrease depending on which ramp one is drawing, followed by a Gaussian random noise for 40 round-trip times. Fig 2.7(a) illustrates the operations transition with increasing the current. A laser starts to work on single mode operation from the threshold till $J = 17.6$. Typical CW transient and the corresponding clean single mode spectrum as in Fig 2.8(a) are seen in this region. At pump current $J = 17.6$, multimode character starts to emerge by the Risken-Nummandal instability as the broader-than-mode-spacing gain curve allows multimodes to oscillate simultaneously [131]. Fig 2.8(b) displays the time trace and the optical spectrum at $J = 20$ which is the current just above the bifurcation point. Five modes lasing simultaneously are seen from the spectrum in the lower panel of Fig 2.8(b). In upper panel of Fig 2.8(b), oscillations at round-trip time are revealed. With increasing the pump, more modes start to emerge in the power spectra and sharp mode-locked pulses are generated. This trend is clearly illustrated in the Fig 2.8(c) and Fig 2.8(d) at pump current $J = 50$ and 75 respectively. More than 20 modes are involved in those operations. The higher the pump current, the more modes emit simultaneously with significant power and the sharper the pulses in the time domain.

At even higher pump current, the nonlinearity induced by the strong output intensity starts to take effect, hence a new frequency doubling regime appears from $J = 85.4$. The amplitude of the oscillation is squeezed and two oscillations are observed within one round trip time as shown in the upper panel in Fig 2.8(e). In the spectrum shown in the lower panel of Fig 2.8(e), one finds odd numbered modes carry negligible power comparing with the even numbered ones. Sidebands at ± 2, ± 4 modes, etc along with the central mode dominate the bandwidth. This corresponds to the period of oscillation being half of the round trip time as mode spacing follows the equation $\Delta \omega = \frac{2\pi}{T}$ where T is the time a pulse makes a round trip around the cavity. In this case when two oscillations occur in one period, the T could effectively be seen as half of its original value, which leaves the mode frequency spacing double.

Further increasing pump current, more complicated dynamics could be found as in Fig 2.8(f). Not only more than one oscillations is seen in one round trip time, the envelope
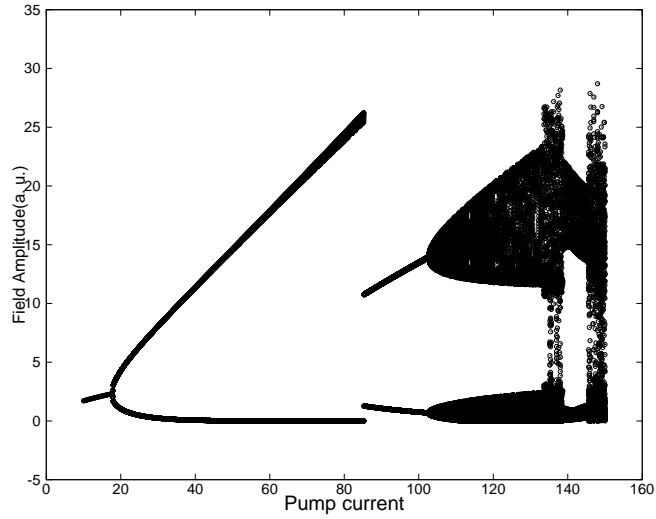
(a) Bifurcation diagram for a current increasing ramp
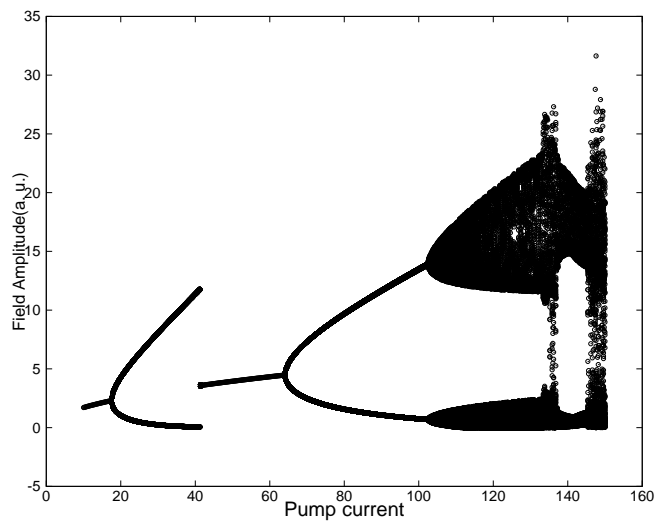
(b) Bifurcation diagram for a current decreasing ramp

FIGURE 2.7: Bifurcation diagrams of ring laser with current up sweeping and down sweeping respectively made by travelling wave approach as in Eq (2.60)-Eq (2.62). Parameters are listed as following: $\delta = 0$, $g = 2$, $T = 1$, $r = 0$, $\varepsilon = 0.1$, $\eta = 10$, $\alpha = 1.58$, $\beta = 0$, $N = 100$
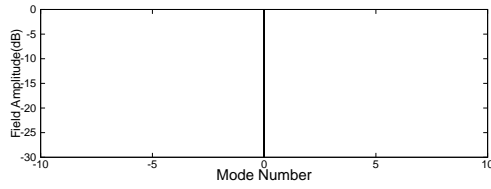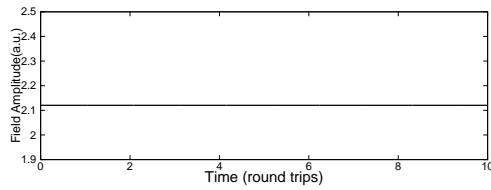
(a) $J = 15$
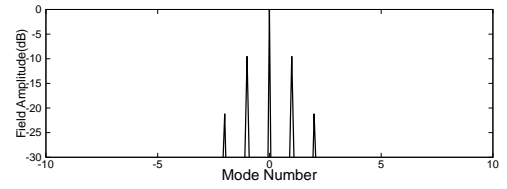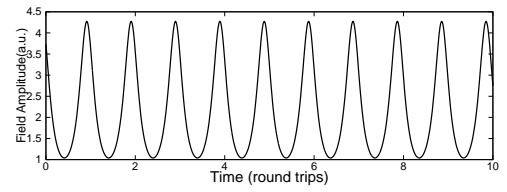
(b) $J = 20$
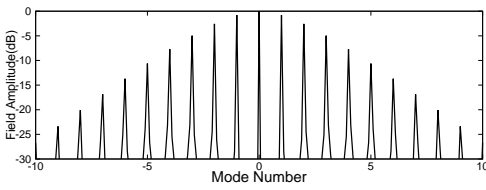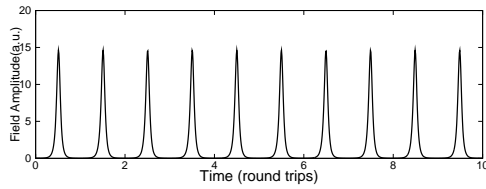
(c) $J = 50$
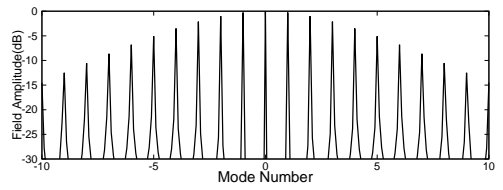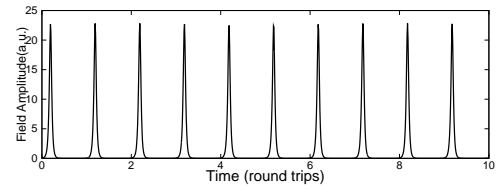
(d) $J = 75$
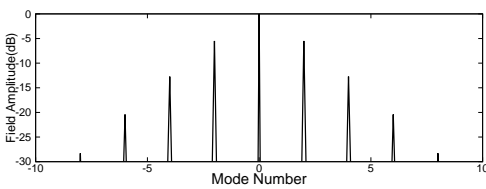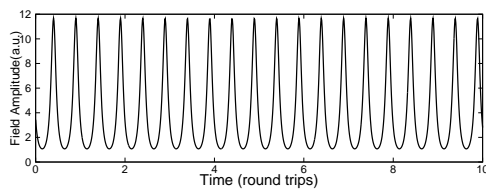
(e) $J = 90$
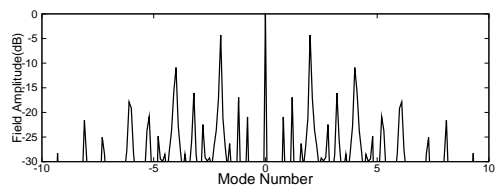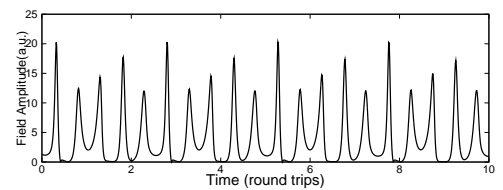
(f) J=125

FIGURE 2.8: Transients and spectra of ring laser working on $J = 15$, $J = 20$, $J = 50$, $J = 75$, $J = 90$ and $J = 125$ respectively during a pump current upward sweeping. Other parameters are the same as those in Fig 2.7

(a) $J = 75$ (b) $J = 50$
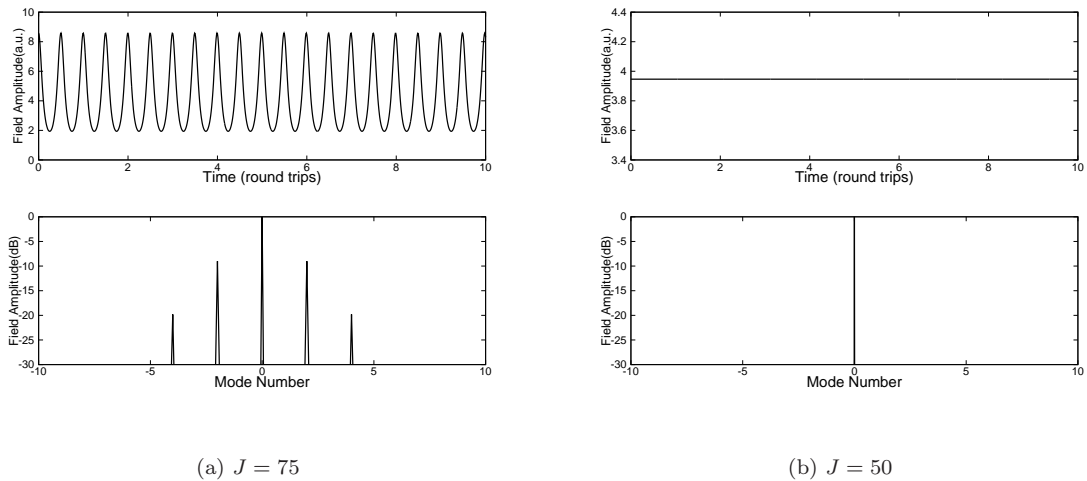
FIGURE 2.9: Transient and spectra of ring laser working on $J = 75$ and 50 with a downward sweeping pump. Other parameters are the same as those in Fig 2.7

of the oscillations are modulated as well. However, this pump is too high above the threshold and the situation might not be seen in the real world.

The down sweeping of the current leads to a bifurcation curve shown in Fig 2.7(b). It looks quite similar to the upward sweeping one except for the region between $J = 41.2$ and $J = 85.4$. Starting from a pump as high as $J = 150$ and decreasing it gradually, the laser shows chaotic oscillations as in Fig 2.8(f) at the beginning, then goes back to the frequency doubling regime as the current enters the region between $J = 85.4$ and $J = 102.6$. By further decreasing the current below 85.4, the two current-light diagrams start to diverge. Instead of suddenly jumping into the mode-locking regime as following the up sweeping diagram reversely, it keeps working on the frequency doubling operation, for instance as in Fig 2.9(a). Fewer modes are seen than in its counterpart on the up sweeping route. To have two oscillations within one round-trip, the spacing between modes is double the original value.

The frequency doubling regime ends at downward sweeping the current to $J = 63.8$ and is followed by single mode operations as seen in Fig 2.9(b). In the corresponding pump region but upwards route, the laser output shows oscillations as in the Fig 2.8(c). However, by keeping decreasing current below $J = 41.2$, the two bifurcation curves converges. The dynamics follow the oscillation, and the monomode route which bifurcates at $J = 17.6$.

To show the influence of the truncation on the bifurcation diagrams, multimode rate equations with different number of modes are used to perform the bifurcation analysis. The bifurcation curve plotted by performing rate equations model with 3 modes, 7 modes and 15 modes are plotted in Fig 2.10.

All three diagrams show similarity at low pump current. In all theses three diagrams, the bifurcations start from single mode operation, bifurcate at current $J = 17.6$ to a multimode oscillation via Risken-Nummandal instability. However, at higher pump, discrepancies emerge. The result of the 3 modes rate equations starts to diverge from that of the travelling wave at as the system just steps into the multimode oscillation regime. Further bifurcations and branches are seen at higher current following. No second multimode operation region is observed even at very high pump in this case. The downward route follows from single mode lasing at high current, complicated dynamics at moderate current, followed by oscillations, and then single mode lasing at low current respectively.

One could easily notice the existence of inner structure as more branches in the multimode regime in the bifurcation diagram plotted from the rate equations with 3 modes, as in Fig 2.10(a). Time traces observed at $J = 27$, $J = 35$ and $J = 45$ are plotted in Fig 2.12(a) - Fig 2.12(c) to investigate this branching effect. Small secondary oscillations between the main ones are seen due to the lacking of necessary modes to make the dynamics express itself in the model. There are even modulations on top of the oscillations when $J = 45$ in Fig 2.12(c).

The spectra shown in the down panels of Fig 2.12(a) - Fig 2.12(c) helps to explain the necessary of more modes in the model for the right dynamics to be shown. As seen in lower panel in Fig 2.12(c), all the three modes emit simultaneously. Unlike spectra in other cases, the modes here smear out strongly. As in the current situation where only 3 modes are taken into account to express strong pulsations which involves a large number of modes, the energy instead of going to high frequency modes will be folded onto the lower ones.

The above discussion shows the adequacy to model usual oscillation by 3 modes. When pump is high and the system enters into the mode locking regime, 3 modes is not good enough as in Fig 2.8(c) and Fig 2.8(d), more than 10 modes are involved in the dynamics. Therefore the bifurcation diagram starts to be messy as pump starts to exceeds $J = 40$.
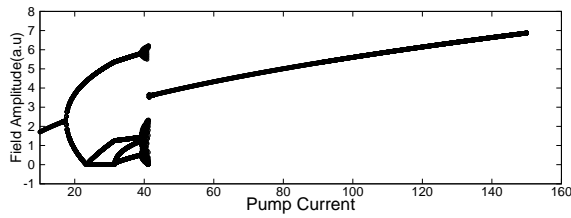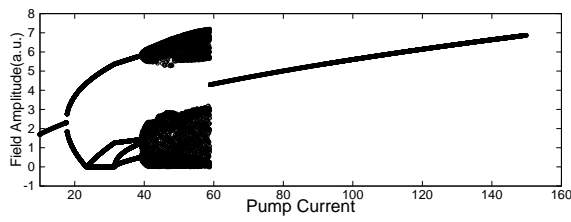
(a) 3 modes
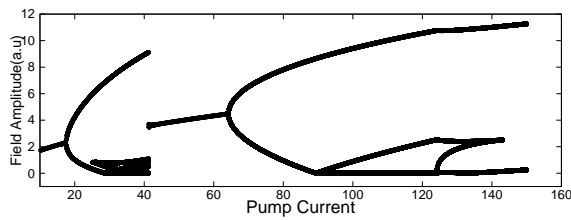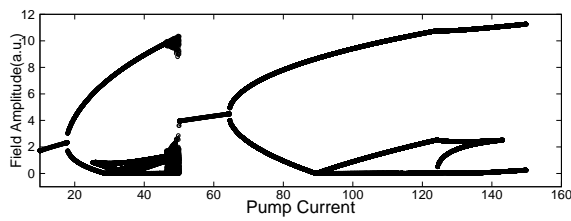
(b) 7 modes
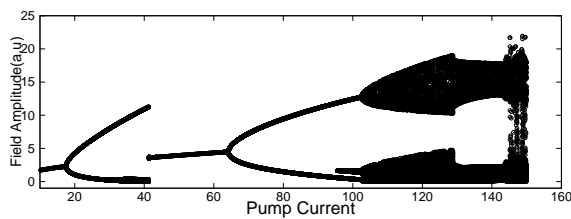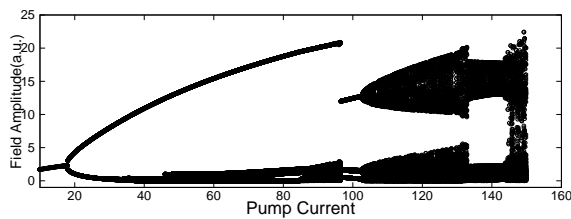
(c) 15 modes

FIGURE 2.10: Bifurcation diagram plotted with rate equations model with (a) 3 modes, (b) 7 modes and (c) 15 modes. The upper panels show the bifurcation diagrams drawn by increasing the pump which the lower ones show those made by down sweeping pump injection. Parameters used here are the same as those in Fig 2.7
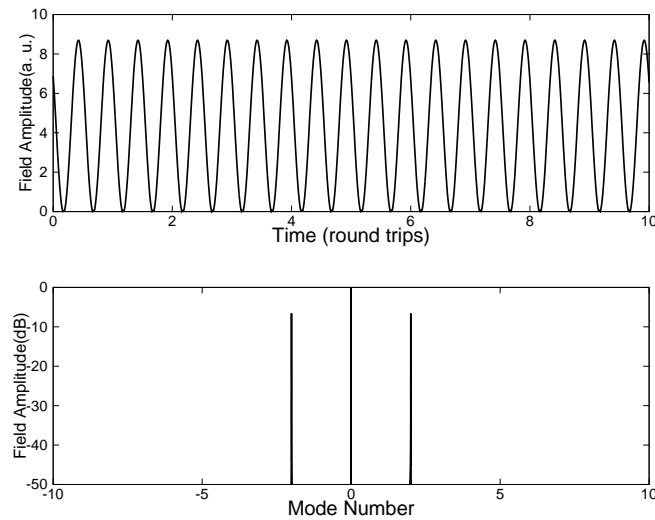
FIGURE 2.11: Transient and spectrum of ring laser working on $J = 90$ following the upward sweeping route made from rate equations with 7 modes. Other parameters are the same as those in Fig 2.7(a) and 2.7(b)

The lacking of frequency doubling regime is definitely due to the limited number of modes as well. As mode spacing doubles in the frequency doubling operation, to have minimum oscillations with 3 modes, a 5 modes rate equations has to be used as 2 mode slots need to be reserved for the nonlasing "± 1" modes.

In the 7 modes case, the second monomode region has been recovered although the bifurcation points do not match what one observed from the travelling wave model. Frequency doubling at $J = 64.4$ by a Hopf bifurcation follows the monomode operation is recovered. Fig 2.11 show the time trace and spectrum at $J = 90$ following the upward sweeping route which is within the frequency doubling region. As shown in Fig 2.8(e), only "0" and "± 2" modes lase, no odd numbered modes are seen in the spectrum.

With 15 modes, the bifurcation curves in Fig 2.10(c) have almost the same profile as the one made from the travelling wave model. Secondary pulses still exist as one sees bifurcation at lower branch of the first multimode region. However they are not significant and expected to disappear completely with further increasing the number of modes.

From the above results, more modes are needed to represent the dynamics at high pump. From Fig 2.10(a) to Fig 2.10(c) it is seen that increasing number of modes into the rate equations smoothes out the high current behaviour and makes the bifurcation diagram closer to that made from the travelling wave approach. Even with 15 modes, the two
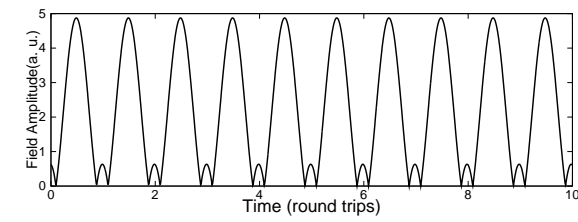
(a) $J = 27$
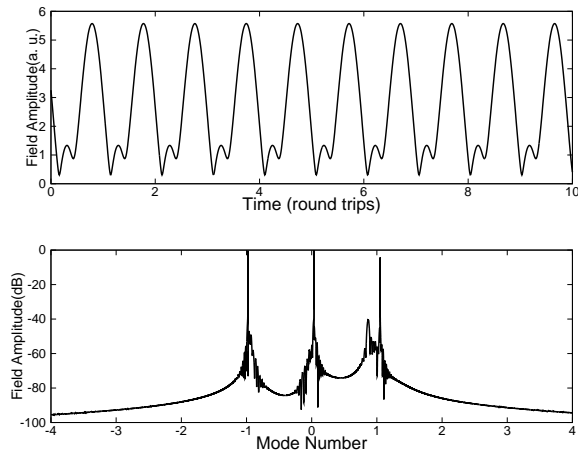
(b) $J = 35$
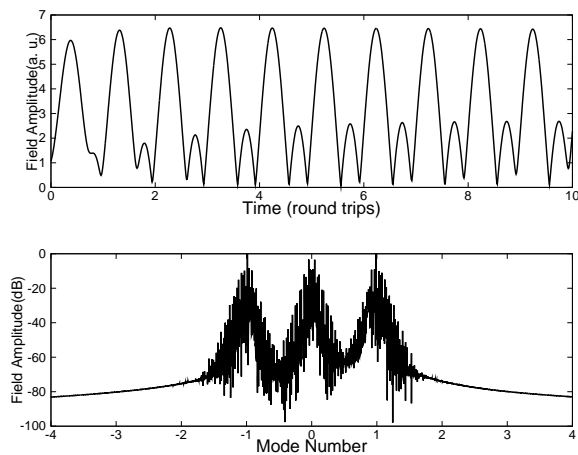
(c) $J = 40$

FIGURE 2.12: Transients and spectra at different pump injection plotted with rate equation with 3 modes. (a) $J = 27$, (b) $J = 35$ and (c) $J = 45$. Parameters used here are the same as those in Fig 2.7

approaches fit quite well to each other. As 100 spatial points are used when making the bifurcation curves from the travelling wave model, the rate equations with 15 modes show superior efficiency and relative good match.

Having said that, the minimum number of modes needed in the modelling varies from operations to operations. To have a reasonably clear idea of the bifurcations in a large range of pump, the author believes 5 modes would be the answer. 3 modes is sensible for a Hopf bifurcation as it is the minimum number one needs to recover the oscillatory operation. However, it is not enough for the frequency doubling operations. 5 modes is the minimum in this case and most common instabilities in mode-locking/multimode lasers.

However different shapes the bifurcation diagrams look like at higher pump end, the lower pump part of the curves always look the same, with the Hopf bifurcation point at the same pump level at $J = 17.6$. A comparison of the bifurcation diagrams made by travelling wave and rate equations with 3, 7 and 15 modes at low pump lever is shown in Fig 2.13. Upward sweeping and downward sweeping diagrams overlap at these currents. It could be seen from the figure that, with more modes the rate equation approach fits better to the travelling wave model. However, even with 3 modes, the behaviours around the bifurcation point at low current by both approaches are reasonably close. This effectively supports the idea of using rate equations approach with very limited number of modes to study the bifurcations of the system.

2.7 The Final Multimode Model

In this section, the discussions in previous sections of this chapter which focus on separate aspects of the modelling are summarised. The final generalized multimode model is presented.

It is based on the consideration that the standing wave pattern due to the unique geometry of ring lasers induces spatially inhomogeneous gain saturation, and hence inhomogeneous refractive index, which behaves like a Bragg grating. A wave is scattered back by the grating and contributes to the waves travelling in the opposite direction. Also, as in FP lasers, beating between co-propagating modes occurs. For the general laser parameters, the length scale of the spatial grating is on the order of the lasing wavelength, eg. about 1μm, which could be washed out in several picoseconds, while
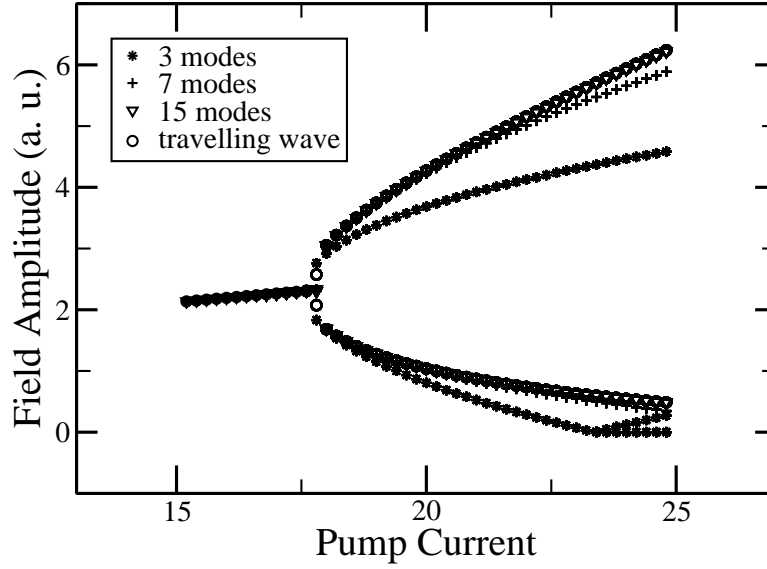
FIGURE 2.13: Comparison of travelling wave result with rate equations ones with 3 modes, 7 modes and 15 modes. The parameter used are the same as those in Fig 2.7

the beating is on the order of the cavity length and is washed out on a nanosecond time scale. Therefore, the first effect is always neglected by the general modelling approach as stated above, and averaged photon densities and carrier density rate equations are used[30]. However, in that paper slowly-varying amplitude is used to describe the optical fields in both directions, and mode beating was hidden. Thus, it is our goal to put counter-propagating effects and multimodes together and present a complete model.

Here the forward and backward wave F and B are decomposed as

$$F = \sum_{p=-M}^{M} F_p(t)e^{ip\Delta kz - ip\Delta\omega t} \tag{2.71}$$

$$B = \sum_{p=-M}^{M} B_p(t)e^{-ip\Delta kz - ip\Delta\omega t}. \tag{2.72}$$

The carrier density as provided previously is

$$\gamma_\parallel^{-1}\frac{dN}{dt} = J - N + D\frac{\partial^2}{\partial z^2}N + \frac{1}{\hbar\omega_c}(iP_T^*E_T + c.c). \tag{2.73}$$

By writing P_T as the convolution of susceptibility and field, Eq (2.73) is written as follows

$$\gamma_{\|}^{-1}\frac{dN}{dt} = J - N + D\frac{\partial^2}{\partial z^2}N + \frac{1}{\hbar\omega_c}[i\sum_{p=-M}^{M}\sum_{q=-M}^{M}(E_p\chi_q^*E_q^* + \tilde{\chi}^*\Delta N E_p E_q^* + c.c)] \quad (2.74)$$

$$= J - N + D\frac{\partial^2}{\partial t^2}N + \frac{1}{\hbar\omega_c}\{i\sum_{p=-M}^{M}E_p\chi_p^*E_p^* + i\sum_{T=1}^{2M}\sum_{p=T-M}^{M}(E_{p-T}\chi_p^*E_p^* + E_p\chi_{p-T}^*E_{p-T}^*)$$

$$+i\tilde{\chi}^*\Delta N[\sum_{p=-M}^{M}E_p E_p^* + \sum_{T=1}^{2M}\sum_{p=T-M}^{M}(E_{p-T}E_p^* + E_p E_{p-T}^*)] + c.c\}$$

here $\tilde{\chi} = \frac{\partial \chi}{\partial N}$, $\chi_p = \chi(\omega_p.N_0)$, $\Delta N = N - N_0$ is the carrier density variation around its steady state. New frequency and spatial components in the dynamics by the product of P_T and E_T are generated.

By separating terms with different spatial periods and using forward and backward fields from Eq (2.20) , Eq (2.75) is written as

$$\gamma_{\|}^{-1}\frac{dN}{dt} = J - N + D\frac{\partial^2}{\partial z^2}N + \frac{2\text{Im}(\tilde{\chi})\Delta N}{\hbar\omega_c}\sum_{p=-M}^{M}(F_p F_p^* + B_p B_p^*)$$

$$+\frac{2}{\hbar\omega_c}\sum_{p=-M}^{M}\text{Im}(\chi_p)(F_p F_p^* + B_p B_p^*) \quad (2.75)$$

$$+\frac{1}{\hbar\omega_c}\{i\sum_{T=1}^{2M}\sum_{p=T-M}^{M}[B_{p-T}B_p^*\chi_p^* - B_p^*B_{p-T}\chi_{p-T} + F_p F_{p-T}^*\chi_{p-T}^* - F_{p-T}^*F_p\chi_p]$$

$$+i\sum_{T=1}^{2M}\sum_{p=-M}^{M}(F_p B_p^*\chi_p^* - B_p^*F_p\chi_p + F_{p-T}B_p^*\chi_p^* - B_{p-T}^*F_p\chi_p$$

$$+F_p B_{p-T}^*\chi_{p-T}^* - F_{p-T}B_p^*\chi_{p-T})e^{2ik_cz} + i\tilde{\chi}\Delta N\sum_{T=1}^{2M}\sum_{p=T-M}^{M}[F_p F_{p-T}^* + B_{p-T}B_p^*$$

$$+(F_p B_p^* + F_{p-T}B_p^* + F_p B_{p-T}^*)e^{2ik_cz}] + c.c\}.$$

Terms with new frequencies and wave vectors are generated but still fall into the slow and fast category. Therefore the carrier density is written as the summation of carrier grating terms with long spatial period components $N_0^{n,m}$ and short spatial period components $N_2^{n,m}$ as

$$N = N_0^{0,0} + \sum_m \sum_n \{N_0^{n,m} e^{i(m\Delta kz - n\Delta\omega t)} + N_2^{n,m} e^{i[(2k_c + m\Delta k)z - n\Delta\omega t]} + c.c\} \qquad (2.76)$$

where m and n are indices of wavevectors and frequencies respectively. As new components are being generated by the production in Eq (2.73), both m and n are summed from $-\infty$ to ∞. However, m and n have to be restricted in a region in real life due to limited capacity of computers. A prior selection is always done before the calculation.

The next step is to substitute Eq (2.76) into Eq (2.73) and separate terms with different wave vectors and frequencies.

The averaged carrier density is

$$
\begin{aligned}
\frac{1}{\gamma_{\parallel}} \frac{dN_0^{0,0}}{dt} =\ & J - N_0^{0,0} + \frac{2}{\hbar\omega_c} \mathrm{Im}(\chi_p) \sum_{p=-M}^{M} (F_p F_p^* + B_p B_p^*) \\
& + \frac{1}{\hbar\omega_c} [i\tilde{\chi}^* \sum_{T=1}^{M} \sum_{p=T-M}^{M} (F_p F_{p-T}^* N_0^{*T,T} + B_{p-T} B_p^* N_0^{*T,-T} + F_p B_p^* N_2^{*2p,0} \\
& + F_{p-T} B_P^* N_2^{*2p-T,-T} + F_p B_{p-T}^* N_2^{*2p-T,T}) + c.c].
\end{aligned}
\qquad (2.77)
$$

The slow grating terms are

$$
\begin{aligned}
\frac{1}{\gamma_{\parallel}} \frac{dN_0^{n,m}}{dt} =\ & i\frac{n\Delta\omega}{\gamma_{\parallel}} N_0^{n,m} - N_0^{n,m} - Dm^2 \Delta k^2 N_0^{n,m} \\
& + \frac{2}{\hbar\omega_c} \mathrm{Im}(\chi) N_0^{n,m} \sum_{p=-M}^{M} (F_p F_p^* + B_p B_p^*) \\
& + \frac{1}{\hbar\omega_c} [i\tilde{\chi}^* \sum_{T=1}^{M} \sum_{p=T-M}^{M} (F_p F_{p-T}^* N_0^{m-T,n-T} + F_p F_{p-T}^* N_0^{*T-m,T-n} \\
& + B_{p-T} B_p^* N_0^{m-T,-n-T} + B_{p-T} B_p^* N_0^{*T-m,-T} + F_p B_p^* N_2^{*2p-m,-n} \\
& + F_{p-T} B_P^* N_2^{*2p-T-m,-n-T} + F_p B_{p-T}^* N_2^{*2p-T-m,T-n}) + c.c].
\end{aligned}
\qquad (2.78)
$$

The carrier densities corresponding to the fast grating terms are

$$\frac{1}{\gamma_\parallel}\frac{dN_2^{n,m}}{dt} = i\frac{n\Delta\omega}{\gamma_\parallel}N_2^{n,m} - N_2^{n,m} - D(2k_c + m\Delta k)^2 N_2^{n,m}$$

$$+\frac{2}{\hbar\omega_c}\text{Im}\,(\chi)\,N_2^{n,m}\sum_{p=-M}^{M}(F_pF_p^* + B_pB_p^*) \tag{2.79}$$

$$+\frac{1}{\hbar\omega_c}[i\tilde{\chi}^*\sum_{T=1}^{M}\sum_{p=T-M}^{M}(F_pF_{p-T}^*N_0^{m-T,n-T} + F_pF_{p-T}^*N_0^{*T-m,T-n}$$

$$+B_{p-T}B_p^*N_0^{m-T,-n-T} + B_{p-T}B_p^*N_0^{*T-m,-T} + F_pB_p^*N_2^{*2p-m,-n}$$

$$+F_{p-T}B_P^*N_2^{*2p-T-m,-n-T} + F_pB_{p-T}^*N_2^{*2p-T-m,T-n}) + c.c].$$

Eq (2.76) is now substituted into the field equations, so that

$$\frac{\partial F_p}{\partial t} = i(\omega_p - v_g\Delta k_p)F_p + \frac{i\omega_c}{2\eta_g^2}\chi(\omega_p, N_0)F_p \tag{2.80}$$

$$+\frac{i\omega_c}{2\eta_g^2}\sum_{q=-M}^{M}\tilde{\chi}[N_0^{p-q,p-q}F_q + N_0^{*q-p,q-p}F_q + N_2^{p-q,p+q}B_q]$$

$$\frac{\partial B_p}{\partial t} = i(\omega_p - v_g\Delta k_p)B_p + \frac{i\omega_c}{2\eta_g^2}\chi(\omega_p, N_0)B_p \tag{2.81}$$

$$+\frac{i\omega_c}{2\eta_g^2}\sum_{q=-M}^{M}\tilde{\chi}[N_0^{p-q,q-p}B_q + N_0^{*q-p,p-q}B_q + N_2^{*q-p,p+q}F_q]$$

As $\frac{\omega_c}{c} = k_c$, the terms in the first parentheses of Eq (2.81) and Eq (2.82) will be 0. the final equation for fields are seen

$$\frac{\partial F_p}{\partial t} = \frac{i\omega_c}{2\eta_g^2}\chi(\omega_p, N_0)F_p + \frac{i\omega_c}{2\eta_g^2}\sum_{q=-M}^{M}\tilde{\chi}[N_0^{p-q,p-q}F_q + N_0^{*q-p,q-p}F_q + N_2^{p-q,p+q}B_q] \tag{2.82}$$

$$\frac{\partial B_p}{\partial t} = \frac{i\omega_c}{2\eta_g^2}\chi(\omega_p, N_0)B_p + \frac{i\omega_c}{2\eta_g^2}\sum_{q=-M}^{M}\tilde{\chi}[N_0^{p-q,q-p}B_q + N_0^{*q-p,p-q}B_q + N_2^{*q-p,p+q}F_q]. \tag{2.83}$$

The above approach generates a large number of carrier fluctuation terms. Each mode index m corresponds to more than one n and *vice versa*. An approach to restrict the

number of m and n is applied in the following. Only components generated by $E_T E_T^*$ are kept, therefore the equation for carrier density reads

$$
\begin{aligned}
\gamma_\parallel^{-1} \frac{dN}{dt} =\ & J - N + D\frac{\partial^2}{\partial z^2}N + \frac{2\mathrm{Im}(\tilde{\chi})\Delta N}{\hbar\omega_c}\sum_{p=-M}^{M}(F_p F_p^* + B_p B_p^*) \\
& + \frac{2\mathrm{Im}(\tilde{\chi})\Delta N}{\hbar\omega_c}\Big\{\sum_{T=1}^{2M}\sum_{p=T-M}^{M}[F_{p-T}^* F_p e^{i(T\Delta kz - T\Delta\omega t)} + B_{p-T}B_p^* e^{i(T\Delta kz + T\Delta\omega t)}] \\
& + \sum_{p=-M}^{M}[F_p B_p^* e^{2ip\Delta kz} + \sum_{T=1}^{2M}\sum_{p=T-M}^{M}F_{p-T}B_p^* e^{i(2p-T)\Delta kz + iT\Delta\omega t} \\
& + B_{p-T}^* F_p e^{i(2p-T)\Delta kz - T\Delta\omega t}]e^{i2k_c z} + c.c\Big\} + \frac{1}{\hbar\omega_c}\Big\{i\sum_{p=-M}^{M}(F_p F_p^* + B_p B_p^*)\chi_p^* \\
& + i\sum_{T=1}^{2M}\sum_{p=T-M}^{M}[(B_{p-T}B_p^*\chi_p^* - B_p^* B_{p-T}\chi_{p-T})e^{iT\Delta kz + iT\Delta\omega t} \qquad (2.84) \\
& + (F_p F_{p-T}^*\chi_{p-T}^* - F_{p-T}^* F_p\chi_p)e^{iT\Delta kz - iT\Delta\omega t}] + i\sum_{p=-M}^{M}(F_p B_p^*\chi_p^* - B_p^* F_p\chi_p)e^{i2p\Delta kz} \\
& + i\sum_{T=1}^{2M}\sum_{p=T-M}^{M}[F_{p-T}B_p^*(\chi_p^* - \chi_{p-T})e^{i(2p-T)\Delta kz + iT\Delta\omega t} \\
& + F_p B_{p-T}^*(\chi_{p-T}^* - \chi_p)e^{i(2p-T)\Delta k - iT\Delta\omega t}]e^{2ik_c z} + c.c\Big\}.
\end{aligned}
$$

The terms in Eq (2.85) could be grouped up into slow and fast variations. Subsequently the carrier density is written as the following correspondingly.

$$
\begin{aligned}
N =\ & N_0 + \Big\{\sum_{l=1}^{2M}(N_1^{l,-l}e^{il\Delta kz - il\Delta\omega t} + N_1^{l,l}e^{il\Delta kz + il\Delta\omega t}) + [\sum_{l=-M}^{M}N_2^{2l,0}e^{2il\Delta kz} \qquad (2.85) \\
& + \sum_{m=1}^{2M}\sum_{l=m-M}^{M}N_2^{2l-m,-m}e^{i(2l-m)\Delta kz - im\Delta\omega t} + N_2^{2l-m,m}e^{i(2l-m)\Delta k + im\Delta\omega t}]e^{i2k_c z} + c.c\Big\}
\end{aligned}
$$

By substituting Eq (2.86) into Eq (2.85), one has the rate equations of the components with different frequencies in Eq (2.86)

The spatially averaged carrier density could be solved from the following equations

$$\frac{1}{\gamma_\parallel}\frac{dN_0}{dt} = J - N_0 + \frac{2}{\hbar\omega_c}\sum_{p=-M}^{M}Im(\chi_p)(F_pF_p^* + B_pB_p^*)$$

$$+\frac{2}{\hbar\omega_c}Im(\tilde{\chi})[\sum_{T=1}^{2M}\sum_{p=T-M}^{M}(F_{p-T}F_p^*N_1^{T,-T} + B_{p-T}^*B_pN_1^{T,T}) \qquad (2.86)$$

$$+\sum_{p=-M}^{M}F_p^*B_pN_2^{2p,0} + \sum_{T=1}^{2M}\sum_{p=T-M}^{M}(F_{p-T}^*B_pN_2^{2p-T,T} + B_{p-T}F_p^*N_2^{2p-T,-T}) + c.c].$$

The rate equations of the "slow" carrier densities are

$$\frac{1}{\gamma_\parallel}\frac{dN_1^{l,-l}}{dt} = -N_1^{l,-l} - Dl^2\Delta k^2 N_1^{l,-l} + \frac{i}{\hbar\omega_c}\sum_{p=l-M}^{M}(F_pF_{p-l}^*\chi_{p-l}^* - F_{p-l}^*F_p\chi_p) \qquad (2.87)$$

$$+\frac{2}{\hbar\omega_c}Im(\tilde{\chi})[N_1^{l,-l}\sum_{p=-M}^{M}(F_pF_p^* + B_pB_p^*) + \sum_{T=1}^{l-1}\sum_{p=T-M}^{M}F_{p-T}^*F_pN_1^{l-T,-(l-T)}$$

$$+\sum_{T=l+1}^{2M}\sum_{p=T-M}^{M}F_{p-T}^*F_pN_1^{*(T-l),-(T-l)} + \sum_{T=1}^{2M-l}\sum_{p=T-M}^{M}F_{p-T}F_p^*N_1^{T+l,-(T+l)}$$

$$+\sum_{p=l-M}^{M}F_pB_p^*N_2^{*2p-l,l} + \sum_{p=-M}^{M-l}F_p^*B_pN_2^{2p+l,-l} + \sum_{p=l-M}^{M}N_2^{2p,0}F_{p-l}^*B_p$$

$$+\sum_{p=-M}^{M-l}N_2^{*2p,0}F_{p+l}B_p^*$$

$$+\sum_{T=1}^{2M-l}\sum_{p=T-M+l}^{M}F_{p-T}B_p^*N_2^{*2p-T-l,T+l} + \sum_{T=1}^{l-1}\sum_{p=T-M}^{M}B_{p-T}^*F_pN_2^{*2p-T-l,l-T}$$

$$+\sum_{T=l+1}^{2M}\sum_{p=T-M}^{M}B_{p-T}^*F_pN_2^{*2p-l-T,-(T-l)} + \sum_{T=1+l}^{2M}\sum_{p=T-M}^{M}F_{p-T}^*B_pN_2^{2p-T+l,T-l}$$

$$+\sum_{T=1}^{l-1}\sum_{p=T-M}^{M+T-l}F_{p-T}^*B_pN_2^{2p+l-T,-(l-T)} + \sum_{T=1}^{2M-l}\sum_{p=T-M}^{M-l}B_{p-T}F_p^*N_2^{2p+l-T,-(T+l)}]$$

and

$$\frac{1}{\gamma_\parallel}\frac{N_1^{l,l}}{dt} = -N_1^{l,l} - Dl^2\Delta k^2 N_1^{l,l} + \frac{i}{\hbar\omega_c}\sum_{p=l-M}^{M}(B_p^*B_{p-l}\chi_p^* - B_{p-l}B_p^*\chi_{p-l}) \qquad (2.88)$$

$$+\frac{2}{\hbar\omega_c}Im(\tilde{\chi})[N_1^{l,l}\sum_{p=-M}^{M}(F_pF_p^* + B_pB_p^*) + \sum_{T=1}^{l-1}\sum_{p=T-M}^{M}B_{p-T}B_p^*N_1^{l-T,l-T}$$

$$+ \sum_{T=l+1}^{2M} \sum_{p=T-M}^{M} B_{p-T} B_p^* N_1^{*T-l,T-l} + \sum_{T=1}^{2M-l} \sum_{p=T-M}^{M} B_{p-T}^* B_p N_1^{l+T,l+T})]$$

$$+ \sum_{p=l-M}^{M} F_p B_p^* N_2^{*2p-l.-l} + \sum_{p=-M}^{M-l} F_p^* B_p N_2^{2p+l.l}$$

$$+ \sum_{p=l-M}^{M} N_2^{2p,0} B_{p-l} F_p^* + \sum_{p=-M}^{M-l} N_2^{*2p,0} F_p B_{p+l}^*$$

$$+ \sum_{T=1+l}^{2M} \sum_{p=T-M}^{M} F_{p-T} B_p^* N_2^{*2p-l-T,T-l} + \sum_{T=1}^{l-1} \sum_{p=T-M}^{M} F_{p-T} B_p^* N_2^{*2p-T-l,-(l-T)}$$

$$+ \sum_{T=1}^{2M-l} \sum_{p=T-M+l}^{M} B_{p-T}^* F_p N_2^{*2p-T-l,-(T+l)} + \sum_{T=1}^{2M-l} \sum_{p=T-M}^{M-l} F_{p-T}^* B_p N_2^{2p-T+l,T+l}$$

$$+ \sum_{T=1}^{l-1} \sum_{p=T-M}^{M+T-l} B_{p-T} F_p^* N_2^{2p-T+l,l-T} + \sum_{T=1+l}^{2M} \sum_{p=T-M}^{M} B_{p-T} F_p^* N_2^{2p-T+l,-(T-l)}].$$

The carrier density corresponding to the fast spatial grating are solved by the following 3 equations

$$\frac{1}{\gamma_\parallel} \frac{N_2^{2l,0}}{dt} = -N_2^{2l,0} - 4Dk_c^2 N_2^{2l,0} + \frac{2}{\hbar\omega_c}\text{Im}(\chi_l)F_l B_l^* + \frac{2}{\hbar\omega_c}\text{Im}(\tilde{\chi})[n_g^{2l,0}\sum_{p=-M}^{M}(F_p F_p^* + B_p B_p^*)$$

$$+ \sum_{T=1}^{M-l} \sum_{p=T-M}^{M} F_{p-T} F_p^* N_2^{2l+T,-T} + \sum_{T=1}^{M+l} \sum_{P=T-M}^{M} B_{P-T} B_P^* N_2^{2l-T,-T} \qquad (2.89)$$

$$+ \sum_{T=1}^{M+l} \sum_{p=T-M}^{M} F_{p-T}^* F_p N_2^{2l-T,T} + \sum_{T=1}^{M-l} \sum_{p=T-M}^{M} B_{p-T}^* B_p N_2^{2l+T,T}$$

$$+ \sum_{T=1}^{l+M} N_2^{T,-T} F_{l-T} B_l^* + \sum_{T=1}^{M-l} F_l B_{l+T}^* N_2^{*T,T} + \sum_{T=1}^{M-l} B_l^* F_{l+T} N_1^{*T,-T} + \sum_{T=1}^{M+l} B_{l-T}^* F_l N_1^{T,T}]$$

$$\frac{1}{\gamma_\parallel} \frac{N_2^{2l-m,-m}}{dt} = -N_2^{2l-m,-m} - D[(2l-m)\Delta k + 2k_c]^2 N_2^{2l-m,+m} + \frac{i}{\hbar\omega_c}F_l B_{l-m}^*(\chi_{l-m}^* - \chi_l)$$

$$+ \frac{2}{\hbar\omega_c}\text{Im}(\chi)\{\sum_{p=T-M}^{M} [\sum_{T=m+1}^{l+M} F_{p-T}^* F_p N_2^{2l-m-T,T-m} + \sum_{T=1+m}^{M+m-l} B_{p-T}^* B_p N_2^{2l-m+T,T-m}$$

$$+ \sum_{T=1}^{m-1} F_{p-T}^* F_p N_2^{2l-T-m,-(m-T)} + \sum_{T=1}^{l+M-m} B_{p-T} B_p^* N_2^{2l-T-m,-(T+m)}$$

$$+ \sum_{T=1}^{M-l} F_{p-T} F_p^* N_2^{T+2l-m,-(T+m)} + \sum_{T=1}^{m-1} B_{p-T}^* B_p N_2^{2l-m+T,-(m-T)}] \qquad (2.90)$$

$$+ \sum_{T=1}^{M-l} N_1^{*m+T,m+T} F_l B_{l+T}^* + \sum_{T=1}^{l-m+M} N_1^{T+m,-(T+m)} F_{l-m-T} B_{l-m}^*$$

$$+ \sum_{T=1+m}^{l+M} N_1^{T-m,T-m} B_{l-T}^* F_l + \sum_{T=1}^{m-1} N_1^{m-T,-(m-T)} B_{l-m}^* F_{l-m+T}$$

$$+ \sum_{T=1}^{m-1} N_1^{*m-T,m-T} B_{l-T}^* F_l + \sum_{T=1}^{M+m-l} N_1^{*T-m,-(T-m)} B_{l-m}^* F_{l-m+T}$$

$$+ \sum_{p=m-M}^{M} F_{p-m}^* F_p N_2^{2(l-m),0} + \sum_{p=m-M}^{M} B_{p-m}^* B_p N_2^{2l,0}$$

$$+ N_1^{m,-m} F_{l-m} B_{l-m}^* + N_1^{*m,m} F_l B_l^* \}$$

$$\frac{1}{\gamma_{\parallel}} \frac{N_2^{2l-m,m}}{dt} = -N_2^{2l-m,m} - D[(2l-m)\Delta k + 2k_c]^2 N_2^{2l-m,+m} + \frac{i}{\hbar\omega_c} F_{l-m} B_l^* (\chi_l^* - \chi_{l-m})$$

$$+ \frac{2}{\hbar\omega_c} \text{Im}(\chi) \{ \sum_{p=T-M}^{M} [\sum_{T=1}^{l+M-m} F_{p-T}^* F_p N_2^{2l-m-T,m+T} + \sum_{T=1}^{m-1} B_{p-T} B_p^* N_2^{2l-T-m,m-T}$$

$$+ \sum_{T=1}^{m-1} F_{p-T} F_p^* N_2^{2l-m+T,m-T} \sum_{T=1}^{M-l} B_{p-T}^* B_p N_2^{2l+T-m,m+T} \qquad (2.91)$$

$$+ \sum_{T=1+m}^{l+M} B_{p-T} B_p^* N_2^{2l-m-T,-(T-m)} + \sum_{T=1+m}^{M+m-l} F_{p-T} F_p^* N_2^{2l-m+T,-(T-m)}]$$

$$+ \sum_{T=1}^{m-1} N_1^{m-T,m-T} F_{l-m} B_{l-m+T}^* + \sum_{T=1+m}^{l+M} N_1^{T-m,-(T-m)} F_{l-T} B_l^*$$

$$+ \sum_{T=1+m}^{M+m-l} N_1^{*T-m,T-m} F_{l-m} B_{l-m+T}^* + \sum_{T=1}^{m-1} N_1^{*(m-T),-(m-T)} F_{l-T} B_l^*$$

$$+ \sum_{T=1}^{l-m+M} N_1^{T+m,T+m} B_{l-m-T}^* F_{l-m} + \sum_{T=1}^{M-l} n_1^{*T+m,-(T+m)} B_l^* F_{l+T}$$

$$+ \sum_{p=m-M}^{M} F_{p-m} F_p^* N_2^{2l,0} + \sum_{p=m-M}^{M} B_{p-m} B_p^* N_2^{2(l-m),0}$$

$$+ F_l B_l^* N_1^{*m,-m} + N_1^{m,m} F_{l-m} B_{l-m}^* \}.$$

The set of equations listed here are the general rate equations with arbitrary number of modes. In general, up to two components of carrier density are kept. One for the averaged term, the other generated by either counter propagating fields or by beating from copropagating modes[66, 67]. However, in this model here, more components of

carrier density could be saved at one's disposal for certain problems. This is the key to model both directional switching and wavelength switching at the same time in Chapter 4.

2.8 Summary

In this chapter, the general modelling consideration has been reviewed and its application to the semiconductor ring lasers has been discussed. The discussion covers aspects including optical field propagation, semiconductor material and its response to the electric magnetic field, peculiarity of the cavity configuration of ring lasers and numerical implementation. A set of ordinary differential equations each corresponds to either an optical mode or a component of carrier density following a certain component after mixing has been derived for a generalised ring laser model which is the basis for the following two chapters. A prior selection of optical component and carrier density has significant effect on the modelling. Different selections will be discussed in the follow chapters.

Chapter 3

Two Mode Study

The simplest case of ring lasers with one mode in each direction is studied in this Chapter. Wave travelling in clockwise direction and counter-clockwise direction interacts both linearly and non-linearly. The cavity construction provides linear backscattering in such way that the output coupler and the facet from output waveguide reflect clockwise wave into counter-clockwise direction and contributes to the counter-clockwise one, and vice versa[98]. Nonlinear interaction is provided by the gain medium itself, like for instance gain competition and four-wave mixing[99]. Standing wave pattern in photon density could be generated by interference of counter propagating waves, which burns holes on carrier density at its maximum position: this effect is called spatial hole burning[66]. This carrier density variation, in turn, behaves like a Bragg grating and scatters light in one direction back into the other. This is considered in this chapter.

One property that distinguishes semiconductor lasers from solid-state ones is the strong carrier diffusion which could wash out that carrier grating mentioned above. This might cause instability of lasing operation[132] and is somehow believed to be one crucial control parameter and is studied theoretically in[97]. On the other hand, Etrich[66] argued that this is an effect small enough to be neglected as the washout time is far quicker than carrier decay rate. However, this effect is kept in this chapter as it is found later that the lasing operation is influenced by its presence.

In this chapter, the general multimode model presented in the previous chapter is simplified to fit the single mode framework at first. Different operating regimes have been identified and bifurcation analysis are performed. At the end of this chapter, directional switching by optical injection is studied as an application of this model.

3.1   Simplified Model

In the single mode framework, there is only one frequency component in each lasing direction. Therefore the total field is reduced to the summation of F and B, which denotes to slow components of clockwise and counter-clockwise wave, respectively.

$$E = Fe^{-i(\omega_c t - k_c z)} + B^{-i(\omega_c t + k_c z)} + c.c. \tag{3.1}$$

The carrier density correspondingly is

$$N = N_0 + N_2 e^{2ik_c z} + N_2^* e^{-2ik_c z}. \tag{3.2}$$

N_0 is the DC component of carrier density. As in single mode approach, there is no beating between co-propagating wave components, hence $N_0^{m,n} = 0$ and $N_2^{m,n} = 0$ in Eq(3.2). However, counter-propagating waves do contribute to the carrier density fluctuation with spatial periodicity as long as half of their wavelength $\frac{\lambda}{2}$, N_2 as a result is kept in above equation.

The reduced field equation for F and B is obtained from Eq(2.82) and Eq(2.83) as

$$\frac{\partial F}{\partial t} = \frac{i\omega_c}{2\eta_g^2}\{\chi(0, N_0)F + \frac{\partial \chi}{\partial N}N_2 B\} \tag{3.3}$$

$$\frac{\partial B}{\partial t} = \frac{i\omega_c}{2\eta_g^2}\{\chi(0, N_0)B + \frac{\partial \chi}{\partial N}N_2^* F\}. \tag{3.4}$$

There are two kinds of backscatterings in the system. One is coherent backscattering which was introduced by coupling between the coupler and the ring cavity, and the reflection from the facets. The other one is incoherent backscattering from impurity distributed in the cavity. The effect of the latter one is cancelled macroscopically. The first one can not be neglected, however is not considered for the time being. The solo influence from the active medium on the dynamics is studied at first.

The corresponding carrier densities equations read

$$\gamma_\parallel^{-1}\frac{dN_0}{dt} = \frac{J}{\gamma_\parallel ed} - N_0 - \frac{\varepsilon_0}{\hbar\omega_c}[i\chi(0,N_0)+c.c](FF^*+BB^*) - \frac{\varepsilon_0}{\hbar\omega_c}(i\frac{\partial\chi}{\partial N}|_{\omega_c,N_0}+c.c)(N_2F^*B+N_2^*FB^*)$$

(3.5)

$$\gamma_\parallel^{-1}\frac{dN_2}{dt} = -N_2 - 4k_c^2DN_2 - \frac{\varepsilon_0}{\hbar\omega_c}[i\frac{\partial\chi}{\partial N}|_{\omega_c,N_0}+c.c]N_2(FF^*+BB^*) - \frac{\varepsilon_0}{\hbar\omega_c}[i\chi(0,N_0)+c.c]FB^*.$$

(3.6)

The susceptibility is written as summation of real and imaginary part

$$\chi = \chi' + i\chi'' \tag{3.7}$$

where the real part corresponds to change of refractive index while the imaginary part corresponds to gain/loss. They are related by Kramers-Kronig relation as mentioned beforehand[1, 121].

On the other hand, susceptibility is usually written as square of refractive index[2]

$$\chi = n^2 - 1. \tag{3.8}$$

Therefore one has a variation of the susceptibility measured from transparency

$$\Delta\chi = 2n(\Delta n' + \Delta n'') \tag{3.9}$$

the carrier density is measured with the respect to transparency, $\Delta N = N - N_{tr}$ where N_{tr} is carrier density at transparency.

It has been pointed out that, above threshold, the peak of the gain spectrum varies almost linearly with the injected carrier density[133]. And so does the refractive index. A phenomenological linewidth enhancement factor α is used to present this linear relation[134]

$$\alpha = \frac{\frac{d\chi''}{dN}}{\frac{d\chi'}{dN}} \tag{3.10}$$

as substitutes Eq(3.9) into Eq(3.10)

$$\alpha = \frac{\frac{dn''}{dN}}{\frac{dn'}{dN}} = \frac{\Delta n''}{\Delta n'} \tag{3.11}$$

$$\chi = \Delta \chi = \Delta \chi + i \Delta \chi. \tag{3.12}$$

It has to be noted that, the definition of α, specifically the sign of it, is related with whether $e^{i\omega t}$ or $e^{-i\omega t}$ is used to represent the phasors of the field. This thesis is based on the latter. In this notation,

$$\Delta n'' = -\frac{G \Delta N}{k} \tag{3.13}$$

$$\Delta n' = -\frac{\alpha G \Delta N}{l}. \tag{3.14}$$

This comes from the requirement of a positive α. As the numerator in Eq (3.11) above $\frac{dn'}{dN}$ is found to be negative in [135] and α is positive at semiconductor lasing wavelength [134], the $\frac{\Delta n''}{\Delta N}$ has to be negative. G is measured in L^2 and the dimension of N is correspondingly L^{-3}. The susceptibility is also measured from transparency.

By putting all terms in and phenomenologically adding internal losses and confinement factor Γ, one obtains

$$\frac{\partial F}{\partial t} = \frac{v_g \Gamma G}{2\eta_g^2}(1 - i\alpha)(\Delta NF + N_2 B) - \frac{F}{\tau_p} \tag{3.15}$$

$$\frac{\partial B}{\partial t} = \frac{v_g \Gamma G}{2\eta_g^2}(1 - i\alpha)(\Delta NB + N_2^* F) - \frac{B}{\tau_p} \tag{3.16}$$

$$\gamma_{\parallel}^{-1}\frac{dN_0}{dt} = \frac{J}{\gamma_{\parallel}ew} - N_0 - \frac{2\varepsilon_0 v_g \Gamma G \Delta N}{\hbar \omega_c^2}(FF^* + BB^*)$$
$$- \frac{2\varepsilon_0 v_g \Gamma G}{\hbar \omega_c^2}(N_2 F^* B + N_2^* FB^*) \tag{3.17}$$

$$\gamma_{\parallel}^{-1}\frac{dN_2}{dt} = -N_2 - 4\gamma_{\parallel}^{-1}k_c^2 DN_2 - \frac{2\varepsilon_0 v_g \Gamma G}{\hbar \omega_c^2}N_2(FF^* + BB^*)$$
$$- \frac{2\varepsilon_0 v_g \Gamma G \Delta N}{\hbar \omega_c^2}FB^*. \tag{3.18}$$

A proper normalization is sought in the following way to make the above four equations dimensionless

$$F, B = \varepsilon_f f, b \tag{3.19}$$

$$\Delta N_0 = \varepsilon_n n \tag{3.20}$$

$$N_2 = \varepsilon_n n_2 \tag{3.21}$$

$$t = \varepsilon_t \tau \tag{3.22}$$

the normalization factors are

$$\epsilon_t = \tau_p \tag{3.23}$$

$$\gamma = \gamma_\parallel \tau_p \tag{3.24}$$

$$\epsilon_f = \sqrt{\frac{\hbar \omega_c^2}{2\varepsilon_0 v_g \Gamma G \gamma_\parallel \tau_p}} \tag{3.25}$$

$$\epsilon_n = \frac{J}{\gamma_\parallel e w} \tag{3.26}$$

$$A = \frac{v_g \Gamma G \tau_p \varepsilon_n}{2 n_g^2} \tag{3.27}$$

$$d = 4\gamma_\parallel^{-1} k_c^2 D. \tag{3.28}$$

$$\tag{3.29}$$

Therefore the equations become

$$\frac{df}{d\tau} = A(nf + n_2 b)(1 - i\alpha) - f \tag{3.30}$$

$$\frac{db}{d\tau} = A(nb + n_2^* f)(1 - i\alpha) - b \tag{3.31}$$

$$\frac{dn}{d\tau} = \gamma - \gamma n(1 + ff^* + bb^*) - \gamma(n_2 f^* b + n_2^* f b^*) \tag{3.32}$$

$$\frac{dn_2}{d\tau} = -\gamma n_2(1 + d + ff^* + bb^*) - \gamma n f b^*. \tag{3.33}$$

These equations are almost the same as those of[97] where a linear gain. The saturation is implicitly included in the interplay between of carrier density and fields [136]. Another popular approach in which gain saturation is explicitly introduced by self- and cross-saturation coefficients to boost the saturation and make the model more accuracy

is taken elsewhere, for example in [19, 106, 107]. However, in such way, the steady state and linear stability analysis is no more solvable analytically, therefore they are not discussed in this chapter. Gain competition and backscattering are separated in these approaches while in this chapter, both of them are provided by nonlinear backscattering from carrier grating.

Three sets of steady state solutions corresponding to different operation regimes could be identified analytically as followings:

1. Trivial solution, eg under lasing threshold. No output in both directions. The injection current is under threshold. A remark should be made here that, this trivial solution is possible even above threshold, although unstable.

$$f = 0 \tag{3.34}$$
$$b = 0 \tag{3.35}$$
$$n = 1 \tag{3.36}$$
$$n_2 = 0. \tag{3.37}$$

2. Unidirectional operation. Lasing output in either directions.

$$f = \sqrt{A-1}e^{-i\alpha\tau} \tag{3.38}$$
$$b = 0 \tag{3.39}$$
$$n = \frac{1}{A} \tag{3.40}$$
$$n_2 = 0 \tag{3.41}$$

or

$$f = 0 \tag{3.42}$$

$$b = \sqrt{A-1}\,e^{-i\alpha\tau} \tag{3.43}$$

$$n = \frac{1}{A} \tag{3.44}$$

$$n_2 = 0. \tag{3.45}$$

3. Bi-directional regime. Lasing in both directions simultaneously. The intensity of counter-propagating waves fluctuates along the cavity therefore the carrier density is not constant but varies along the cavity

$$f = b \neq 0 \tag{3.46}$$

$$n \neq 0 \tag{3.47}$$

$$n_2 \neq 0. \tag{3.48}$$

3.2   Below Lasing Threshold

A linear stability analysis is taken in this section to study the lasing condition properties. Small linear perturbations are added onto steady states found in previous section

$$f = \delta f \tag{3.49}$$

$$b = \delta b \tag{3.50}$$

$$n = 1 + \delta n \tag{3.51}$$

$$n_2 = \delta g. \tag{3.52}$$

Where δf, δb, δn and δg are small perturbations. By substituting those solutions back into Eq (3.30)-(3.33), one gets

$$\dot{\delta f} = (A - 1 - i\alpha)\,\delta f \tag{3.53}$$

$$\dot{\delta b} = (A - 1 - i\alpha)\,\delta b \tag{3.54}$$

$$\dot{\delta n} = -\gamma \delta n \tag{3.55}$$

$$\dot{\delta g} = -\gamma \delta g\,(1 + d)\,. \tag{3.56}$$

The eigenvalues of the above system can be calculated separately as none of those equations are coupled. As Eq (3.53) and (3.54) are identical and in a very simple from, it is straightforward to see the eigenvalues are complex conjugate $\lambda_1 = \lambda_2 = A - 1 - i\alpha$, $\lambda_3 = \lambda_4 = A - 1 + i\alpha$. Eq(3.55) has eigenvalue $\lambda_5 = -\gamma$.

By expressing δg in Eq (3.56) as a phasor, one has eigenvalues $\lambda_6 = -\gamma(1 - i\alpha)$ and $\lambda_7 = 0$. The latter one indicates the existence of arbitrary phase of the carrier grating.

The real parts of those eigenvalues keep negative as long as $A < 1$. In the other words, the system stays stable as A is smaller than 1. Any small perturbation applied on the system decays monotonically or with oscillation, depends on whether the λs are complex or not. Therefore $A = 1$ is the first threshold. The laser evolves to some other state with oscillation as long as A exceed this threshold, as the first four eigenvalues have positive real parts and nonzero imaginary parts.

3.3   Uni-directional Operation and Relaxation Oscillations

As there is no anisotropy between laser directions in the cavity studied in this thesis so far, unidirectional operations in both the two opposite directions are degenerate. Therefore, in this section, forward lasing operation is studied. The result could be applied to the backward lasing operation.

Linear stability analysis is used again. The solutions with linear perturbation are listed as following

$$
\begin{aligned}
f &= \sqrt{A-1}\,e^{-\alpha\tau} + \delta f & (3.57)\\
b &= \delta b & (3.58)\\
n &= \frac{1}{A} + \delta n & (3.59)\\
n_2 &= \delta g. & (3.60)
\end{aligned}
$$

By substituting them into Eq (3.30)-(3.33) and rearranging the order of the equations

$$
\begin{aligned}
\dot{\delta f} &= A\sqrt{A-1}\,(1-i\alpha)\,\delta n & (3.61)\\
\dot{\delta n} &= -\frac{\gamma}{A}\sqrt{A-1}\,(\delta f + \delta f^*) - \gamma A \delta n & (3.62)\\
\dot{\delta b} &= A\sqrt{A-1}\,(1-i\alpha)\,\delta g^* & (3.63)\\
\dot{\delta g} &= -\frac{\gamma}{A}\sqrt{A-1}\,\delta b^* - \gamma\delta g\,(d+A)\,. & (3.64)
\end{aligned}
$$

As δf, δb and δg are actually complex quantities, the rate equations of their complex conjugates are supplied to make the system complete. The Jacobian reads

$$
\begin{pmatrix} R & 0 \\ 0 & S \end{pmatrix} \tag{3.65}
$$

where

$$
R = \begin{pmatrix} 0 & 0 & A\sqrt{A-1}(1-i\alpha) \\ 0 & 0 & A\sqrt{A-1}(1+i\alpha) \\ -\frac{\gamma\sqrt{A-1}}{A} & -\frac{\gamma\sqrt{A-1}}{A} & -\gamma A \end{pmatrix} \tag{3.66}
$$

and

$$S = \begin{pmatrix} 0 & 0 & 0 & A\sqrt{A-1}(1-i\alpha) \\ 0 & 0 & A\sqrt{A-1}(1+i\alpha) & 0 \\ 0 & -\frac{\gamma\sqrt{A-1}}{A} & -\gamma(A+d) & 0 \\ -\frac{\gamma\sqrt{A-1}}{A} & 0 & 0 & -\gamma(A+d) \end{pmatrix}. \tag{3.67}$$

The matrix could be decomposed in a 3×3 matrix and a 4×4 matrix, in another word, the 7th ordered characteristic polynomial is composed of a cubic polynomial and a 4th order one. The smaller matrix corresponds the dynamics of lasing mode f and carrier density n. It has the same form as that of equations governing the stability of a single mode FP laser[66]. On the other hand, the larger matrix determines the stability of nonlasing mode b and carrier grating g.

The characteristic polynomial of the matrix composed of f, f^* and n reads

$$P_3(\lambda) = [\lambda^2 + \gamma A\lambda + 2\gamma(A-1)]\lambda \tag{3.68}$$

whose solutions are

$$\lambda_1 = 0 \tag{3.69}$$

and

$$\lambda_{2,3} = -\frac{\gamma A \pm \sqrt{\gamma^2 A^2 - 8(A-1)\gamma}}{2}. \tag{3.70}$$

The solution λ_1 indicates an arbitrary phase. In the case of $A > 1$, or above threshold, the solutions $\lambda_{2,3}$ are either negative real quantities or complex quantities with negative real parts. In this case, the subsystem of f and n, eg the lasing mode, is always stable. It is called an attractor as trajectories around it will be asymptotically attracted inside it.

Any perturbation applied on the steady state lasing mode will decay exponentially with rotation at the relaxation oscillation frequency. The damping rate is a combination of time constants corresponding to real part of λ_2 and λ_3. In the case that λ_2 and λ_3 are complex values, the perturbation will be damped out in oscillatory way with frequency determined by imaginary part of λ_2 and λ_3.

A typical decay of perturbation by relaxation oscillation is shown in Fig. 3.1. The projection of the attractor on the intensity carrier density plane is a node as Fig. 3.2. The projection of the solution is asymptotically ringing towards the node.
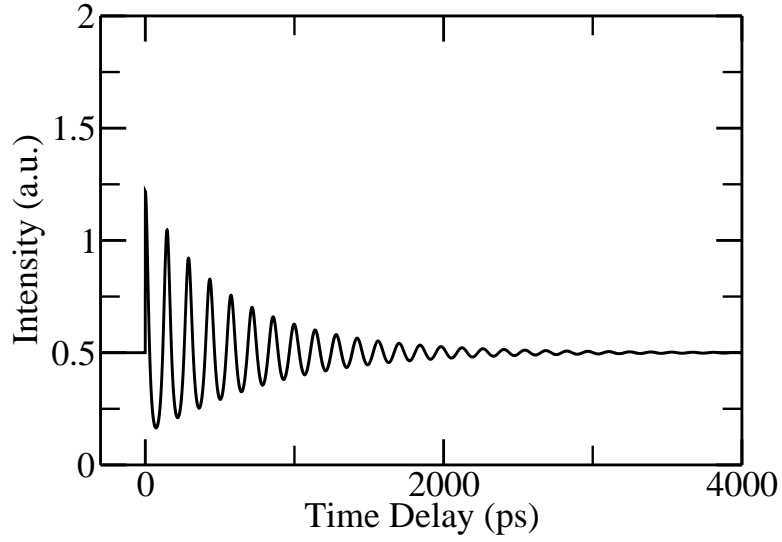
FIGURE 3.1: Transient of relaxation oscillation at $A = 1.5A_{th}$, $\gamma = 0.002$ $\alpha = 3$, $d = 120$
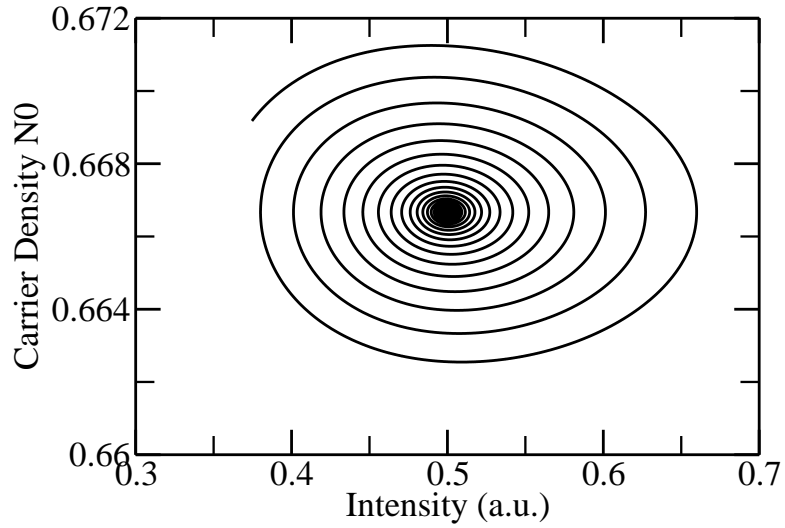
FIGURE 3.2: Phase-space projection of relaxation oscillation at Fig 3.1

The characteristic polynomial of the subsystem of b, b^*, g and g^*, for the nonlasing mode, reads

$$P_4(\lambda) = \{\lambda[\gamma(d + A) + \lambda] + \gamma(A - 1)\}^2 + \alpha^2\gamma^2(A - 1)^2. \tag{3.71}$$

The corresponding eigenvalues fulfil the requirement $P_4(\lambda) = 0$ which gives us

$$\lambda^2 + \gamma(d + A)\lambda + \gamma(A - 1)(1 \pm i\alpha) = 0. \tag{3.72}$$

Therefore the solution will be

$$\lambda_{1,3} = -\frac{\gamma(d+A) \pm \sqrt{\gamma^2(d+A)^2 - 4\gamma(A-1)(1+i\alpha)}}{2} \tag{3.73}$$

$$\lambda_{2,4} = \lambda_{1,3}^*. \tag{3.74}$$

These can be expressed as

$$\lambda_{1,3} = -\frac{\gamma(d+A)}{2}[1 \pm \sqrt{1 - \frac{4(A-1)(1+i\alpha)}{\gamma(d+A)^2}}]. \tag{3.75}$$

The second term in the square root is small, therefore as $\sqrt{1-x} = 1 - x + O(x^2)$,

$$\lambda_{1,3} = -\frac{\gamma(d+A)}{2}[1 \pm (1 - \frac{4(A-1)(1+i\alpha)}{\gamma(d+A)^2})]. \tag{3.76}$$

By further simplification, one has

$$\lambda_1 = -\gamma(d+A)\left[1 - \frac{2(A-1)(1+i\alpha)}{\gamma(d+A)^2}\right] \tag{3.77}$$

$$\lambda_3 = -\frac{2(A-1)(1+i\alpha)}{(d+A)} \tag{3.78}$$

when A is just about threshold, eg $A-1$ is slight above 0, it is easy to see Eq (3.78) with a negative real part. Eq (3.77) could be proven to be negative as well. Therefore this operation is stable just above threshold.

When A is sufficiently large, the eigenvalues are

$$\lambda_1 = \lambda_3^* = -2 - 2i\alpha \tag{3.79}$$

$$\lambda_2 = \lambda_4^* = -\gamma d - \gamma A + 2 + 2i\alpha. \tag{3.80}$$

It is quite straightforward to see that all λs have negative real parts. Therefore at high current injection operation, the nonlasing mode is stable. In the wide range between just above lasing threshold and very high current, the real part of λ_2 and λ_4 could either

be constantly negative or switch between positive and negative a couple of times.

The former case is trivial in that lasing state keeps stable all the time with varying current injection. It is interesting to study the second case, where the operation change via Hopf bifurcation, eg real part of eigenvalues switch from negative to positive or vice versa with smoothly tuning of A, could happen. To spot boundaries of operations, one assumes the eigenvalue is purely imaginary $\lambda = iy$, y is real, and substitutes this condition into Eq (3.71). The real and imaginary parts are separated

$$y^2 = \gamma(A-1) \tag{3.81}$$

$$(d+A)y = \pm(A-1)\alpha. \tag{3.82}$$

An equation is obtained by solving above equations

$$(A-1)^2 + (A-1)\left(2d+2-\frac{\alpha^2}{\gamma}\right) + (d+1)^2 = 0. \tag{3.83}$$

The solution

$$A - 1 = \frac{\frac{\alpha^2}{\gamma} - 2(d+1) \pm \sqrt{\frac{\alpha^4}{\gamma^2} - \frac{4(d+1)\alpha^2}{\gamma}}}{2} \tag{3.84}$$

for above equation to have real solutions, the difference inside the square root should be always positive. This gives the boundary for the possibility for a uni-directional operation to be stable, which is

$$d < \frac{\alpha^2}{4\gamma} - 1. \tag{3.85}$$

It is proven that Eq (3.84) always has two positive solutions. They correspond the two Hopf bifurcations for the stable and unstable unidirectional operation switch.

Eq (3.84) is plotted in Fig 3.3 to show boundary of steady uni-directional operation regime in $A - d$ space. α is set to be 3 which is typical value from semiconductor quantum well lasers. γ is 0.15 here.
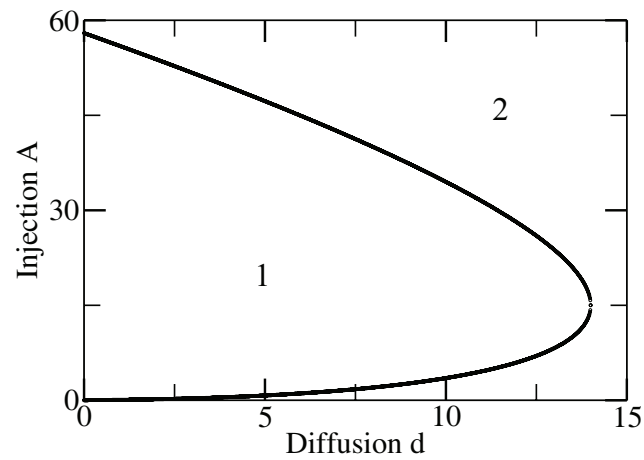
FIGURE 3.3: Region of stable uni-directional operation $\gamma = 0.15$ $\alpha = 3$. The unidirectional operation is always stable at large diffusion. For small diffusion, the unidirectional is only stable at small and large current but unstable in between. Regions marked 1 and 2 are for unstable and stable uni-directional operations respectively.

As Fig. 3.3 shows, the unidirectional operation is always stable when diffusion d is larger than a threshold. However, for d below that value, unidirectional operation is still stable at low and high inject, but unstable in between.

3.4 CW Bidirectional Operation

The laser could also work in a CW-bidirectional operation in which light is travelling in both directions inside the cavity. The total intensity has a standing wave pattern which therefore induces a Bragg grating in the carrier density. In this case, optical fields in both directions and the carrier grating term all have nonzero solution at steady state. The solutions in the following form are sought

$$f = f_0 e^{-i(\omega_f \tau + \phi_f)} \tag{3.86}$$

$$b = b_0 e^{-i(\omega_b \tau + \phi_b)} \tag{3.87}$$

$$n_2 = n_{20} e^{-i(\omega_{n2} \tau + \phi_{ng})}. \tag{3.88}$$

By substituting Eq(3.86),(3.87) and (3.88) into Eq(3.30)-(3.33), one has

$$\dot{f_0} = An_0 f_0 + An_{20} b_0 \left(\cos\Delta\phi - \alpha\sin\Delta\phi \right) - f_0 \tag{3.89}$$

$$\dot{b_0} = An_0 b_0 + An_{20} f_0 \left(\cos\Delta\phi + \alpha\sin\Delta\phi \right) - b_0 \tag{3.90}$$

$$\dot{n_0} = -\gamma - \gamma n_0 \left(1 + f_0^2 + b_0^2 \right) - 2\gamma n_{20} f_0 b_0 \cos\Delta\phi \tag{3.91}$$

$$\dot{n_{g0}} = -\gamma n_{20} \left(1 + d + f_0^2 + b_0^2 \right) - \gamma n_0 f_0 b_0 \cos\Delta\phi \tag{3.92}$$

$$\begin{aligned}
\dot{\Delta\phi} &= \dot{\phi}_{n2} + \dot{\phi}_b - \dot{\phi}_f \\
&= \gamma \frac{n_0}{n_{20}} f_0 b_0 \sin\Delta\phi - A \frac{n_{20}}{b_0} f_0 \left(\sin\Delta\phi - \alpha\cos\Delta\phi \right) \\
&\quad - A \frac{n_{20}}{f_0} b_0 \left(\sin\Delta\phi + \alpha\cos\Delta\phi \right).
\end{aligned} \tag{3.93}$$

It can be seen that only the phase combination $\Delta\phi = \phi_{n2} + \phi_b - \phi_f$ plays a role in determining the static bi-directional operation, instead of individual phases. Its exact value could be solved from Eq (3.89) and Eq (3.90).

The symmetrical solution with identical amplitude for waves travelling in both directions, i.e. $f_0 = b_0$, is sought in this section. By substituting this condition into Eq (3.89) and (3.90), it requires that $\sin\Delta\phi = 0$. Hence $\cos\Delta\phi$ could be either -1 or 1.

If $\cos\Delta\phi = 1$, e.g. $\Delta\phi = 0$, Eq(3.89)-(3.91) becomes

$$A(n_{00} + n_{20}) = 0 \tag{3.94}$$

$$n_{00}(1 + f_0^2) + 2n_{20}f_0^2 = 1 \tag{3.95}$$

$$n_{20}(1 + d + 2f_0^2) + n_{00}f_0^2 = 0. \tag{3.96}$$

This set of equation is unphysical as every single term in the left hand side of Eq(3.96) is positive. Therefore $\Delta\phi = 0$ is excluded as a solution. This is interpreted as follows: $\Delta\phi = 0$ corresponds to the situation where the carrier grating and the standing wave formed by counter-propagating mode are in-phase. In other words, the standing wave has its peak at the point of maximum carrier density. This can not last long as the carriers and photons recombining at those peaks are stronger than those at the nulls. Therefore the carriers are depleted and carrier density maximum moves $\frac{\pi}{2}$ away.

If $\cos\Delta\phi = -1$, i.e $\Delta\phi = \pi$. Eq (3.89)-(3.93) become

$$A(n_{00} - n_{20}) = 0 \tag{3.97}$$

$$n_{00}(1 + f_0^2) - 2n_{20}f_0^2 = 1 \tag{3.98}$$

$$n_{20}(1 + d + 2f_0^2) - n_{00}f_0^2 = 0. \tag{3.99}$$

Let $I = f_0^2 = b_0^2$ be the steady state intensity; from the three equations Eq (3.97) - Eq (3.99);

$$2I^2 + (4 + 2d - A)I + (1 + d)(1 - A) = 0. \tag{3.100}$$

The solution for I is

$$I = \frac{A - 2d - 4 \pm \sqrt{A^2 + 4d^2 + 4Ad + 8d + 8}}{4}. \tag{3.101}$$

The "−" solution is discarded as current above threshold gives negative intensity. Therefore the steady state solution reads
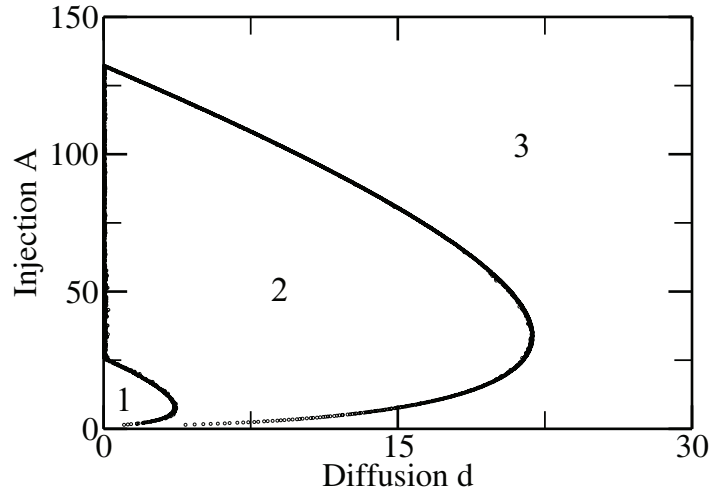
FIGURE 3.4: Region of stable bi-directional operation $\gamma = 0.15$ $\alpha = 3$. Regions marked 1,2,3 are for unstable, stable and unstable bi-directional operations respectively.

$$f_0^2 = b_0^2 = \frac{A - 2d - 4 + \sqrt{A^2 + 4d^2 + 4Ad + 8d + 8}}{4} \tag{3.102}$$

$$n_{00} = \frac{A + 2d + 4 - \sqrt{A^2 + 4d^2 + 4Ad + 8d + 8}}{2A} \tag{3.103}$$

$$n_{20} = \frac{A + 2d + 2 - \sqrt{A^2 + 4d^2 + 4Ad + 8d + 8}}{2A}. \tag{3.104}$$

The stability of bi-directional operation is studied by a linear stability analysis as in previous sections. However it is impossible to do this analytically as trigonometric functions occur in Eq (3.89)-(3.93). Therefore, instead of analytically writing the Jacobian matrix of the above system and solving characteristic polynomials as in previous sections, numerical solutions are pursued.

Let

$$x = (f, b, n_0, n_2, \Delta\phi) \tag{3.105}$$

being a 5 dimensional vector. The equations Eq (3.89) - Eq (3.93) are expressed as following

$$\frac{dx}{d\tau} = M(x) \tag{3.106}$$

where $M(x)$ corresponds to coefficients of Eq(3.89)-(3.93). Let $x = x_0 + \delta x$ where x_0 is bi-directional steady state solutions satisfying to Eq(3.95)-(3.96) and δx is a perturbation on x_0. Therefore

$$\frac{d\delta x}{d\tau} = J(M)\delta x \qquad (3.107)$$

where $J(M)$ is the Jacobian of matrix M.

$$J(M)_{ij} = \frac{M(x_{0i} + \delta x_i) - M(x_{0i})}{dx_j}. \qquad (3.108)$$

This way, elements of Jacobian $J(M)$ are calculated along with the consequent eigenvalues.

The stable bi-directional operation is shown in Fig. (3.4). As in the uni-directional case, stable bi-directional lasing only happens below a certain diffusion threshold. At low diffusion coefficient, four Hopf bifurcations occur with increasing drive current.
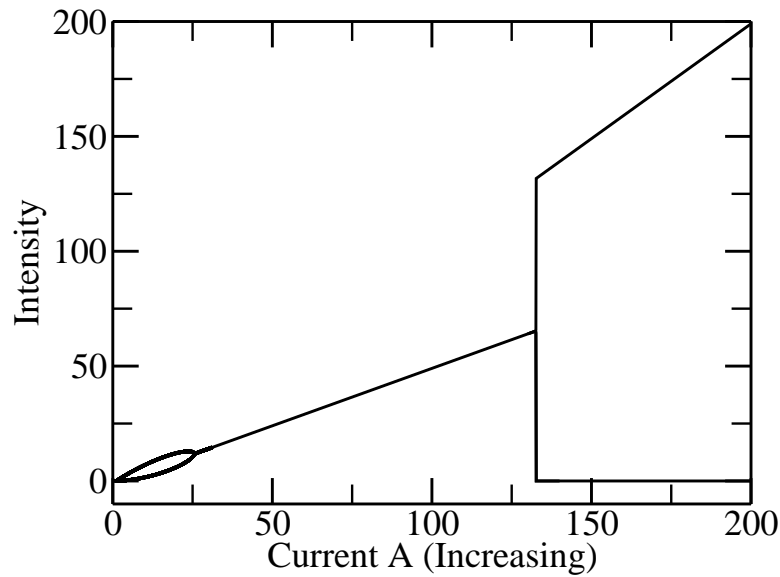
FIGURE 3.5: Bifurcation diagram with increasing current $\gamma = 0.15$ $\alpha = 3$, $d = 0$. The laser works from bi-directional oscillation to uni-directional CW operation via bi-directional CW operation by increasing current.

3.5 Transition Between Different Regimes of Operation

The previous sections discussed the condition for each state to be stable. By varying different control parameters, e.g. diffusion coefficient and injection current, the system might switch between different operations. Since there is no linear backscattering in this model, carrier grating exists as sole source for coupling between counterpropagating modes. Strong carrier diffusion literately washes out this coupling and makes the two lasing modes independent. In this case, only one of the two couterpropagating modes has sufficient gain to lase. As Fig. 3.3 shows, for a certain current A, the laser only works in unidirectional regime as d becomes large. On the other end, small d indicates persistent carrier grating by inefficient diffusion and thus strong coupling between counterpropagating modes. As shown in Fig. 3.4, laser always works on the bi-direction operation, either CW or oscillates as discussed later.

The analyses provided in previous sections are instructive. However, supplementary information is needed to characterize device behaviours. By comparing Fig. 3.3 and Fig. 3.4, overlap areas of stable bi-directional and uni-directional operation are found. This indicates the existence of bistable states and possible hysteresis behaviours with control parameters.

This could be shown from bifurcation analysis in which different operation regimes are recorded by starting a laser from a steady state and slowly tuning a control parameter. The tuning is assumed adiabatic so that the laser is assumed to be in equilibrium during the whole process apart from an abrupt hopping between the different operation regimes.
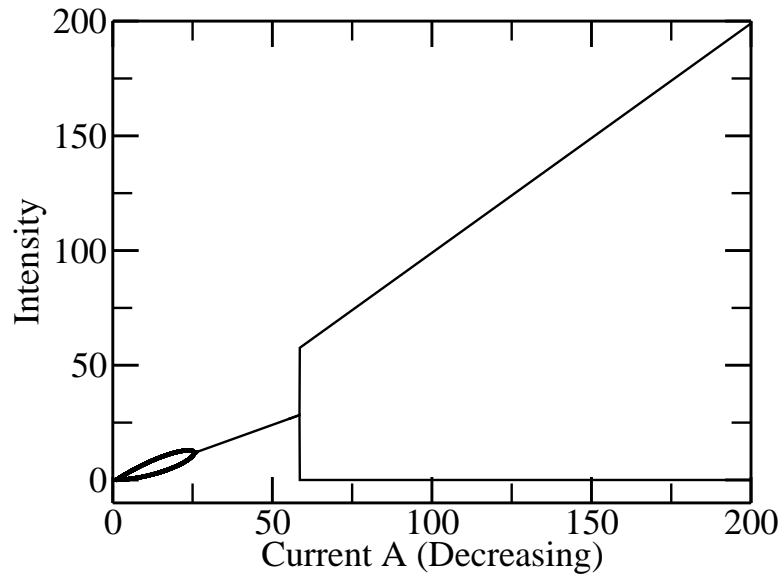
FIGURE 3.6: Bifurcation diagram with decreasing current $\gamma = 0.15$ $\alpha = 3$, $d = 0$. The laser works from uni-directional CW operation to bi-directional oscillation via bi-directional CW operation by decreasing current.

Numerically, this is implemented by integrating the rate equations in a very long time interval and then slightly changing the control parameter and giving the steady solution a small random perturbation.

Fig. 3.5 and Fig. 3.6 show for $d = 0$ a bifurcation diagram with carrier injection increased and decreased respectively. Both figure shows bi-directional oscillation, bi-directional CW and uni-directional lasing. Differences on values between different operations are shown. This corresponds to the overlap of stable regimes as mentioned before. For small d, one gets the same bifurcation diagrams.

At small d and A, both uni- and bi- directional operation are unstable. It is interesting to address the operation of this area. By running simulations in this area, it is shown that a bi-directional oscillatory regime is found as in Fig. 3.7. The phase portrait Fig. 3.8 shows periodicity. However, at certain parameters, chaotic time traces are observed. As γ is reduced to 0.002, a chaotic regime is seen from Fig. 3.9.

3.6 Directional Switching

Studies on directional switching by a single mode rate equation model have been conducted by several groups recently[30, 32, 101]. The switching between two stable lasing
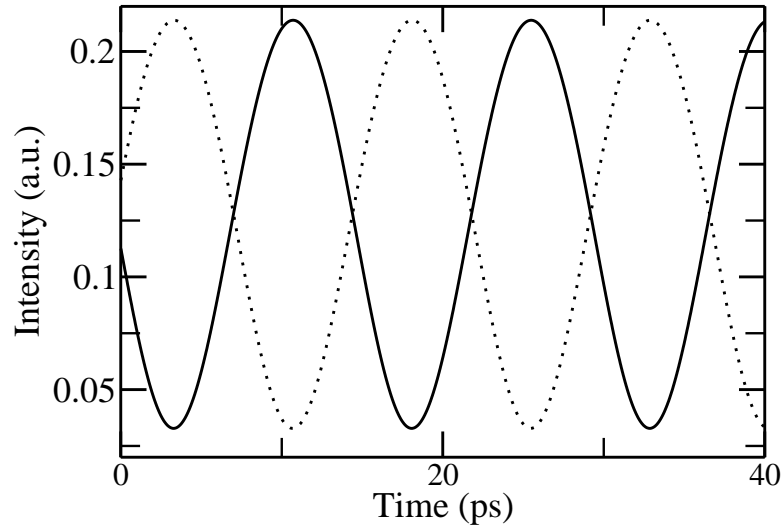
FIGURE 3.7: Transient at $A = 1.3$ $\gamma = 0.15$ $\alpha = 3$, $d = 0$
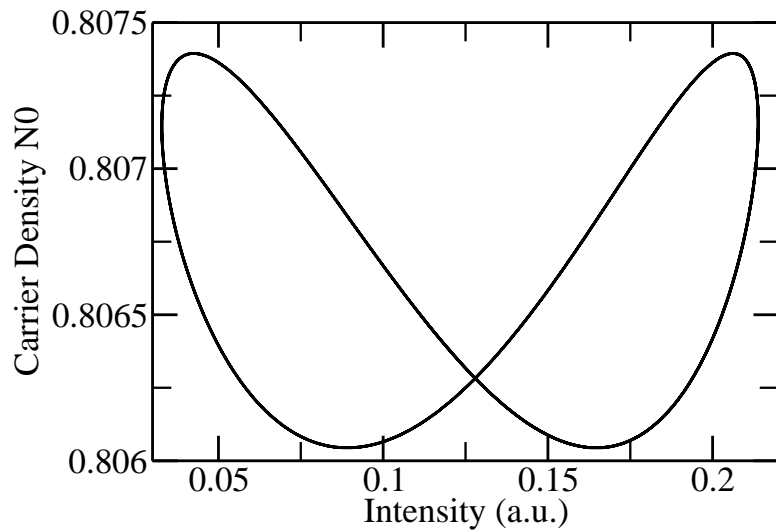
FIGURE 3.8: Phase portrait at $\gamma = 0.15$ $\alpha = 3$, $d = 0$

directions has been studied and its time constant has been characterised[30, 32]. To the best knowledge of the author, all of them neglected the effect of the carrier grating by assuming it washed out by strong diffusion in a very short time scale. In this section, a model with carrier density and diffusion is presented to study directional switching as an extension of the previous section.

To model real devices, a couple of amendments are applied to the model presented in the previous section. As mentioned in the previous section, the output coupling introduces backscattering between two counter-propagating modes. Therefore a complex term ρ is
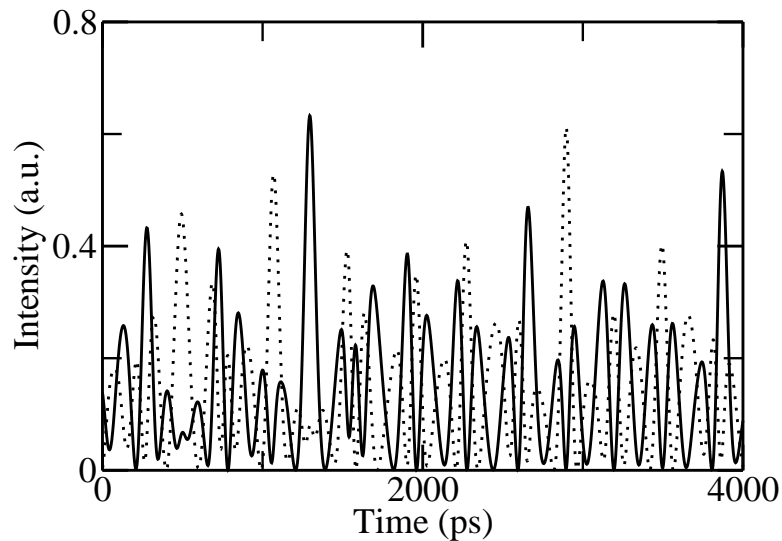
FIGURE 3.9: Transient at $A = 1.3$ $\gamma = 0.002$ $\alpha = 3$, $d = 0$

added into the original rate equations as in[98]. This qualitatively changes the bifurcation diagrams of Fig. 3.3 and Fig. 3.4 and introduces a new operation regime where bidirectional oscillation in modal power is observed, eg alternate oscillation [28, 98]. The conservative part ρ_c, eg. the imaginary part of ρ, and dissipative part ρ_d, eg. the real part of ρ, governs the bifurcation diagram in such way [19, 28], that ρ_c favours alternate oscillations while ρ_d favours CW operation. The values of ρ_c and ρ_d used in this chapter are listed later

The equations for N and N_2 are kept the same as in the previous section. The injection is coherently added into the field equation of f [137]. As symmetry exists between forward and backward propagating waves, it is assumed that the laser starts in forward lasing operation and a trigger pulse is injected into the backward direction. The pulse shape is not critical to the system response according to [32]. In this section, the injection is taken as a Gaussian pulse envelope.

Before discussing the results, the values to be used are listed here. As picosecond switching time is relevant, a small cavity size is used, say of radius 50μm, and the photon lifetime is 1ps. The carrier decay rate $\gamma_\parallel$ is 1ns^{-1}, the differential gain G is 2^{-19}m^2, and the thickness of quantum well w is set to 10nm. The confinement factor Γ is 0.2. α is 3. Normal diffusion coefficient is $D = 13.8\text{cm}^2\text{s}^{-1}$ which corresponds to $d = 60$ after normalisation. As the study here is focused on switching between uni-directional bistable states, a reasonably large diffusion will be adopted to make sure there is no bidirectional oscillatory operation just above threshold; $d = 120$ is used in this calculation

here.

The injection term is added to the right hand side of Eq (3.15) as [103, 137]

$$\frac{\partial F}{\partial t} = \frac{v_g G \Gamma}{2n_g^2}(1 - i\alpha)(\Delta N F + N_2 B) - \frac{F}{\tau_p} + \frac{1}{T_{trig}}\sqrt{\frac{E_{trig}}{\sqrt{2\pi}\sigma\varepsilon A v_g}}e^{-\frac{t^2}{4\sigma^2}} + \rho B \quad (3.109)$$

where E_{trig} is the energy of the Gaussian shaped trigger pulse with FWHM $2\sqrt{2\ln 2}\sigma$. T_{trig} is the coupling coefficient. A is the cross-section area of the active medium. After normalized by

$$f_{trig} = \frac{1}{\varepsilon_f}\sqrt{\frac{E_{trig}}{\sqrt{2\pi}\sigma\varepsilon A v_g}} \quad (3.110)$$

$$\tau_{trig} = \frac{T_{trig}}{\tau_p} \quad (3.111)$$

$$\sigma_{trig} = \frac{\sigma}{\tau_p} \quad (3.112)$$

$$\rho' = \rho\tau_p \quad (3.113)$$

the forward field equation reads

$$\frac{\partial f}{\partial \tau} = A(nf + n_2 b)(1 - i\alpha) - f + \frac{1}{\tau_{trig}}f_{trig}e^{-\frac{\tau^2}{\sigma_{trig}^2}} + \rho' b. \quad (3.114)$$

The time trace of a typical switching dynamics is shown in Fig. 3.10. The laser is working on a steady state at $1.5A_{th}$, where A_{th} is threshold current. A Gaussian pulse with 10 ps FWHM is injected into the nonlasing direction at $t = 0$. The switching is characterized by slow decay superimposed with a fast oscillation.

There are some arguments on the way to define switching time as during directional switching, the nonlasing mode experiences strong spikes right after the trigger pulse was injected and then; slowly settling down. Each of those dynamics has different time constants, sometime even with different orders of magnitude. The ring lasers discussed here are mainly for photonic networks or storage where fast switching dynamics is favourable. After the power of the nonlasing mode exceeds that of the lasing mode, switching is accomplished. Therefore the switching time is defined as the time between the nonlasing
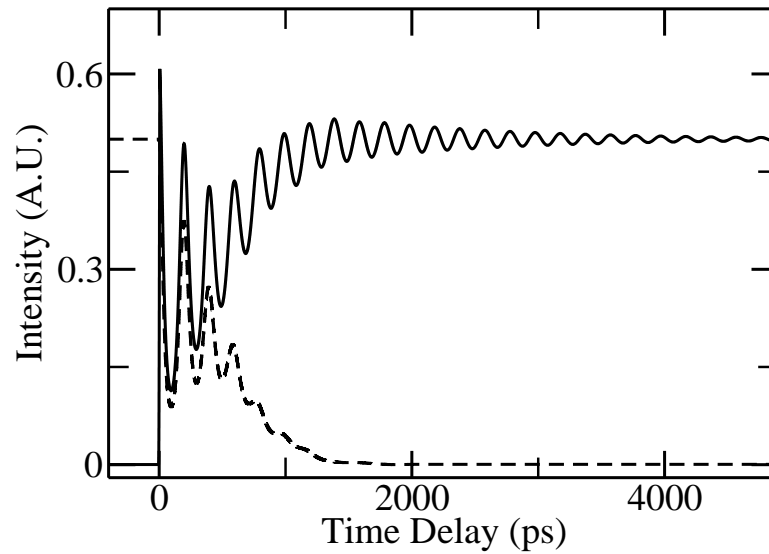
FIGURE 3.10: A typical time trace of switching dynamics. A Gaussian pulse is injected onto the nonlasing direction at $t = 0$. $A = 1.1$, $\gamma = 0.001$, $\alpha = 3$, $d = 120$. The dashed line and the solid line are intensities of light in the lasing and nonlasing direction before the trigger pulse comes in respectively.

mode's rise in power from 10% of steady state lasing power to 90% of it.

First the switching time's dependence on the injection current is studied. The trigger pulse is fixed to constant energy equal to 0.4% of energy stored inside cavity at $A = 1.5A_{th}$. The trigger pulsewidth is 10ps. Switching time increases almost linearly with current injection as shown in Fig. 3.11. This is explained as the uni-directional operation is more stable at higher injection current, or in another word, in a deeper potential well. To move it from one potential well to another takes longer time.

The trigger pulse plays an important role in the dynamics as a driving force for switching to take place. Therefore it is worth studying the switching dynamics as a function of various pulse parameters.

As shown in Fig. 3.12, the switching time decreases with higher trigger pulse energy or shorter pulsewidth for the trigger pulses with the same energy. This is understood as both shorter pulsewidth or higher pulse energy provides more power to trigger the switching, therefore the switching takes place in shorter time.

Even with the same amount of energy, the way energy is distributed inside the pulse profile is not trivial for the switching dynamics. As a consequence, the response of a
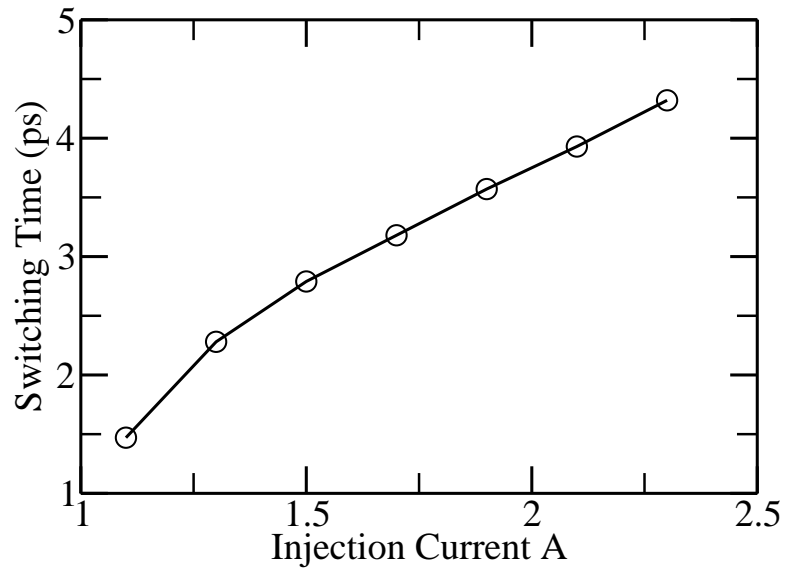
FIGURE 3.11: Switching time dependence on injection current. $\gamma = 0.001$, $\alpha = 3$, $d = 120$, injection pulse at 10 ps FWHM, $\tau_{trig} = 25$, $E_{inj} = 0.4\%$.
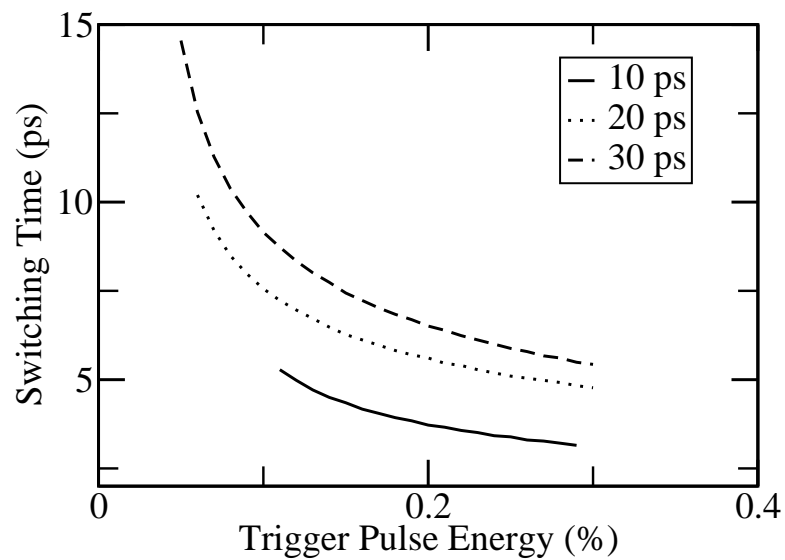
FIGURE 3.12: Switching time dependence on trigger pulse energy. $\gamma = 0.001$ $\alpha = 3$, $d = 120$, $A = 1.5$.
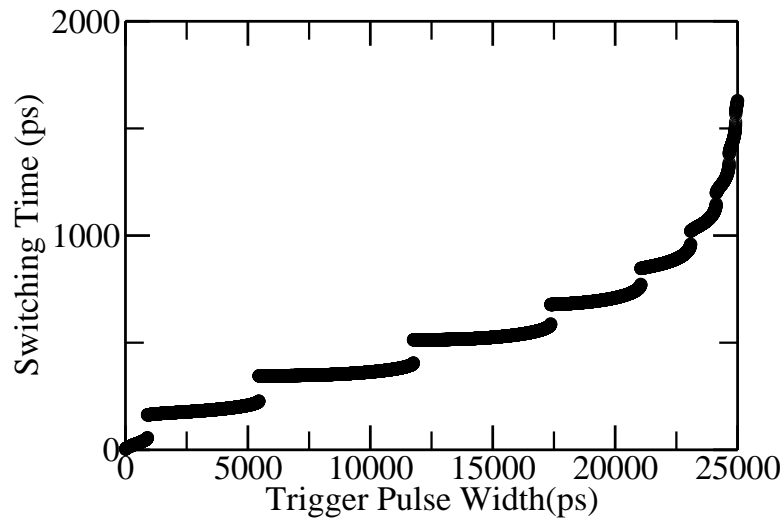
FIGURE 3.13: Switching time dependence on trigger pulse width $\gamma = 0.15\ \alpha = 3$, $d = 0$, $E_{inj} = 0.2\%$.
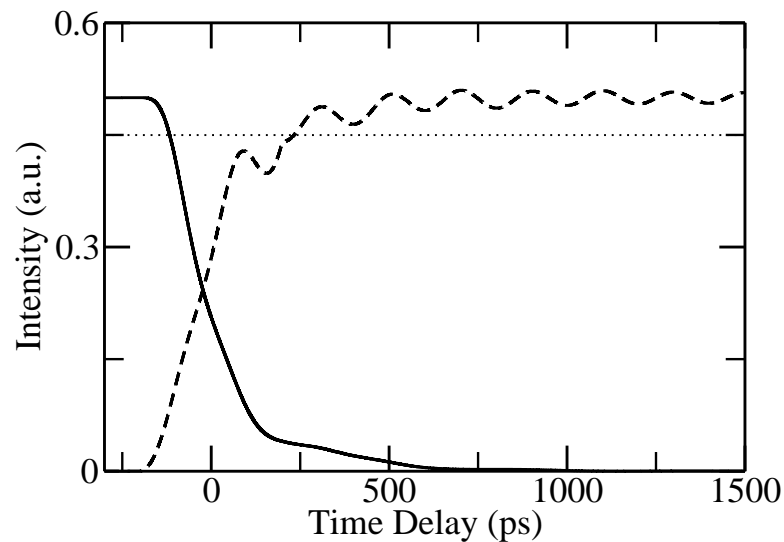
FIGURE 3.14: Transient with longer injection pulse $\gamma = 0.001\ \alpha = 3$, $d = 120$, $E_{inj} = 0.2\%$.

ring laser to Gaussian pulses with the same amount of energy but different pulsewidth has been studied as follows.

As shown in Fig. 3.13, the switching time increases with the pulsewidth of the trigger exponentially. With short trigger pulses, the injection power is strong enough to boost the first spike of nonlasing mode to 90% of steady state power as in Fig. 3.10. However, with longer trigger pulses, the energy is distributed within a longer time slot, therefore the injected power is not strong enough to bring the first spike above 90%, as in Fig. 3.14. The switching is finished in more than one relaxation oscillation period. For longer

trigger pulse, the nonlasing mode might wait for the 3rd or even the 4th spike to reach the 90% threshold. Therefore discontinuities are seen in Fig. 3.13.

3.7 Conclusion

The bi-directional single mode ring laser model has been presented in this chapter. The stability of the unidirectional and bidirectional CW operation has been studied and their boundaries are identified in term of carrier diffusion and current injection. The significance of the carrier diffusion on the dynamics are studied in this chapter. This results fit previous publications well [66, 132]. Lasing directional switching has also been studied in this chapter. Although the diffusion was widely neglected, it is included here. Directional switching and time dependence on parameters, especially those of optical injected Gaussian pulses have been studied.

Chapter 4

Four Mode Study

Two mode rate equation model as the one presented in the previous chapter has been widely used in identifying operation regimes[105, 106] and studying directional switching [30, 101]. However, issues such as wavelength switching are out of the scope of such model as only one frequency component is not enough to model the wavelength change. Recently, wavelength change accompanying directional switching is observed in [20]. To successfully model this phenomenon, more than one mode in each direction has to be considered in the model.

As an extension of the model in the previous chapter, a model with two modes in each direction is presented in this chapter. Both wavelength and directional switching are addressed. The multimode nature in each direction of this model provides the possibility to explain the experiment results.

4.1 Mathematical Formulation

The derivation starts from the carrier density and field part of the Maxwell-Bloch equation for the two level model. The polarization will be supplemented later.

In the RWA approximation, with detuning $\delta = (\omega_A - \omega_C)/\gamma_\perp$ and diffusion coefficient $D = \tilde{D}/\gamma_{||}$, one has

$$\partial_t E_\pm \pm v_g \partial_z E_\pm = P_\pm - \kappa E_\pm \tag{4.1}$$

$$\gamma_{||}^{-1} \partial_t N_0 = J - N_0 - D\frac{\partial^2}{\partial z^2} N_0 - \gamma_{||}^{-1} \left(P_+ E_+^* + E_+ P_+^* + P_- E_-^* + E_- P_-^* \right) \tag{4.2}$$

$$\gamma_{||}^{-1} \partial_t N_2 = -\left(1 + 4Dk_0^2\right) N_2 + 4ik_0 D \partial_z N_2 - D\frac{\partial^2}{\partial z^2} N_2$$
$$-\gamma_{||}^{-1} \left(P_+ E_-^* + E_+ P_-^* \right) \tag{4.3}$$

where $\gamma_{||}$ is the carrier decay rate and κ is the cavity loss. N_0 is the slow carrier density component in terms of spatial frequency. N_2 is the carrier density component with spatial period as short as $2k$.

In this chapter, two adjacent modes are considered in each direction. Therefore the field and corresponding polarisation can be written

$$E_\pm = E_\pm^{(1)} + E_\pm^{(2)} e^{\pm i\Delta kz - i\Delta\omega t} \tag{4.4}$$

$$P_\pm = P_\pm^{(1)} + P_\pm^{(2)} e^{\pm i\Delta kz - i\Delta\omega t} \tag{4.5}$$

where $\Delta k = \Delta\omega / v_g$. Both Δk and $\Delta\omega$ are small as compared to k_0, ω_C and they define the mode spacing.

4.1.1 Decomposition of Carrier Density

Although the carrier density is written as components with long and short spatial periodicity N_0 and N_2 respectively, each of them could be further decomposed to the slower terms in both space and time. Inserting Eq (4.4) and (4.5) in the carrier equations Eq (4.2) and (4.3), one finds that the interaction between the field and the medium gives rise to new sources that form dynamic gratings, and the carriers have to be expressed as

$$N_0 = N + \left(N_+ e^{i\Delta kz + i\Delta\omega t} + c.c. \right) + \left(N_- e^{i\Delta kz - i\Delta\omega t} + c.c. \right) \tag{4.6}$$

$$N_2 = G_1 + G_+ e^{i\Delta kz + i\Delta\omega t} + G_- e^{+i\Delta kz - i\Delta\omega t} + G_2 e^{2i\Delta kz}. \tag{4.7}$$

Substituting Eq (4.6) and (4.7) into Eq (4.2) and (4.3), the equations for all the components in Eq (4.4) and (4.5) are as the following

$$\gamma_{||}^{-1}\partial_t N = J - N - \gamma_{||}^{-1}\sum_{\pm,j}\left(P_{\pm}^{(j)}E_{\pm}^{(j)*} + c.c.\right) \tag{4.8}$$

$$\gamma_{||}^{-1}\partial_t N_+ + i\frac{\Delta\omega}{\gamma_{||}}N_+ = -\left[1 + D\left(\Delta k\right)^2\right]N_+ - \gamma_{||}^{-1}\left(P_-^{(2)*}E_-^{(1)} + E_-^{(2)*}P_-^{(1)}\right) \tag{4.9}$$

$$\gamma_{||}^{-1}\partial_t N_- - i\frac{\Delta\omega}{\gamma_{||}}N_- = -\left[1 + D\left(\Delta k\right)^2\right]N_- - \gamma_{||}^{-1}\left(P_+^{(1)*}E_+^{(2)} + E_+^{(1)*}P_+^{(2)}\right) \tag{4.10}$$

$$\gamma_{||}^{-1}\partial_t G_1 = -\left(1 + 4Dk_0^2\right)G_1 - \gamma_{||}^{-1}\left(P_-^{(1)*}E_+^{(1)} + E_-^{(1)*}P_+^{(1)}\right) \tag{4.11}$$

$$\gamma_{||}^{-1}\partial_t G_+ + i\frac{\Delta\omega}{\gamma_{||}}G_+ = -\left[1 + D\left(2k_0 + \Delta k\right)^2\right]G_+$$
$$\qquad\qquad -\gamma_{||}^{-1}\left(P_-^{(2)*}E_+^{(1)} + E_-^{(2)*}P_+^{(1)}\right) \tag{4.12}$$

$$\gamma_{||}^{-1}\partial_t G_- - i\frac{\Delta\omega}{\gamma_{||}}G_- = -\left[1 + D\left(2k_0 + \Delta k\right)^2\right]G_-$$
$$\qquad\qquad -\gamma_{||}^{-1}\left(P_-^{(1)*}E_+^{(2)} + E_-^{(1)*}P_+^{(2)}\right) \tag{4.13}$$

$$\gamma_{||}^{-1}\partial_t G_2 = -\left[1 + D\left(2k_0 + 2\Delta k\right)^2\right]G_2$$
$$\qquad\qquad -\gamma_{||}^{-1}\left(P_-^{(2)*}E_+^{(2)} + E_-^{(2)*}P_+^{(2)}\right). \tag{4.14}$$

To make the equation looks clean and tidy, forward and backward waves are named in different symbols to emphasize.

$$E_+^{(j)} = F_{(j)} \tag{4.15}$$
$$E_-^{(j)} = B_{(j)}. \tag{4.16}$$

By rearranging the above equations and moving all terms except derivatives to the right hand sides, the new set of equations is obtained

$$\gamma_{||}^{-1}\partial_t N = J - N - \gamma_{||}^{-1}\sum_{\pm,j}\left(P_\pm^{(j)}E_\pm^{(j)*} + c.c.\right) \tag{4.17}$$

$$\gamma_{||}^{-1}\partial_t N_+ = -\left[1 + D\left(\Delta k\right)^2 + i\frac{\Delta\omega}{\gamma_{||}}\right]N_+ - \gamma_{||}^{-1}\left(P_-^{(2)*}B_1 + B_2^*P_-^{(1)}\right) \tag{4.18}$$

$$\gamma_{||}^{-1}\partial_t N_- = -\left[1 + D\left(\Delta k\right)^2 - i\frac{\Delta\omega}{\gamma_{||}}\right]N_- - \gamma_{||}^{-1}\left(P_+^{(1)*}F_2 + F_1^*P_+^{(2)}\right) \tag{4.19}$$

$$\gamma_{||}^{-1}\partial_t G_1 = -\left(1 + 4Dk_0^2\right)G_1 - \gamma_{||}^{-1}\left(P_-^{(1)*}F_1 + B_1^*P_+^{(1)}\right) \tag{4.20}$$

$$\gamma_{||}^{-1}\partial_t G_+ = -\left[1 + D\left(2k_0 + \Delta k\right)^2 + i\frac{\Delta\omega}{\gamma_{||}}\right]G_+ - \gamma_{||}^{-1}\left(P_-^{(2)*}F_1 + B_2^*P_+^{(1)}\right) \tag{4.21}$$

$$\gamma_{||}^{-1}\partial_t G_- = -\left[1 + D\left(2k_0 + \Delta k\right)^2 - i\frac{\Delta\omega}{\gamma_{||}}\right]G_- - \gamma_{||}^{-1}\left(P_-^{(1)*}F_2 + B_1^*P_+^{(2)}\right) \tag{4.22}$$

$$\gamma_{||}^{-1}\partial_t G_2 = -\left[1 + D\left(2k_0 + 2\Delta k\right)^2\right]G_2 - \gamma_{||}^{-1}\left(P_-^{(2)*}F_2 + B_2^*P_+^{(2)}\right) \tag{4.23}$$

while the field equations are just that trivial

$$\partial_t F_j = P_+^{(j)} - \kappa F_j \tag{4.24}$$

$$\partial_t B_j = P_-^{(j)} - \kappa B_j \tag{4.25}$$

4.1.2 Polarization

The polarization is written here as suggested in Chapter 2

$$P_\pm = \tilde{\chi}E_\pm + \acute{\tilde{\chi}}N_{\pm 2}E_\mp \tag{4.26}$$

where

$$\chi E_\pm = \tilde{\chi}(\omega_0 + i\partial_t, N_0)E_\pm \tag{4.27}$$

$$\acute{\chi}E_\pm = \acute{\tilde{\chi}}E_\pm = \frac{\partial\chi}{\partial N}(\omega_0 + i\partial_t, N_0)E_\pm \tag{4.28}$$

$\tilde{\chi}$ and $\acute{\tilde{\chi}}$ here stand for the operator of gain and the modification of gain by grating terms. They act on the fields $E_\pm$ but not carrier densities $N_{\pm 2}$. χ and $\acute{\chi}$ are the corresponding values.

As with Balle's definitions in [95] and [94] with interchanging the meaning of real and imaginary part of the susceptibility here

$$P = E(\frac{\Lambda + 1}{2\Lambda}\chi - \frac{\Lambda - 1}{2\Lambda}\chi^*) + \acute{\chi}\Delta N E. \tag{4.29}$$

It has to be noted that, a factor of i differs between the susceptibility used here and that in [94, 95]. In this chapter, real and imaginary parts of susceptibility are defined corresponds to gain and refractive index while the definition is the opposite way round in the references cited. The same is applied to the definition of polarization.

By adding and subtraction χ to the above equation

$$P = \chi E + (\chi + \chi^*)\frac{1 - \Lambda}{2\Lambda}E + \acute{\chi}\Delta N E. \tag{4.30}$$

Here $\Lambda = \sqrt{1 + \varepsilon s_0 |E|^2}$. εs_0 is a small number representing the gain compression due to spectral hole burning. Its dominant effect is an almost frequency independent reduction of the gain[29, 95]. The terms on the right hand side of Eq (4.30) corresponding to linear gain, nonlinear gain and coupling of forward and backward modes respectively. By Taylor expansion of the nonlinear gain term of the above equation to its first order,

$$P = \chi E - \frac{1}{4}\varepsilon s_0(\chi + \chi^*)|E|^2 E + \acute{\chi}\Delta N E. \tag{4.31}$$

Nonlinear susceptibility is a third-order effect which corresponds to nonlinear gain saturation, from its negative sign. It is defined by

$$\chi_{NL} = -\frac{1}{4}\varepsilon s_0(\chi + \chi^*)|E|^2 = -\frac{1}{2}\varepsilon s_0\Re(\chi)|E|^2. \tag{4.32}$$

The third order property is confirmed in this equation (i.e. polarization is cubic in E).

Here the nonlinear gain saturation χ_{NL} is studied. The nonlinear polarization is written as

$$P^{NL} = \chi_{NL}E = P_+^{NL}e^{ikz} + P_-^{NL}e^{-ikz}. \tag{4.33}$$

By substituting Eq (4.32) into Eq (4.33) and using

$$E = Fe^{ikz} + B^{-ikz} \tag{4.34}$$

the " $+$ " and " $-$ " nonlinear polarization components are

$$P_+^{NL} = -\frac{1}{2}\Re(\chi)\varepsilon s(|F|^2 + 2|B|^2)E_+ \tag{4.35}$$

$$P_-^{NL} = -\frac{1}{2}\Re(\chi)\varepsilon s(|B|^2 + 2|F|^2)E_-. \tag{4.36}$$

The effect of self saturation is always a half of that of cross saturation. In the study here, there are two modes in each direction. By further taking this point and substituting Eq (4.4) and Eq (4.5) into the above equations, one has

$$P_{1,+}^{NL} = -\frac{1}{2}\varepsilon s\Re\left(\chi_1\right)\left(|F_1|^2 + 2|B_1|^2 + 2|F_2|^2 + 2|B_2|^2\right)F_1 = \chi_{1,+}^{NL}F_1 \tag{4.37}$$

$$P_{1,-}^{NL} = -\frac{1}{2}\varepsilon s\Re\left(\chi_1\right)\left(|B_1|^2 + 2|F_1|^2 + 2|F_2|^2 + 2|B_2|^2\right)B_1 = \chi_{1,-}^{NL}B_1 \tag{4.38}$$

$$P_{2,+}^{NL} = -\frac{1}{2}\varepsilon s\Re\left(\chi_2\right)\left(|F_2|^2 + 2|F_1|^2 + 2|B_1|^2 + 2|B_2|^2\right)F_2 = \chi_{2,+}^{NL}F_2 \tag{4.39}$$

$$P_{2,-}^{NL} = -\frac{1}{2}\varepsilon s\Re\left(\chi_2\right)\left(|B_2|^2 + 2|F_1|^2 + 2|F_2|^2 + 2|B_2|^2\right)B_2 = \chi_{2,-}^{NL}B_2. \tag{4.40}$$

Therefore the polarization can be written as the medium reaction to the optical field, both linearly and nonlinearly, plus the contribution from the carrier grating as follows

$$P_+^{(1)} = \left[\chi_1\left(N\right) + \chi_{1,+}^{NL}\right]F_1 + \acute{\chi}_1\left(G_1B_1 + N_-^*F_2 + G_+B_2\right) \tag{4.41}$$

$$P_-^{(1)} = \left[\chi_1\left(N\right) + \chi_{1,-}^{NL}\right]B_1 + \acute{\chi}_1\left(G_1^*F_1 + N_+B_2 + G_-^*F_2\right) \tag{4.42}$$

$$P_+^{(2)} = \left[\chi_2\left(N\right) + \chi_{2,+}^{NL}\right]F_2 + \acute{\chi}_2\left(G_2B_2 + N_-F_1 + G_-B_1\right) \tag{4.43}$$

$$P_-^{(2)} = \left[\chi_2\left(N\right) + \chi_{2,-}^{NL}\right]B_2 + \acute{\chi}_2\left(G_2^*F_2 + N_+^*B_1 + G_+^*F_1\right). \tag{4.44}$$

4.1.3 Scaling of the Equations

Before further analysis, the magnitudes of different quantities have to be studied. The following order estimates of the carrier and the photon lifetime are made

$$\kappa \sim 10^{11}\text{s}^{-1} \tag{4.45}$$

$$\gamma_{||} \sim 10^{9}\text{s}^{-1} \tag{4.46}$$

$$\tilde{D} \sim 10^{-3}\text{ms}^{-1} \tag{4.47}$$

An effective index of 3 and a device of diameter 333μm that operates at $\lambda = 1.55\mu$m are assumed. The optical cavity length is therefore 1mm. Thus

$$v_g = 10^{8}\text{ms}^{-1} \tag{4.48}$$

$$k_0 \sim 5 \times 10^{6}\text{m}^{-1} \tag{4.49}$$

$$\omega_0 \sim 5 \times 10^{14}\text{s}^{-1} \tag{4.50}$$

$$\Delta k \sim 6.28 \times 10^{3}\text{m}^{-1} \tag{4.51}$$

$$\Delta \omega \sim 6.28 \times 10^{11}\text{s}^{-1}. \tag{4.52}$$

All of the above values are typical for semiconductor ring lasers. Furthermore, the time constants in the rate equation of the components of carrier densities Eq (4.17)-(4.18) are

$$4\frac{\tilde{D}}{\gamma_{||}}k_0^2 \sim 10^{11}/10^9 \sim 100 \tag{4.53}$$

$$\frac{\tilde{D}}{\gamma_{||}}(\Delta k)^2 \sim 4 \times 10^4/10^9 \sim 4 \times 10^{-5} \tag{4.54}$$

$$\frac{\tilde{D}}{\gamma_{||}}k_0\Delta k \sim \pi \times 10^{-2} \tag{4.55}$$

$$\frac{\Delta \omega}{\gamma_{||}} \sim 6.28 \times 10^2. \tag{4.56}$$

Since $\tilde{D}(\Delta k)^2/\gamma_{||} \ll \Delta \omega/\gamma_{||}$ this term should be safely disregarded at some point.

For the later analysis, a time scale order is defined as the ratio of the two time scales by

$$T = \frac{\kappa}{\gamma_{||}}$$

$$\sim 10^2 \tag{4.57}$$

and a smallness parameter

$$
\begin{aligned}
\varepsilon &= T^{-1} \\
&\sim 10^{-2}
\end{aligned}
$$

(4.58)

The magnitudes of time constants in Eq (4.53)-(4.56) are

$$
\begin{aligned}
4Dk_0^2 &= dT \\
\frac{\Delta\omega}{\gamma_{||}} &= \mu T \\
d &\sim O(1) \\
\mu &\sim O(1) \\
\frac{\tilde{D}}{\gamma_{||}} k_0 \Delta k &\sim \varepsilon \\
\frac{\tilde{D}}{\gamma_{||}} (\Delta k)^2 &\sim \varepsilon^2.
\end{aligned}
$$

As the gratings are small, the corresponding terms are scaled as

$$
\begin{aligned}
N_\pm &= \varepsilon n_\pm \\
G_\pm &= \varepsilon g_\pm \\
G_{1,2} &= \varepsilon g_{1,2}.
\end{aligned}
$$

As a consequence, the polarisation is expressed as

$$
P_\pm^{(1,2)} = \left[\chi_{1,2}(N) + \chi_{1,2}^{NL}\right](F,B)_{1,2} + O(\varepsilon).
$$

(4.59)

The Eq (4.18) of the grating term with short spatial periodicity n_+ up to first order is

$$
\varepsilon \gamma_{||}^{-1} \partial_t n_+ = -(\varepsilon + i\mu) n_+ - \gamma_{||}^{-1}\left(P_-^{(2)*} B_1 + B_2^* P_-^{(1)}\right).
$$

(4.60)

Upon identification of the leading order terms it is found that

$$n_+ \;=\; -\frac{1}{i\mu}\gamma_{||}^{-1}\left[\chi_2^*\left(N\right)B_2^*B_1 + \chi_1\left(N\right)B_2^*B_1\right] + O\left(\varepsilon\right). \tag{4.61}$$

Then noticing that the gain difference is small and that the gratings are already evaluated at first order, one can safely neglect the gain curvature in the grating expression and get

$$n_+ \;\sim\; -\frac{2}{i\mu}\gamma_{||}^{-1}\left(B_1 B_2^*\right)\Re\left(\chi\right). \tag{4.62}$$

Using the same procedure for all the other gratings components in Eq (4.19)-(4.23), one has

$$n_+ \;=\; -\frac{2}{i\mu}\gamma_{||}^{-1}\left(B_1 B_2^*\right)\Re\left(\chi\right) \tag{4.63}$$

$$n_- \;=\; \frac{2}{i\mu}\gamma_{||}^{-1}\left(F_1^* F_2\right)\Re\left(\chi\right) \tag{4.64}$$

$$g_+ \;=\; -\frac{2}{d+i\mu}\gamma_{||}^{-1}\left(B_2^* F_1\right)\Re\left(\chi\right) \tag{4.65}$$

$$g_- \;=\; -\frac{2}{d-i\mu}\gamma_{||}^{-1}\left(B_1^* F_2\right)\Re\left(\chi\right) \tag{4.66}$$

$$g_1 \;=\; -\frac{2}{d}\gamma_{||}^{-1}\left(B_1^* F_1\right)\Re\left(\chi\right) \tag{4.67}$$

$$g_2 \;=\; -\frac{2}{d}\gamma_{||}^{-1}\left(B_2^* F_2\right)\Re\left(\chi\right). \tag{4.68}$$

The equation for the population inversion benefits only slightly from such simplification. The leading order in ε gives

$$\gamma_{||}^{-1}\partial_t N \;=\; J - N - \gamma_{||}^{-1}\sum_{\pm,j}\left[\chi_j\left(N\right)\left|E_\pm^{(j)}\right|^2 + \chi_j^*\left(N\right)\left|E_\pm^{(j)}\right|^2\right] \tag{4.69}$$

$$\sim\; J - N - \gamma_{||}^{-1}\sum_{\pm,j}\left(2\Re\left[\chi_j\left(N\right)\right]\left|E_\pm^{(j)}\right|^2\right) \tag{4.70}$$

$$\sim\; J - N - 2\gamma_{||}^{-1}\Re\left(\chi\left(N\right)\right)\left(\left|F_1\right|^2 + \left|B_1\right|^2 + \left|F_2\right|^2 + \left|B_2\right|^2\right). \tag{4.71}$$

By substituting Eq (4.63)-(4.68) into Eq (4.41)-(4.44), and then the field equations, the final form of the model reads

$$\partial_t F_1 = \left[\chi_1(N) + \chi_{1,+}^{NL} - \kappa_1\right] F_1$$
$$+ 2\varepsilon\gamma_{||}^{-1}\acute{\chi}_1(N)\,\Re(\chi)\left(-\frac{1}{d}|B_1|^2 + \frac{i}{\mu}|F_2|^2 - \frac{1}{d+i\mu}|B_2|^2\right) F_1 \quad (4.72)$$

$$\partial_t B_1 = \left[\chi_1(N) + \chi_{1,-}^{NL} - \kappa_1\right] B_1$$
$$+ 2\varepsilon\gamma_{||}^{-1}\acute{\chi}_1(N)\,\Re(\chi)\left(-\frac{1}{d}|F_1|^2 + \frac{i}{\mu}|B_2|^2 - \frac{1}{d+i\mu}|F_2|^2\right) B_1 \quad (4.73)$$

$$\partial_t F_2 = \left[\chi_2(N) + \chi_{2,+}^{NL} - \kappa_2\right] F_2$$
$$+ 2\varepsilon\gamma_{||}^{-1}\acute{\chi}_2(N)\,\Re(\chi)\left(-\frac{1}{d}|B_2|^2 - \frac{i}{\mu}|F_1|^2 - \frac{1}{d-i\mu}|B_1|^2\right) F_2 \quad (4.74)$$

$$\partial_t B_2 = \left[\chi_2(N) + \chi_{2,-}^{NL}\kappa_2\right] B_2$$
$$+ 2\varepsilon\gamma_{||}^{-1}\acute{\chi}_2(N)\,\Re(\chi)\left(-\frac{1}{d}|F_2|^2 - \frac{i}{\mu}|B_1|^2 - \frac{1}{d-i\mu}|F_1|^2\right) B_2 \quad (4.75)$$

$$\gamma_{||}^{-1}\partial_t N = J - N - 2\gamma_{||}^{-1}\Re(\chi(N))\left(|F_1|^2 + |B_1|^2 + |F_2|^2 + |B_2|^2\right). \quad (4.76)$$

Although the gain is asymmetric around its peak, within a small detuning, it is approximately parabolic in shape, which can be modelled by a Taylor expansion around its peak frequency to the second order,

$$\chi_1 = \chi(N) + \frac{\Delta\omega}{2}\frac{\partial\chi}{\partial\omega} + \left(\frac{\Delta\omega}{2}\right)^2\frac{\partial^2\chi}{\partial^2\omega}$$
$$\chi_2 = \chi(N) - \frac{\Delta\omega}{2}\frac{\partial\chi}{\partial\omega} + \left(\frac{\Delta\omega}{2}\right)^2\frac{\partial^2\chi}{\partial^2\omega},$$

where

$$\chi_{1,2}(N) = \chi_0(1 - i\alpha)N \quad (4.77)$$

and the carrier and frequency dependence of $\frac{\partial\chi}{\partial\omega}$, $\frac{\partial^2\chi}{\partial\omega^2}$ and $\acute{\chi}_{1,2}$ are neglected such that

$$\acute{\chi}_{1,2} \sim \acute{\chi}$$
$$= \chi_0(1 - i\alpha).$$

Substituting them into Eq (4.72)-(4.76) and scaling with

$$E_{new} = \sqrt{\frac{\chi_0}{\gamma_{||}}} E_{old}$$

one has

$$
\begin{aligned}
\partial_t F_1 &= (1 - i\alpha)\chi_0 N \left(1 - \frac{2\varepsilon}{d}|B_1|^2 + 2i\frac{\varepsilon}{\mu}|F_2|^2 - 2\varepsilon\frac{d - i\mu}{d^2 + \mu^2}|B_2|^2\right) F_1 \\
&\quad - \left[\chi_0\varepsilon(s|F_1|^2 + c|B_1|^2 + c|F_2|^2 + c|B_2|^2)N + (\kappa - \delta\kappa)\right] F_1 \quad\quad (4.78) \\
\partial_t B_1 &= (1 - i\alpha)\chi_0 N \left(1 - 2\frac{\varepsilon}{d}|F_1|^2 + 2i\frac{\varepsilon}{\mu}|B_2|^2 - 2\varepsilon\frac{d - i\mu}{d^2 + \mu^2}|F_2|^2\right) B_1 \\
&\quad - \left[\chi_0\varepsilon(s|B_1|^2 + c|F_1|^2 + c|F_2|^2 + c|B_2|^2)N + (\kappa - \delta\kappa)\right] B_1 \quad\quad (4.79) \\
\partial_t F_2 &= (1 - i\alpha)\chi_0 N \left(1 - 2\frac{\varepsilon}{d}|B_2|^2 - 2i\frac{\varepsilon}{\mu}|F_1|^2 - 2\varepsilon\frac{d + i\mu}{d^2 + \mu^2}|B_1|^2\right) F_2 \\
&\quad - \left[\chi_0\varepsilon(s|F_2|^2 + c|B_1|^2 + c|F_1|^2 + c|B_2|^2)N + (\kappa + \delta\kappa)\right] F_2 \quad\quad (4.80) \\
\partial_t B_2 &= (1 - i\alpha)\chi_0 N \left(1 - 2\frac{\varepsilon}{d}|F_2|^2 - 2i\frac{\varepsilon}{\mu}|B_1|^2 - 2\varepsilon\frac{d + i\mu}{d^2 + \mu^2}|F_1|^2\right) B_2 \\
&\quad - \left[\chi_0\varepsilon(s|B_2|^2 + c|F_1|^2 + c|B_1|^2 + c|F_2|^2)N + (\kappa + \delta\kappa)\right] B_2 \quad\quad (4.81) \\
\gamma_{||}^{-1}\partial_t N &= J - N - 2N\left(|F_1|^2 + |B_1|^2 + |F_2|^2 + |B_2|^2\right) \quad\quad\quad\quad\quad\quad (4.82)
\end{aligned}
$$

where $s = \frac{s_0\gamma_{||}}{\chi_0}$ is self-saturation. $c = 2s$ is the cross-saturation coefficient. An interplay between the shift of gain spectrum and losses happens when operation current is changed. $\kappa = (\kappa_2 + \kappa_1)/2$, $\delta\kappa = (\kappa_2 - \kappa_1)/2$ are the mean and difference of losses due to that effect. The linear coupling from the coupler reflections is neglected for the purpose of study the solo effect of gain material on the dynamics. In this case there is a nice phase invariance and it is desirable to write equations only for the intensities. Notice however that bidirectional solutions are either totally lost or in the best case very unlikely. Since the unidirectional regime is relevant here, this should not be a problem. Reducing the problem to the dynamics of the intensities only, one has

$$\partial_t I_1^+ = 2\left[\chi_0 N\left(1 - 2\frac{\varepsilon}{d}I_1^- + 2\varepsilon\frac{\alpha}{\mu}I_2^+ - 2\varepsilon\frac{d-\alpha\mu}{d^2+\mu^2}I_2^-\right) - (\kappa-\delta\kappa)\right]I_1^+$$
$$-2\varepsilon\chi_0 N\left[sI_1^+ + c\left(I_1^- + I_2^+ + I_2^-\right)\right]I_1^+ \tag{4.83}$$

$$\partial_t I_1^- = 2\left[\chi_0 N\left(1 - 2\frac{\varepsilon}{d}I_1^+ + 2\varepsilon\frac{\alpha}{\mu}I_2^- - 2\varepsilon\frac{d-\alpha\mu}{d^2+\mu^2}I_2^+\right) - (\kappa-\delta\kappa)\right]I_1^-$$
$$-2\varepsilon\chi_0 N\left[sI_1^- + c\left(I_1^+ + I_2^+ + I_2^-\right)\right]I_1^- \tag{4.84}$$

$$\partial_t I_2^+ = 2\left[\chi_0 N\left(1 - 2\frac{\varepsilon}{d}I_2^- - 2\varepsilon\frac{\alpha}{\mu}I_1^+ - 2\varepsilon\frac{d+\alpha\mu}{d^2+\mu^2}I_1^-\right) - (\kappa+\delta\kappa)\right]I_2^+$$
$$-2\varepsilon\chi_0 N\left[sI_2^+ + c\left(I_1^+ + I_1^- + I_2^-\right)\right]I_2^+ \tag{4.85}$$

$$\partial_t I_2^- = 2\left[\chi_0 N\left(1 - 2\frac{\varepsilon}{d}I_2^+ - 2\varepsilon\frac{\alpha}{\mu}I_1^- - 2\varepsilon\frac{d+\alpha\mu}{d^2+\mu^2}I_1^+\right) - (\kappa+\delta\kappa)\right]I_2^-$$
$$-2\varepsilon\chi_0 N\left[sI_2^- + c\left(I_1^+ + I_1^- + I_2^+\right)\right]I_2^- \tag{4.86}$$

$$\gamma_\parallel^{-1}\partial_t N = J - N - 2N\left(I_1^+ + I_1^- + I_2^+ + I_2^-\right). \tag{4.87}$$

It can be written in a compact way

$$\partial_t I_j^\pm = 2\left[\chi_0 N\left(1 - 2\frac{\varepsilon}{d}I_j^\mp - (-1)^j\,2\varepsilon\frac{\alpha}{\mu}I_{3-j}^\pm - 2\varepsilon\frac{d+(-1)^j\,\alpha\mu}{d^2+\mu^2}I_{3-j}^\mp\right) - (\kappa\mp\delta\kappa)\right]I_j^\pm$$
$$-2\chi_0\varepsilon\{sI_j^\pm + c(I_j^\mp + I_{3-j}^\pm + I_{3-j}^\mp)\}I_j^\pm \tag{4.88}$$

$$\gamma_\parallel^{-1}\partial_t N = J - N - 2N\left(I_1^+ + I_1^- + I_2^+ + I_2^-\right). \tag{4.89}$$

4.1.4 The Final Form of the Equations

In the case that $\chi_0 = \kappa$, which only amounts to redefining the transparency current, one gets

$$\partial_\sigma I_1^+ = 2\{N\left[1 - 2\varepsilon s I_1^+ - 2\varepsilon\left(\frac{1}{d}+c\right)I_1^- - 2\varepsilon\left(c-\frac{\alpha}{\mu}\right)I_2^+ - 2\varepsilon\left(c+\frac{d-\alpha\mu}{d^2+\mu^2}\right)I_2^-\right]$$
$$-\left(1 - \varepsilon\frac{\delta}{2}\right)\}I_1^+ \tag{4.90}$$

$$\partial_\sigma I_1^- = 2\{N\left[1 - 2\varepsilon s I_1^- - 2\varepsilon\left(\frac{1}{d}+c\right)I_1^+ - 2\varepsilon\left(c-\frac{\alpha}{\mu}\right)I_2^- - 2\varepsilon\left(c+\frac{d-\alpha\mu}{d^2+\mu^2}\right)I_2^+\right]$$
$$-\left(1 - \varepsilon\frac{\delta}{2}\right)\}I_1^- \tag{4.91}$$

$$\partial_\sigma I_2^+ = 2\{N\left[1 - 2\varepsilon s I_2^+ - 2\varepsilon\left(\frac{1}{d}+c\right)I_2^- - 2\varepsilon\left(c+\frac{\alpha}{\mu}\right)I_1^+ - 2\varepsilon\left(c+\frac{d+\alpha\mu}{d^2+\mu^2}\right)I_1^-\right]$$

$$-\left(1+\varepsilon\frac{\delta}{2}\right)\}I_2^+ \tag{4.92}$$

$$\partial_\sigma I_2^- = 2\{N\left[1-2\varepsilon s I_2^- - 2\varepsilon\left(\frac{1}{d}+c\right)I_2^+ - 2\varepsilon\left(c+\frac{\alpha}{\mu}\right)I_1^- - 2\varepsilon\left(c+\frac{d+\alpha\mu}{d^2+\mu^2}\right)I_1^+\right]$$

$$-\left(1+\varepsilon\frac{\delta}{2}\right)\}I_2^- \tag{4.93}$$

$$\frac{1}{\varepsilon}\partial_\sigma N = J - N - 2N\left(I_1^+ + I_1^- + I_2^+ + I_2^-\right). \tag{4.94}$$

The equation is normalised with the following definition

$$\delta = \frac{2\delta\kappa}{\varepsilon\kappa} \tag{4.95}$$

and scaled in time with respect to the photon lifetime $\sigma = \kappa t$.

Removing a factor of 2 by the scaling $I_{new} = 2I_{old}$ to make the equations look tidy

$$\partial_\sigma I_1^+ = 2\{N\left[1-\varepsilon s I_1^+ - \varepsilon\left(\frac{1}{d}+c\right)I_1^- - \varepsilon\left(2s-\frac{\alpha}{\mu}\right)I_2^+ - \varepsilon\left(c+\frac{d-\alpha\mu}{d^2+\mu^2}\right)I_2^-\right]$$

$$-\left(1-\varepsilon\frac{\delta}{2}\right)\}I_1^+$$

$$\partial_\sigma I_1^- = 2\{N\left[1-\varepsilon s I_1^- - \varepsilon\left(\frac{1}{d}+c\right)I_1^+ - \varepsilon\left(2s-\frac{\alpha}{\mu}\right)I_2^- - \varepsilon\left(c+\frac{d-\alpha\mu}{d^2+\mu^2}\right)I_2^+\right]$$

$$-\left(1-\varepsilon\frac{\delta}{2}\right)\}I_1^-$$

$$\partial_\sigma I_2^+ = 2\{N\left[1-\varepsilon s I_2^+ - \varepsilon\left(\frac{1}{d}+c\right)I_2^- - \varepsilon\left(2s+\frac{\alpha}{\mu}\right)I_1^+ - \varepsilon\left(c+\frac{d+\alpha\mu}{d^2+\mu^2}\right)I_1^-\right]$$

$$-\left(1+\varepsilon\frac{\delta}{2}\right)\}I_2^+$$

$$\partial_\sigma I_2^- = 2\{N\left[1-\varepsilon s I_2^- - \varepsilon\left(\frac{1}{d}+c\right)I_2^+ - \varepsilon\left(2s+\frac{\alpha}{\mu}\right)I_1^- - \varepsilon\left(c+\frac{d+\alpha\mu}{d^2+\mu^2}\right)I_1^+\right]$$

$$-\left(1+\varepsilon\frac{\delta}{2}\right)\}I_2^-$$

$$\frac{1}{\varepsilon}\partial_\sigma N = J - N\left(1+I_1^+ + I_1^- + I_2^+ + I_2^-\right).$$

This is the final form of the equations. In the following sections when analysis is performed on them, the sign of μ is fixed to be negative, which means that modes 2 are reds and 1 are blue. If δ is positive then 1 are stable and blue. Decreasing δ from positive to negative means that instability occurs from blue to red that is from 1 to 2.

4.2 Result and Discussion

4.2.1 Motion on the slow manifold

From this point only the slow time intermodal dynamics is considered. During the modal dynamics the carriers are always around the steady state which is in this case $N = 1$. A singular perturbation with the same smallness parameter is used, a perturbation of the carriers, scale parameters and go to the carrier time scale $\gamma_{||}$,

$$\varepsilon = \frac{1}{T} \tag{4.96}$$

$$N = 1 + \varepsilon n \tag{4.97}$$

$$P = J - 1 \tag{4.98}$$

$$\frac{\delta\kappa}{\kappa} = \varepsilon\delta \tag{4.99}$$

$$\tau = \gamma_{||} t \tag{4.100}$$

and one has

$$\partial_\tau I_j^\pm = 2\frac{1}{\varepsilon}[\varepsilon n - (1 + \varepsilon n)\left(2\frac{\varepsilon}{d}I_j^\mp + (-1)^j 2\varepsilon\frac{\alpha}{\mu}I_{3-j}^\pm + 2\varepsilon\frac{d + (-1)^j \alpha\mu}{d^2 + \mu^2}I_{3-j}^\mp\right)$$
$$-\varepsilon\frac{\delta}{2}]I_j^\pm \tag{4.101}$$

$$\varepsilon\partial_\tau n = P - \varepsilon n - 2(1 + \varepsilon n)\left(I_1^+ + I_1^- + I_2^+ + I_2^-\right) \tag{4.102}$$

which gives, after simplification where only terms at $O(\varepsilon)$ are retained in the field equation and use of the scaling $I_j^\pm \to I_j^\pm/2$,

$$\frac{1}{2}\partial_\tau I_1^+ = [n - sI_1^+ - (c + \frac{1}{d})I_1^- - (c - \frac{\alpha}{\mu})I_2^+ - (c - \frac{d - \alpha\mu}{d^2 + \mu^2})I_2^- + \frac{\delta}{2}]I_1^+ \tag{4.103}$$

$$\frac{1}{2}\partial_\tau I_1^- = [n - sI_1^- - (c + \frac{1}{d})I_1^+ - (c - \frac{\alpha}{\mu})I_2^- - (c - \frac{d - \alpha\mu}{d^2 + \mu^2})I_2^+ + \frac{\delta}{2}]I_1^- \tag{4.104}$$

$$\frac{1}{2}\partial_\tau I_2^+ = [n - sI_2^+ - (c + \frac{1}{d})I_2^- - (c + \frac{\alpha}{\mu})I_1^+ - (c + \frac{d + \alpha\mu}{d^2 + \mu^2})I_1^- - \frac{\delta}{2}]I_2^+ \tag{4.105}$$

$$\frac{1}{2}\partial_\tau I_2^- = [n - sI_2^- - (c + \frac{1}{d})I_2^+ - (c + \frac{\alpha}{\mu})I_1^- - (c + \frac{d + \alpha\mu}{d^2 + \mu^2})I_1^+ - \frac{\delta}{2}]I_2^- \tag{4.106}$$

$$\varepsilon\partial_\tau n = P - \varepsilon n - (1 + \varepsilon n)\left(I_1^+ + I_1^- + I_2^+ + I_2^-\right). \tag{4.107}$$

A singular perturbation is used here to simplify the above equations. This is done by noticing the smallness parameter ε in front of the left hand side of Eq (4.107). When $\varepsilon = 0$, the set of equations is singular with dramatic behaviour change from the original one as Eq (4.107) is no more a differential equation but an algebraical one, hence the system losses one degree of freedom. This could always be thought as simplifications arise by considering the motion on the slow manifold where the total intensity is almost a constant. In this scenario, relaxation oscillations are lost as they have a fast time scale. A degree of freedom is lost as the leading order in ε is singular. If one defines the incoherent total intensity as

$$S = I_1^+ + I_1^- + I_2^+ + I_2^- \tag{4.108}$$

$O(1)$ terms in the carrier equation give

$$0 = P - S \tag{4.109}$$

A very important result comes from this equation, which is that steady state single mode operation always has amplitude equal to P. It will be used in the following analysis. The equation for total intensity S is obtained by summing Eq (4.103)-(4.106) together

$$
\begin{aligned}
\frac{1}{2}\dot{S} &= nS - sS^2 - (c + \frac{2}{d})(I_1^+ I_1^- + I_2^+ I_2^-) - c(I_1^+ I_2^+ + I_1^- I_2^-) \\
&\quad - (c + \frac{2d}{d^2 + \mu^2})(I_1^+ I_2^- + I_1^- I_2^+) + \frac{\delta}{2}(I_1^+ + I_1^- - I_2^- - I_2^+).
\end{aligned} \tag{4.110}
$$

Since the conservation law $\dot{S} = 0$, the expression of n is

$$
\begin{aligned}
n &= sP + \frac{2(s + \frac{1}{d})}{P}(I_1^+ I_1^- + I_2^+ I_2^-) + \frac{2s}{P}(I_1^+ I_2^+ + I_1^- I_2^-) + \frac{2(s + \frac{d}{d^2 + \mu^2})}{P}(I_1^+ I_2^- + I_1^- I_2^+) \\
&\quad + \frac{\delta}{2P}(I_2^+ + I_2^- - I_1^+ - I_1^-).
\end{aligned} \tag{4.111}
$$

The stability of single mode operation is first studied in this section. As shown in Eq(4.109), the intensity of any mode of this operation is P as long as current is kept at the same level.

4.2.2   Linear Stability Analysis

The purpose of the model presented in this chapter is to explain the asymmetrical behaviour of laser wavelength switching accompanied by directional reversal. Although the experimental result is observed under continuous increasing or decreasing bias current[20], the gain spectrum shift due to Joule heating is seen as the driving force behind, and hence the origin of the asymmetrical dynamic behaviours.

As shown in Eq (4.103)-(4.107), inside the square brackets, intensities I_1^+ I_1^- I_2^+ I_2^- are multiplied by combinations of self-saturation, cross-saturation, diffusion and α in different order. Therefore, for each mode in the dynamics, contributions from other modes are not identical. This is seen as the source of asymmetrical dynamics observed during wavelenght switching.

Linear stability analysis is applied to the system. The idea is to assume that the laser starts on a certain frequency and to check the stability of the other frequency components, both forward and backward, on a continuous sweeping of δ, which simulates the gain curve thermal drift. At a certain point where wavelength shift occurs, the new lasing direction will be decided by the eigenvalues of the linearised perturbed system.

First, assume that the laser works on F_1 mode and its transition to mode 2 is studied. In this case, mode 1 experiences lower loss than mode 2 at the beginning, A downwards sweeping of δ is performed to model the lasing wavelength red shift. During the transition, the loss of mode 1 increases while that of mode 2 decrease. At a certain δ, both modes experience the same amount of loss. Then the loss of mode 1 exceeds that of mode 2.

The small perturbations made on F_2 and B_2 are δF_2 and δB_2. By substituting $I_1^+ = P$ and Eq (4.111) into Eq (4.105) and (4.106), one has

$$\begin{pmatrix} \dot{\delta I_2^+} \\ \dot{\delta I_2^-} \end{pmatrix} = 2 \begin{pmatrix} -Ps - \frac{\delta}{2} - P\frac{\alpha}{\mu} & 0 \\ 0 & -Ps - \frac{\delta}{2} - P\frac{d+\alpha\mu}{d^2+\mu^2} \end{pmatrix} \begin{pmatrix} \delta I_2^+ \\ \delta I_2^- \end{pmatrix}. \tag{4.112}$$

As the matrix in Eq (4.112) is diagonal, the eigenvalues, which denoted as λ_1 and λ_2, are just the diagonal elements

$$\lambda_1 = -Ps - \frac{\delta}{2} - P\frac{\alpha}{\mu} \qquad (4.113)$$

$$\lambda_2 = -Ps - \frac{\delta}{2} - P\frac{d + \alpha\mu}{d^2 + \mu^2}. \qquad (4.114)$$

As solution of diagonal matrix, the eigenvectors corresponding to λ_1 and λ_2 are $v_1 = \begin{pmatrix} 1 \\ 0 \end{pmatrix}$ and $v_2 = \begin{pmatrix} 0 \\ 1 \end{pmatrix}$ respectively. They correspond to single mode lasing in the F_2-direction and B_2 direction respectively in a Cartesian system based on F_2 and B_2, as displayed in Fig. 4.2.

In the case here, P is fixed at 1 by assuming the laser works at a moderate value above lasing threshold. Therefore the real parts of the eigenvalues are

$$\lambda_1 = -s - \frac{\delta}{2} - \frac{\alpha}{\mu} \qquad (4.115)$$

$$\lambda_2 = -s - \frac{\delta}{2} - \frac{d + \alpha\mu}{d^2 + \mu^2}. \qquad (4.116)$$

The eigenvalues as functions of δ are shown in the Fig 4.1 for typical operation parameters. The parameters used here are $\mu = 1$, $\alpha = 2$, $d = 1$, $s = 1$. λ_1 and λ_2 are plotted in black and red curves respectively. To make stable single mode lasing in the F_1 direction, δ has to be on the positive end of the diagram, where both λ_1 and λ_2 are negative. With decreasing δ, which simulates the red shift of the gain peak, λ_1 and λ_2 starts to approach 0. λ_1 reaches 0 at first at $\delta = 1$ and then is positive while λ_2 is still negative. Therefore, F_1 is not stable any more from that point after perturbation. The system evolves to the direction of the eigenvector corresponding to λ_1, eg v_1, which is the F_2 direction, exponentially at the rate corresponding to λ_1. No B_2 mode lasing as any perturbation will be damped out because of the negative eigenvalue corresponding to it. Moving δ downwards will make the real part of λ_2 become 0 and positive consequently at $\delta = -1$. However, this is irrelevant since λ_1 is already positive and the system has evolved to another state whose dynamics is not governed by the above matrix and eigenvalues in Fig. 4.1.

It could be seen that the equations for the case of B_1 to mode 2 switching can be obtained by exchanging δF_2 and δB_2 in Eq (4.112). Therefore the analysis of this scenario
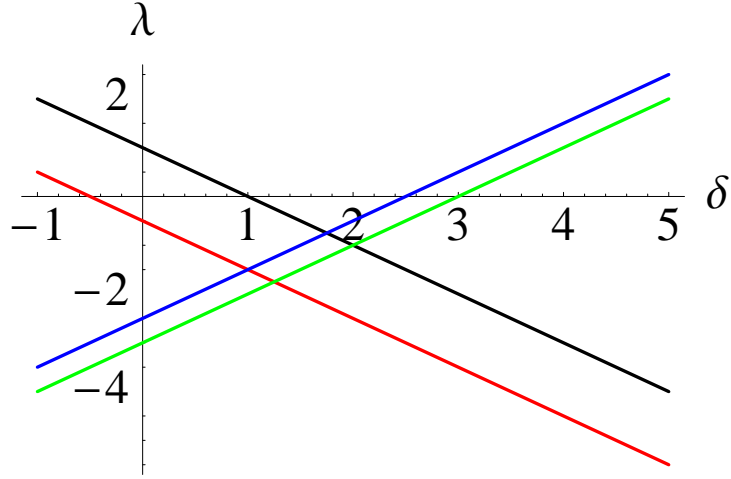
FIGURE 4.1: Real parts of eigenvalues at $\mu = -1$ $\alpha = 2$, $d = 1$, $P = 1$, $s = 1$. λ_1 to λ_4 are drawn in black, red, green and blue respectively. Bifurcation points are $\delta = 1$ and $\delta = 2.5$ for gain curve red shift and blue shift respectively.
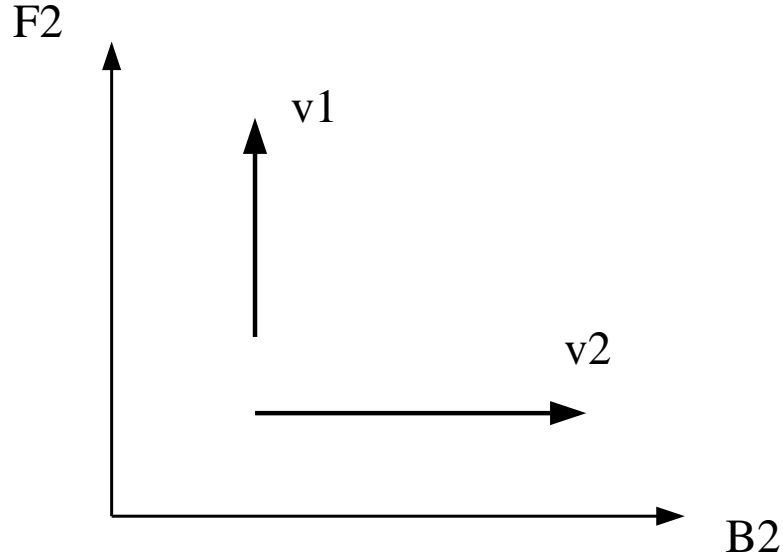
FIGURE 4.2: Schematic diagram of eigenvectors v_1 and v_2 in the scenario without backscattering

is the same as the one considered above. Thus the details will be neglected here.

Similarly, to study the directionality of the emission during wavelength switching from mode 2 to mode 1, it is assumed that the laser starts from F_2 and the relative stability of F_1 or B_1 after mode jump is studied. The matrix reads

$$\begin{pmatrix} \dot{\delta I_1^+} \\ \dot{\delta I_1^-} \end{pmatrix} = 2 \begin{pmatrix} -Ps + \frac{\delta}{2} + P\frac{\alpha}{\mu} & 0 \\ 0 & -Ps + \frac{\delta}{2} - P\frac{d-\alpha\mu}{d^2+\mu^2} \end{pmatrix} \begin{pmatrix} \delta I_1^+ \\ \delta I_1^- \end{pmatrix}. \tag{4.117}$$

The real parts of eigenvalues are

$$\lambda_3 = -Ps + \frac{\delta}{2} + P\frac{\alpha}{\mu} \tag{4.118}$$

$$\lambda_4 = -Ps + \frac{\delta}{2} - P\frac{d - \alpha\mu}{d^2 + \mu^2}, \tag{4.119}$$

and at $P = 1$ as in previous the analysis

$$\lambda_3 = -s + \frac{\delta}{2} + \frac{\alpha}{\mu} \tag{4.120}$$

$$\lambda_4 = -s + \frac{\delta}{2} - \frac{d - \alpha\mu}{d^2 + \mu^2}. \tag{4.121}$$

Similarly, the eigenvectors corresponding to λ_3 and λ_4 are $v_3 = \begin{pmatrix} 1 \\ 0 \end{pmatrix}$ and $v_4 = \begin{pmatrix} 0 \\ 1 \end{pmatrix}$ respectively. They correspond to F_1 and B_1 respectively.

The λ_3 and λ_4 as a function of δ are plotted as green and blue curves in Fig. 4.1. λ_4 reaches positive earlier than λ_3 when δ is increased from negative value. This corresponds to a F_2 to B_1 hop.

To summarize, the model predicts blue shift in the lasing direction while the directions remain stable during red shift. This is exactly opposite to the experimental observation[20]. Therefore a modification of the current model is needed to resolve this contradiction. Before further analysis, a more careful look at the Equations of λs Eq (4.115)(4.116)(4.120)(4.121) is conducted to gain better understanding of the model.

First, as stated above, the first one between λ_1 and λ_2 that changes its sign from negative to positive during the downwards sweeping of δ determines whether or not a red shift of lasing wavelength is accompanied by directional switching. By looking at Eq (4.115)(4.116), it is found that λ_1 and λ_2 are degenerate at $d = 0$. In this case, no efficient dissipation of the carrier grating is provided. After bifurcation, a persistent standing wave pattern on carrier density is formed and bi-directional operation is obtained. Thus transition from a single mode unidirectional operation to a bi-directional operation is possible by varying δ when there is no carrier diffusion. The same happens for a gain blue shift.

When diffusion is not negligible, it can be worked out from Eq (4.115) and (4.116) that λ_1 is always larger than λ_2 for reasonable lasing parameters, therefore λ_1 always reaches positive first, hence F_1 to F_2 switching. A schematic diagram of relative stabilities of the phase space is drawn in Fig 4.3. Solid lines and dotted lines are stable and unstable states respectively. Both F_1 to F_2 and F_1 to B_2 transitions are possible with downward sweeping δ. However, as the route of former one comes early than the latter, one always expects a F_1 to F_2 transition.

The same approach is applied to the mode 2 to mode 1 switching where it can be proven that λ_4 is always larger than λ_3 from Eq (4.120) and (4.121). It is always a directional flip accompanied by wavelength switching. Therefore, it is always true from this model that the gain curve blue shift is accompanied by directional switching while no such switching occurs for gain spectrum red shift which is exactly opposite to the experiment results. This contradiction is handled in the next section.

The effect of the the linewidth enhancement factor α, which contributes the asymmetry to the gain profile by moving the lasing mode to the blue side, is now discussed here.

When $\alpha = 0$, the laser is not a semiconductor one any longer and the gain spectrum is symmetrical, more appropriate to solid state lasers and gas lasers, rather than quantum well semiconductor lasers. This symmetry has an important implementation. The λ_1 is still relevant to red shift while, unlike the case when $\alpha \neq 0$, λ_3 starts to be relevant to blue shift, thus no directional flip accompanies wavelength shift whether it is a red one or a blue one. λ_1 and λ_3 dependence on δ is displayed in Fig 4.4. The value of δ for λ_1 and λ_3 equal to 0 is symmetrical with respect to the origin. Therefore, there is no difference between the blue shift and the red shift in terms of dynamics as both are without reversal and happen at $\delta = 0$.

The existence of saturation in the system brings bistable states. In Fig 4.5, F_1 is stable for $\delta < 1$ while F_2 is stable for $\delta > -1$. In the region in between where $-1 < \delta < 1$, both F_1 and F_2 could be stable. The lasing direction is determined by the laser's previous state. In other words, a hysteresis exists in this region. A schematic diagram is seen in Fig 4.3 to illustrate this situation.

By letting $s = 0$, both dominant eigenvalues λ_1 and λ_3 change sign at $\delta = 0$. No bistable states and consequence hysteresis occur in this scenario. Wavelength hopping happens
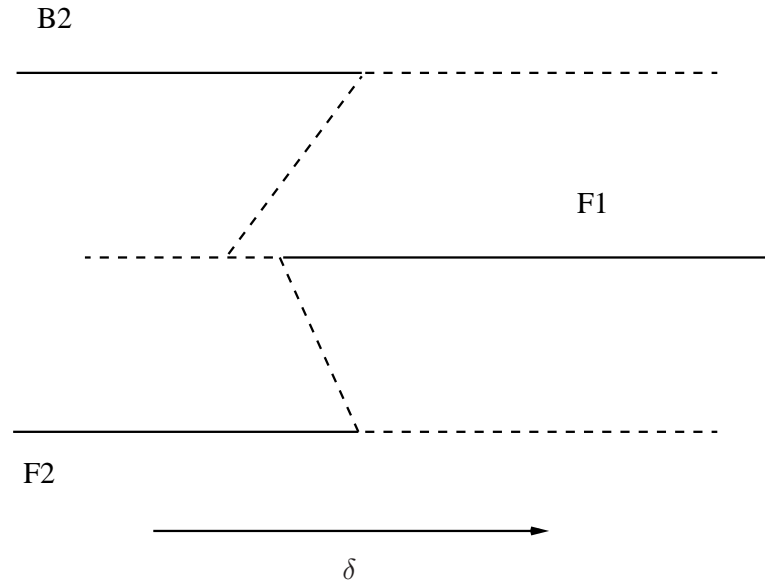
FIGURE 4.3: Schematic diagram of the stabilities of F_1 B_1 and F_2 single mode lasing states. Solid lines and dotted lines illustrate stable and unstable states respectively
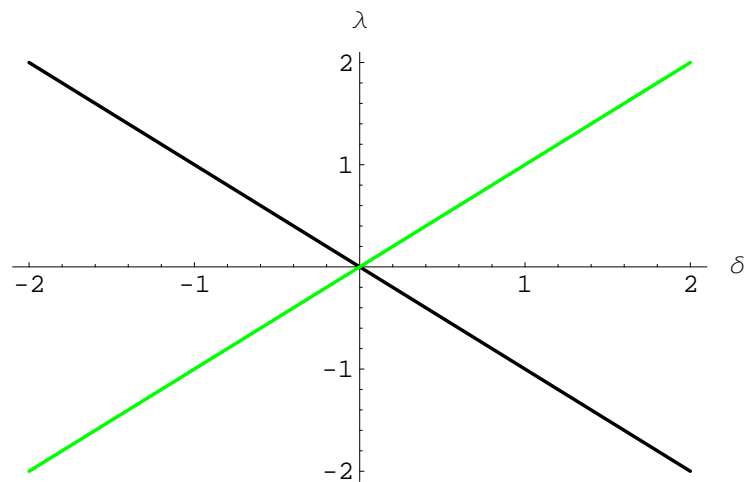
FIGURE 4.4: Typical eigenvalues dependence on δ in the case without α and s. $\mu = -1$, $d = 1$, $P = 1$. Black and green correspond to λ_1 and λ_3 respectively. The bifurcation of upwards and downward sweeping occurs at the same point $\delta = 0$

as long as a nonlasing mode starts to have larger gain than the lasing one does.

The above can be proved by a bifurcation curve produced by numerically solving Eq (4.103)-(4.107)

Fig 4.6 and 4.7 show the bifurcation of a lasing mode with respect to gain curve shift δ. Fig 4.6 is for δ sweeping from positive to negative while Fig 4.7 is for the opposite sweeping. The Eq (4.103)-(4.107) are numerically solved for steady state values at a certain δ. Then for a new δ which is a little smaller (larger) than the previous one, the steady state solutions with a small random perturbation is fed to the equations as initial
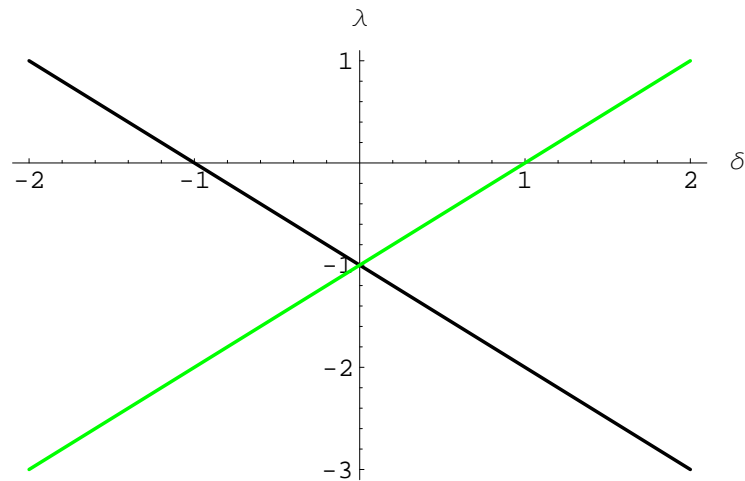
FIGURE 4.5: Typical eigenvalues dependence on δ in the case without α but with s. $\mu = -1$, $d = 1$, $P = 1$, $s = 1$. Black and green correspond to λ_1 and λ_3 respectively. The bifurcation of upwards and downward sweeping occurs symmetrically with the respect of the origin.
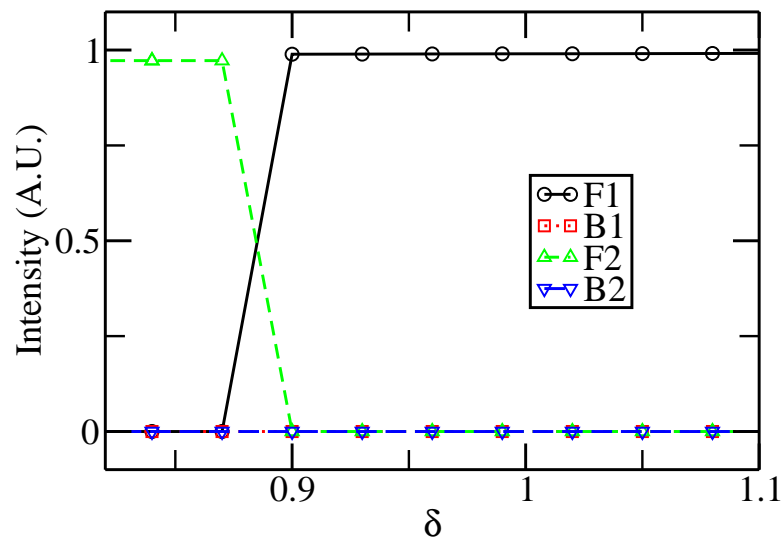
FIGURE 4.6: Bifurcation curve by sweeping δ downwards. $\mu = -1$, $\alpha = 2$, $d = 1$, $P = 1$, $s = 1$. Bifurcation happens at $\delta = 0.9$. F_1 to F_2 switching is obtained.

conditions. The new steady state is obtained and used as the initial condition for the next iteration. Both the bifurcation point and the switching scenario correspond to the result obtained from the linear stability analysis, eg the switching is exactly opposite to the experimental results. Therefore a further amendment is made.
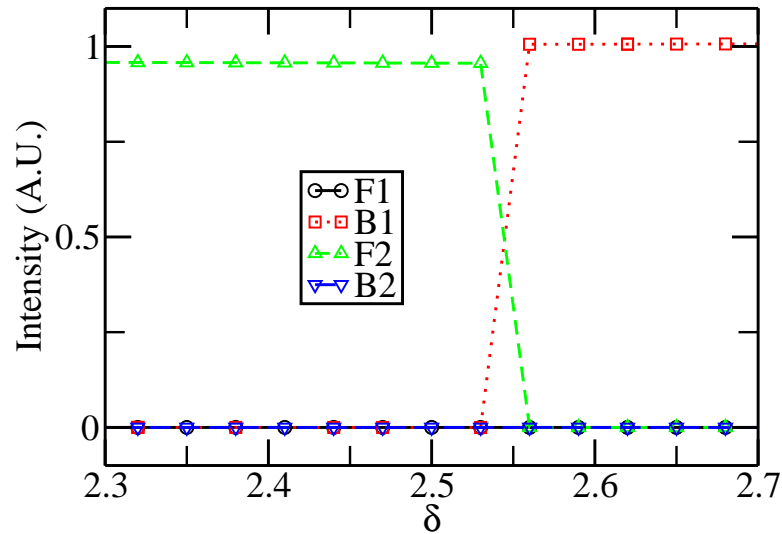
FIGURE 4.7: Bifurcation curve by sweeping δ upwards. $\mu = -1$, $\alpha = 2$, $d = 1$, $P = 1$, $s = 1$. Bifurcation happens at $\delta = 2.53$. F_2 to B_1 switching is obtained.

4.3 Effect of Backscattering

Neglecting the backscattering from the output coupler and the facets of the output waveguide might be misleading, as such an approach in the previous section produces results opposite to those observed in experiments. By adding backscattering terms, the matrix is qualitatively changed from diagonal to nondiagonal. In this section, such a modification is made in an attempt to reproduce results which fit experiments. To what extent the modified model works in the experiment is also studied

As a coherent effect, backscattering can not be added easily to rate equations of intensities used in the previous section. Therefore equations Eq (4.78)-(4.82) with normalization as performed in the previous section are used as a starting point

$$
\begin{aligned}
\partial_t F_1 &= (1 - i\alpha) \left\{ N \left[1 - \varepsilon \frac{1}{d} |B_1|^2 + \varepsilon \frac{i}{\mu} |F_2|^2 - \varepsilon \left(\frac{d - i\mu}{d^2 + \mu^2} \right) |B_2|^2 \right] - \left(1 - \varepsilon \frac{\delta}{2} \right) \right\} F_1 \\
&\quad + \varepsilon \rho_F e^{i\theta_1} B_1 - N\varepsilon s(|F_1|^2 + 2|B_1|^2 + 2|F_2|^2 + 2|B_2|^2)F_1 + R_{sp} \qquad (4.122) \\
\partial_t B_1 &= (1 - i\alpha) \left\{ N \left[1 - \varepsilon \frac{1}{d} |F_1|^2 + \varepsilon \frac{i}{\mu} |B_2|^2 - \varepsilon \frac{d - i\mu}{d^2 + \mu^2} |F_2|^2 \right] - \left(1 - \varepsilon \frac{\delta}{2} \right) \right\} B_1 \\
&\quad + \varepsilon \rho_B e^{i\theta_1} F_1 - N\varepsilon s(|B_1|^2 + 2|F_1|^2 + 2|F_2|^2 + 2|B_2|^2)B_1 + R_{sp} \qquad (4.123) \\
\partial_t F_2 &= (1 - i\alpha) \left\{ N \left[1 - \varepsilon \frac{1}{d} |B_2|^2 - \varepsilon \frac{i}{\mu} |F_1|^2 - \varepsilon \frac{d + i\mu}{d^2 + \mu^2} |B_1|^2 \right] - \left(1 + \varepsilon \frac{\delta}{2} \right) \right\} F_2 \\
&\quad + \varepsilon \rho_F e^{i\theta_2} B_2 - N\varepsilon s(|F_2|^2 + 2|F_1|^2 + 2|B_1|^2 + 2|B_2|^2)F_2 + R_{sp} \qquad (4.124) \\
\partial_t B_2 &= (1 - i\alpha) \left\{ N \left[1 - \varepsilon \frac{1}{d} |F_2|^2 - \varepsilon i \frac{1}{\mu} |B_1|^2 - \varepsilon \frac{d + i\mu}{d^2 + \mu^2} |F_1|^2 \right] - \left(1 + \varepsilon \frac{\delta}{2} \right) \right\} B_2 \\
&\quad \varepsilon \rho_B e^{i\theta_2} F_2 - N\varepsilon s(|B_2|^2 + 2|F_1|^2 + 2|B_1|^2 + 2|F_2|^2)B_2 + R_{sp} \qquad (4.125) \\
\frac{1}{\varepsilon} \partial_t N &= J - N - N \left(|F_1|^2 + |B_1|^2 + |F_2|^2 + |B_2|^2 \right). \qquad (4.126)
\end{aligned}
$$

The reflection coefficient and phase shift are denoted by ρ and θ in the above equations. R_{sp} is a Gaussian profiled noise to represent spontaneous emission. Its usage is discussed later.

4.3.1 Linear Stability Analysis

As in the previous study when backscattering is not considered, the linear stability analysis is performed at the beginning. The steady state solutions of carrier density and photon density of the model without backscattering are used as it is believed that their introduction influences coherent effects more seriously than particle densities.

First, the possibility of directional switching when the gain curve thermally drifts to red is studied. It is assumed that the laser starts on the F_1 mode. The steady state solution is

$$
|F_{10}|^2 = \frac{2J - 2 + \varepsilon\delta}{2 + 2\varepsilon s J + \varepsilon\delta} \qquad (4.127)
$$

$$
N_0 = \frac{2 + 2\varepsilon s J - \varepsilon\delta}{2 + 2\varepsilon s}. \qquad (4.128)
$$

Let $P_0 = J - 1$; the linear perturbations δF_2 and δB_2 applied to F_2 and B_2 obey
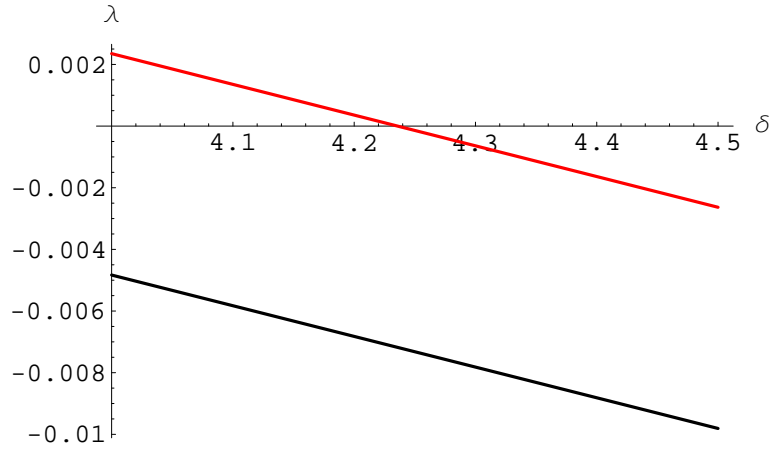
FIGURE 4.8: Real part of eigenvalues λ with gain red curve shift δ at $\mu = -1$, $\alpha = 2$, $d = 0.3$, $J = 6$, $s = 1$, $\theta_2 = 1.4$, $\rho_F = 4$, $\rho_B = 4$. Black and red curves are λ_1 and λ_2 respectively. The switching occurs at $\delta = 4.25$

$$\begin{pmatrix} \delta \dot{F}_2 \\ \delta \dot{B}_2 \end{pmatrix} = \begin{pmatrix} L_{11} & L_{12} \\ L_{21} & L_{22} \end{pmatrix} \begin{pmatrix} \delta F_2 \\ \delta B_2 \end{pmatrix} \tag{4.129}$$

where elements of the transformation matrix are

$$L_{11} = (1 - i\alpha)N_0\left(1 - \varepsilon\frac{i}{\mu}P_0\right) - (1 + \varepsilon\frac{\delta}{2}) - \varepsilon c N_0 P_0 \tag{4.130}$$

$$L_{12} = \varepsilon\rho_F e^{\theta_2} \tag{4.131}$$

$$L_{21} = \varepsilon\rho_B e^{\theta_1} \tag{4.132}$$

$$L_{22} = (1 - i\alpha)N_0\left(1 - \varepsilon\frac{1}{d - i\mu}P_0\right) - (1 + \varepsilon\frac{\delta}{2}) - \varepsilon c N_0 P_0. \tag{4.133}$$

The eigenvalues' dependence on δ during a gain curve red shift is plotted in Fig. 4.8. λ_1 and λ_2 are plotted in black and red respectively. As λ_2 reaches positive before λ_1 does at $\delta = 4.25$ on the way of decreasing δ, the onset of the lasing mode switching follows the direction of the corresponding eigenvector v_2 with the rate of λ_2. Unlike the eigenvectors of the matrix without backscattering, the eigenvectors here point to neither pure F_2 nor B_2 direction but to a combination of the both. Therefore it is the relation between the F_2 and the B_2 components of v_2 that determines the direction of lasing after a lasing mode red shift. A schematic diagram is drawn to show this situation in Fig. 4.9. The dotted line is exactly at 45° from B_2 and F_2 axis. Drawing eigenvectors from the origin, those eigenvectors below the dotted line have a larger B_2 component, therefore a tendency to the B_2 direction, while those above the dotted line have an F_2
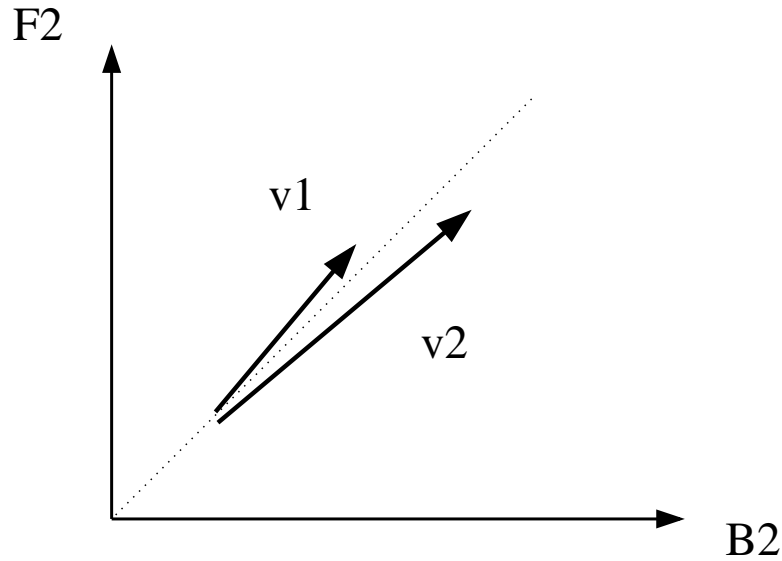
FIGURE 4.9: Schematic diagram of the direction of eigenvectors v_1 and v_2 in the case with backscattering. Both v_1 and v_2 are not pointing to pure F_2 or B_2 direction but with an angle

tendency.

The task now is to find if the eigenvector v_2 sits above the dotted line or fall below it. Both ρ_F and ρ_B are set to have the same value ρ. The study shows that the relative of values of B_2 and F_2 components are functions of ρ and θ. To make sure that the switching has a tendency of F_1 to B_2, proper parameters have to be selected carefully. In Fig.4.10 the direction of the eigenvector v_2 as a function of θ_2 with a period of 2π is plotted at the bifurcation point $\delta = 4.3$. The ratio of the 2 directional components $\frac{B_2}{F_2}$ is smaller than 1 for most of the θ_2. This means v_2 is prone to F_2 direction at most of the time. However it is the small region of $0.97 < \theta_2 < 1.6$ that gives a desirable result, e.g. a more B_2 oriented eigenvector in this case.

The corresponding $\frac{B_2}{F_2}$ dependence on the reflection from the coupler ρ at $\delta = 4.3$ is plotted in Fig. 4.11. ρ_2 has to be larger than 3 to achieve red shift with right directionality selection.

The case of directional switching during a gain curve blue shift is studied in the same way. It is assumed that the laser starts from F_2. The steady state solution used are
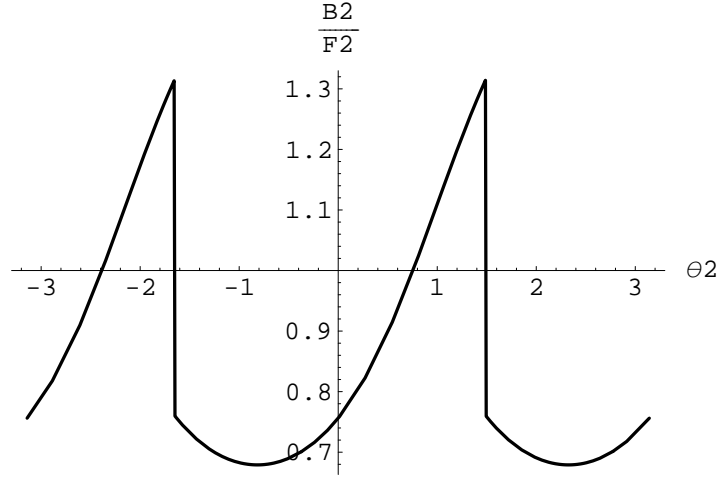
FIGURE 4.10: The direction of v_2 measured by the ratio of its 2 components $\frac{B_2}{F_2}$ dependence on δ. $\mu = -1$, $\alpha = 2$, $d = 0.3$, $s = 1$, $J = 6$, $\rho = 4$, $\delta = 4.3$
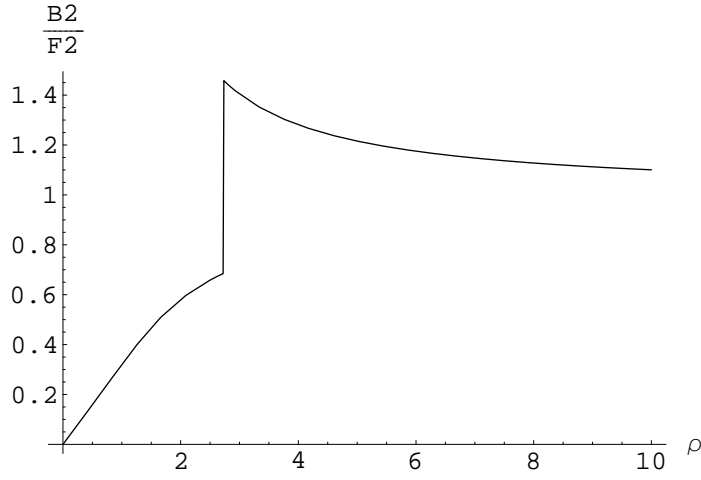
FIGURE 4.11: The dependence of $\frac{B_2}{F_2}$ on ρ. $\mu = -1$, $\alpha = 2$, $d = 0.3$, $s = 1$, $J = 6$, $\theta_2 = 1.4$, $\delta = 4.3$

$$|F_{20}|^2 = \frac{2J - 2 - \varepsilon\delta}{2 - 2\varepsilon\delta + 2\varepsilon sJ} \tag{4.134}$$

$$N_0 = \frac{2 + \varepsilon\delta + 2\varepsilon sJ}{2 + 2\varepsilon s}. \tag{4.135}$$

The similar linear perturbation on the system follows

$$\begin{pmatrix} \delta\dot{F}_1 \\ \delta\dot{B}_1 \end{pmatrix} = \begin{pmatrix} L_{11} & L_{12} \\ L21 & L_{22} \end{pmatrix} \begin{pmatrix} \delta F_1 \\ \delta B_1 \end{pmatrix} \tag{4.136}$$

where the elements of the transformation matrix are
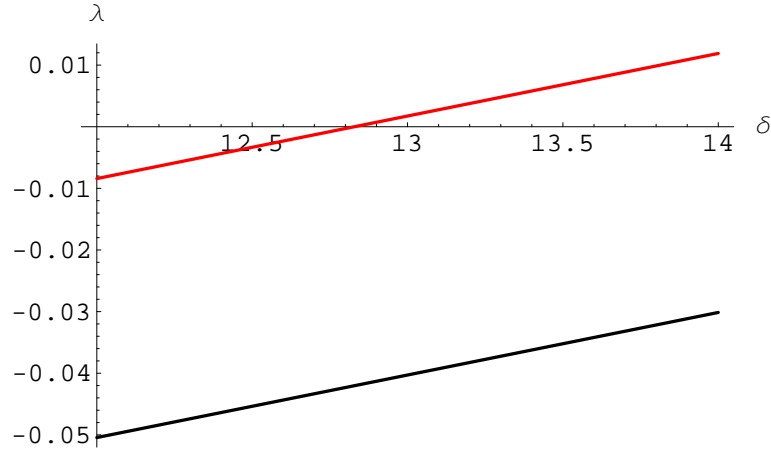
FIGURE 4.12: Real part of eigenvalues λ with gain curve blue shift δ at $\mu = -1$ $\alpha = 2$, $d = 0.3$, $J = 6$, $s = 1$, $\theta_1 = -1$, $\rho = 4$. Switching occurs at $\delta = 12.8$. Black and red curve are λ_3 and λ_4 respectively
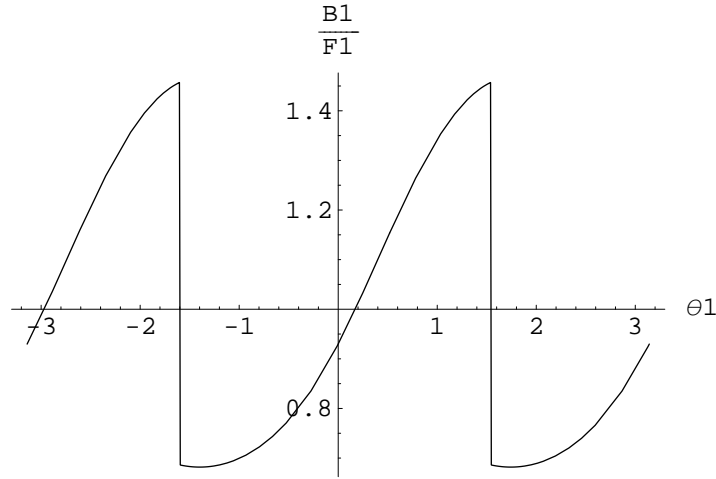
FIGURE 4.13: The direction of v_2 measured by the ratio of its 2 components $\frac{B_1}{F_1}$ dependence on δ. $\mu = -1$, $\alpha = 2$, $d = 0.3$, $s = 1$, $J = 6$, $\rho = 4$, $\delta = 12.8$

$$L_{11} = (1 - i\alpha)N_0 \left(1 + \varepsilon \frac{i}{\mu} P_0\right) - \left(1 - \varepsilon \frac{\delta}{2}\right) - \varepsilon c N_0 P_0 \tag{4.137}$$

$$L_{12} = \varepsilon \rho_F e^{\theta_1} \tag{4.138}$$

$$L_{21} = \varepsilon \rho_B e^{\theta_1} \tag{4.139}$$

$$L_{22} = (1 - i\alpha)N_0 \left(1 - \varepsilon \frac{1}{d - i\mu} P_0\right) - (1 - \varepsilon \frac{\delta}{2}) - \varepsilon c N_0 P_0. \tag{4.140}$$

The figure of the real parts of the eigenvalues λ_3 and λ_4 versus on δ is shown in Fig. 4.12. λ_3 and λ_4 are drawn in black and red curves respectively. From this figure, lasing mode switching at $\delta = 12.8$ follows the direction of v_4. Fig. 4.13 and 4.14 are $\frac{B_1}{F_1}$ of v_4 as
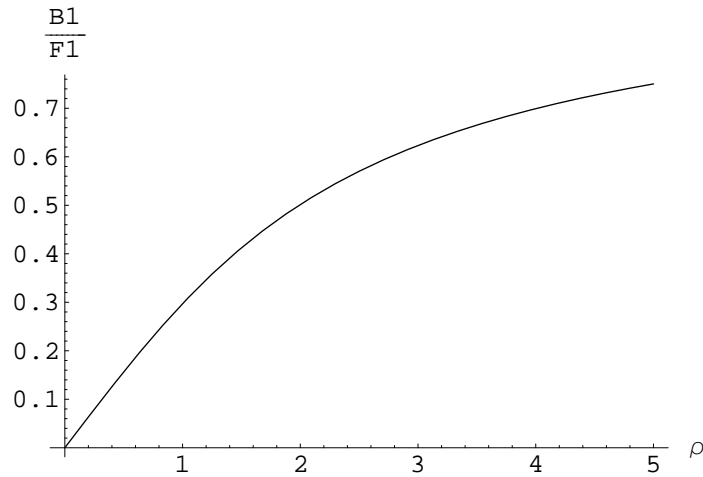
FIGURE 4.14: The dependence of $\frac{B_1}{F_1}$ on ρ. $\mu = -1$, $\alpha = 2$, $d = 0.3$, $s = 1$, $J = 6$, $\theta_1 = -1$, $\delta = 12.8$

a function of θ_1 and ρ_1. They may be used to optimise the parameters used in the model.

It is desirable to have v_1 and v_2 (v_3 and v_4) to have large a split to distinguish them when the onset of lasing mode switching is triggered by gain curve shift. Values to optimize and make desirable switching are obtained from Fig. 4.10, 4.11, 4.13 and 4.14. The selected values are listed here: $\theta_1 = -1$, $\theta_2 = 1.4$, $\rho = 4$.

4.3.2 Numerical Bifurcation Study

To supplement the linear stability analysis, numerical bifurcation with δ is studied. The method used here is the same as the one used in the previous section. Up and down sweeping of δ, which corresponds to gain spectrum blue shift and red shift respectively, are plotted in Fig. 4.15 and 4.16.

The above figures show that the bifurcation point predicted by linear stability analysis matches that measured from Fig. 4.8 and 4.12. However, although both of the methods obtain identical directionality of the lasing after gain curve blue shift, the expected directional reverse accompanied by gain curve red shift for certain parameters suggested from linear stability analysis is not guaranteed here. Repeated numerical downward sweeping of δ reveals that the red shift could end up at either direction with a certain probability.
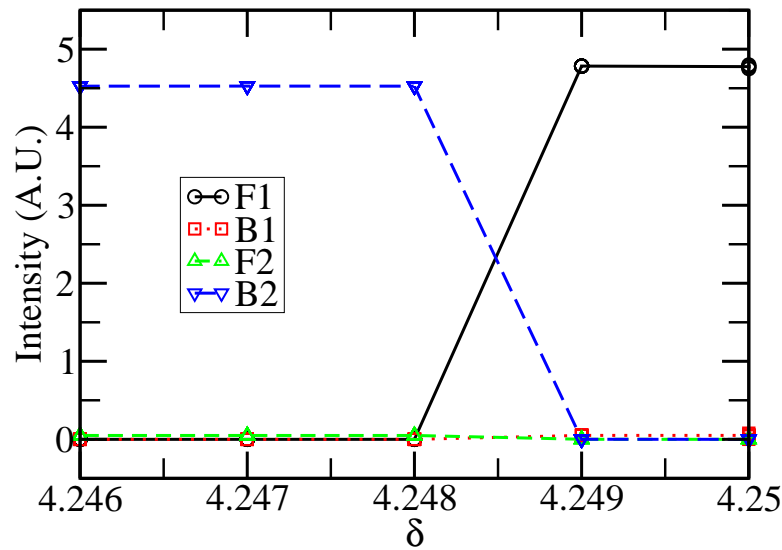
FIGURE 4.15: Bifurcation curve with sweeping of δ downwards. $\mu = -1$, $\alpha = 2$, $d = 0.3$, $P = 5$, $s = 1$, $\theta_1 = -1$, $\theta_2 = 1.4$, $\rho = 4$. Bifurcation occurs at $\delta = 4.249$, F_1 to B_2 switching is obtained

The four-mode dynamics at a bifurcation point calculated by two separate downwards numerical sweepings of δ are plotted in Fig. 4.17 and 4.18. The bifurcation occurs at $\delta = 4.24$. Both F_2 and B_2 modes have their power increase, while F_1 decays with time. From the time trace, at the offset of the mode switching, B_2 always has a power superior to F_2 before a couple of oscillations and power transfer between them. The ratio of intensity of those two modes, $\frac{B_2}{F_2}$ is around 1.6, which is the same as that calculated from linear stability analysis, at the beginning of the dynamics and persists for a long time. This is the indication that the dynamics follows the route predicted by linear stability analysis at the onset. However, a complex dynamics involving all the four modes happens in the middle of the switching process. It is explained in such way that the process is so sensitive to noise that dynamics could take either F_2 or B_2 as exit although the initial states are identical.

The effect of the noise on the exit which the system selected is studied in the following. Gaussian noise functions with 0 mean and various variances are used and the the number of times the system reaches F_2 or B_2 is recorded for each variance. As with the small variance, the noise is most likely to stay within a small region around the mean value. The effect of such Gaussian noise with small variance is almost along the direction of trajectory. On the contrary, the noise with large variance perturbs the system on its trajectory's transverse direction which is more likely to push the dynamics from one attractor to another attractor given that there are two attractors sitting next to each other.
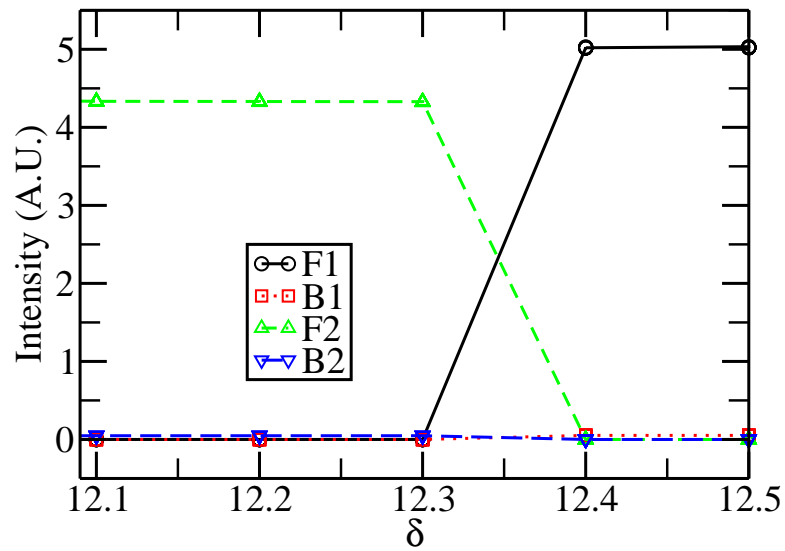
FIGURE 4.16: Bifurcation curve with sweeping of δ upwards. $\mu = -1$, $\alpha = 2$, $d = 0.3$, $P = 5$, $s = 1$, $\theta_1 = -1$, $\theta_2 = 1.4$, $\rho = 4$. Bifurcation occurs at $\delta = 12.3$, F_2 to F_1 switching is obtained
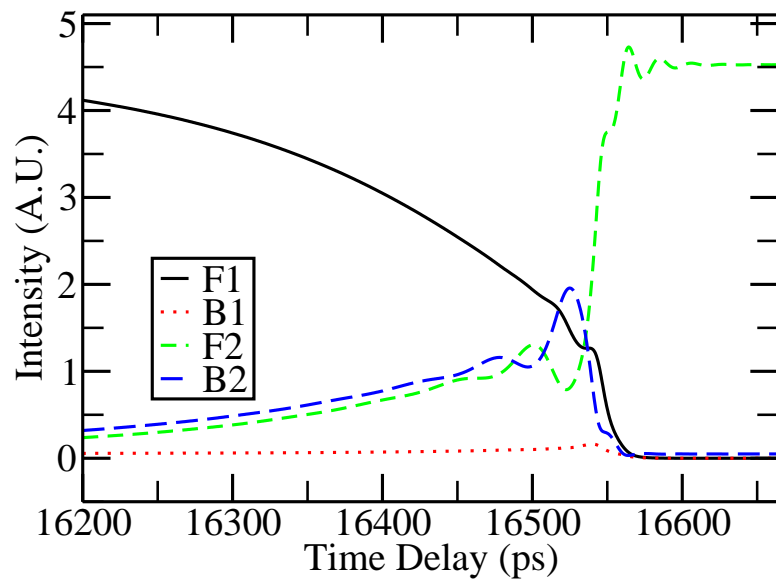
FIGURE 4.17: Undesirable mode dynamics of gain curve red shift at $\delta = 4.249$. $\mu = -1$, $\alpha = 2$, $d = 0.3$, $J = 6$, $s = 1$, $\rho = 4$, $\theta_1 = -1$, $\theta_2 = 1.4$.
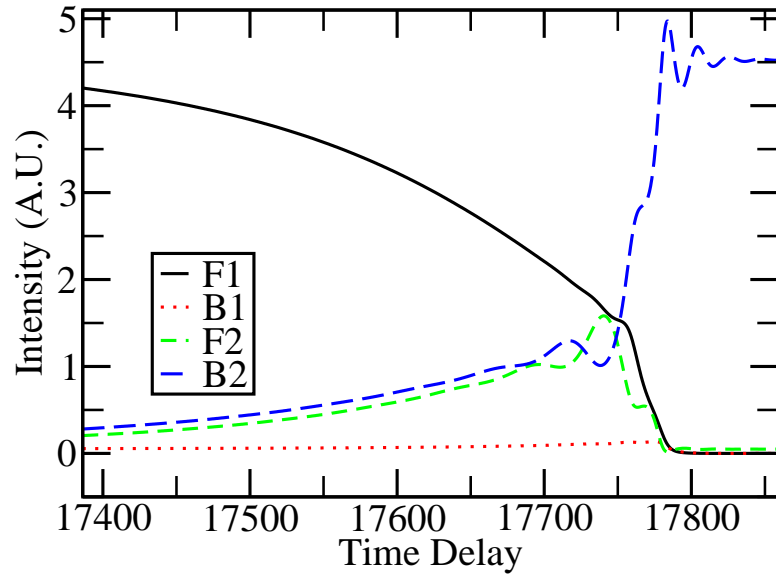
FIGURE 4.18: Desirable mode dynamics of gain curve red shift at $\delta = 4.249$. $\mu = -1$, $\alpha = 2$, $d = 0.3$, $J = 6$, $s = 1$, $\rho = 4$, $\theta_1 = -1$, $\theta_2 = 1.4$.

A statistical approach is taken to study the effect of the noise. The δ sweeping is taken for 4000 times with different variance of the noise. The possibility of the system reaching B_2 after wavelength switching is recorded in Fig. 4.19. The system is likely to reach F_2 when noise with small variance is applied, while B_2 is more probable with noise of large variance. This is to say, the system is more likely to have F_1 to F_2 switching naturally which is not observed experimentally. However, with the aid of the noise, the gain red shift goes to the 'right' direction. It is also needed to note that, the large variance strongly moves the bifurcation point of δ.

4.4   Conclusion

In conclusion, the directional switching of the lasing during a mode jump in frequency is studied in this chapter. The combination of the gain curve drift due to ohmic heating and backscattering from the output waveguide are seen as the mechanism. The backscattering is seen as the vital part to the 'right' switching behaviour from the linear stability analysis. However, a complex dynamics exists between the onset of switching and its final state, which makes the lasing direction non-deterministic from the model, although the onset of switching points to a right direction. A comparison with the model presented in [29] sees some possible improvement of the model. This is discussed in the next Chapter.
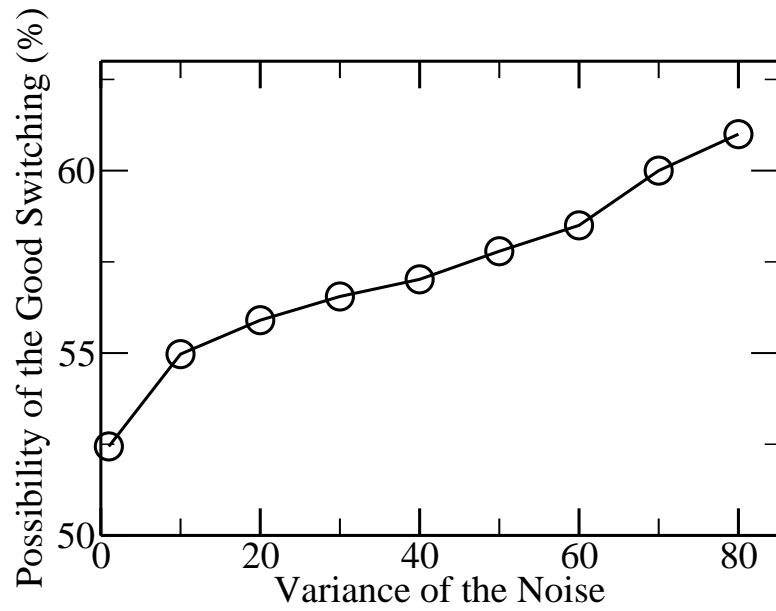
FIGURE 4.19: The possibility of good switching as a function of the variance of the Gaussian noise during gain curve red shift. $\mu = -1$, $\alpha = 2$, $d = 0.3$, $J = 6$, $s = 1$, $\rho = 4$, $\theta_1 = -1$, $\theta_2 = 1.4$.

Chapter 5

Conclusions and Discussions

5.1   Conclusions

In this thesis, a numerical method based on spectral decomposition solving partial differential equations applied to the Maxwell-Bloch equations has been proposed to study the dynamics of the semiconductor ring lasers. Contribution to the dynamics from the nonlinear polarization for each individual mode has been identified by phase matching. A set of coupled rate equations has been developed. Lasers with a priori number of modes have been studied. Also, the diffusion coefficient is proved to be significant to the dynamics and taken into account.

To summarize, the main advantages of the spectral method developed in the thesis are listed here

1. The method suits problems with regular cavity geometry, for example ring lasers by providing a fast convergence.

2. Modes are expressed explicitly. Linear stability analysis is applied on selected modes to study their relative stability.

3. The model is numerically efficient as the spectral method is only applied to the spatial coordinate. Solutions have been solved by marching along the time which is numerically cheaper compared with a full spectral decomposition on both space and time.

4. A good form of susceptibility from Balle [95] could be used instead of calculating the polarizations microscopically. Spectral hole burning is taken into account without complex calculation.

5. Dynamics faster than picosecond scale are hidden in the susceptibility.

6. The numerical algorithm is relatively easy to implement to the programme code.

The general multimode rate equation model used in this thesis has been presented in Chapter 2. A comparison between travelling wave model and multimode rate equation model on two level uni-directional ring laser is performed. According to that, although the number of modes needed in the model varies with the dynamics to be expressed, and moderate number of modes has to be included to recover the strong pulsation operations obtained from the travelling wave model, rate equations with very limited number of modes are good to study the bifurcations at low pump injection.

In Chapter 3, the method is applied to the bi-directional single mode semiconductor lasers. Diffusion as an important parameter has been considered in this chapter. Its influence on the different operating regimes is analysed by linear stability analysis. The boundaries of different regimes have been identified. This result fits those achieved by other studies[66, 97]. The phase sensitive interaction via the included carrier grating between conterpropagating lasing modes and optically triggered directional switching have been studied as well. The switching time dependence on lasing parameters is studied, for which the result has been compared with [32]. A good agreement has been shown although in [32] explicit nonlinear gain saturation has been used in the approach and a carrier grating is not included

In Chapter 4, the bi-directional multi-mode semiconductor lasers with two modes in each lasing direction have been used to study the wavelength switching accompanying directional switching. Comparing with the model in Chapter 3, the approach in this chapter corresponds to an increase of the degrees of freedom by two. The asymmetry introduced by the backscattering from the output coupler is the key to different dynamic behaviour and consequences from gain curve red shift and blue shift. This has been confirmed by steady state analysis.

5.2 Future Works

The rate equation approach for the lasing mode bifurcation with gain curvature shift which has been observed experimentally has been justified analytically. However, the direction after bifurcation from numerical calculation shows a dependence on the direction of the perturbation exerted on the trajectory. A discrepancy of the travelling wave

approach in [29] and the rate equations is observed as the bifurcation from the numerical result of the travelling wave approach always goes to the good direction which fits the experiments well.

A comparison between the travelling wave approach and the rate equation has been conducted and one main differences between those two approach is found. The rate equation approach adopted in this thesis is under the assumption of a perfect cavity without geometrical symmetry broken induced by energy exchange from the coupler. This is to say, the spatial profile dose not change all the way along the cavity. However, in the case of travelling wave modelling, the amplitude of the light is dependent on the position. As it gets amplified when travelling within the active medium and attenuated in the coupler. Therefore one possible future work could be to recover the spatial profile missing in the rate equations. Travelling wave approach could be used to serve such purpose. Attempts to deal with the spatial profile has also been reported[67].

From the last chapter, complicated dynamics are indicated close to the bifurcation point. Attractors close to each other might exist as noise could trigger switching from the same starting points and end up at different operations. A travelling wave model also shows that the transition of switching involves 6 modes in the intermediate dynamics[29]. It is worthwhile to have a comprehensive investigation in the bifurcation point and the structure around it.

Bibliography

[1] A. Yariv. *Quantum Electronics, 3rd Edition.* Wiley, January 1989. ISBN 0471609978.

[2] E. Hecht. *Optics.* Pearson Education, Inc., 2002.

[3] A. Javan, W. R. Bennett, and D. R. Herriott. Population inversion and continuous optical maser oscillation in a gas discharge containing a He-Ne mixture. *Physical Review Letters*, 6(3):106–110, Feb 1961. doi: 10.1103/PhysRevLett.6.106.

[4] T. H. Maiman. Stimulated optical radiation in ruby. *Nature*, 187:493–393, 1960.

[5] G. H. B. Thompson. *Physics of Semiconductor Laser Devices.* John Wiley & Sons, 1980.

[6] R. N. Hall, G. E. Fenner, J. D. Kingsley, T. J. Soltys, and R. O. Carlson. Coherent light emission from GaAs junctions. *Physical Review Letters*, 9(9):366–368, Nov 1962. doi: 10.1103/PhysRevLett.9.366.

[7] M. I. Nathan, W. P. Dumke, G. Burns, Jr. F. H. Dill, and G. Lasher. Stimulated emission of radiation from GaAs p-n junctions. *Applied Physics Letters*, 1(3):62–64, 1962. doi: 10.1063/1.1777371. URL http://link.aip.org/link/?APL/1/62/1.

[8] Jr. N. Holonyak and S. F. Bevacqua. Coherent (visble) light emission from $GaAs_{1-x}P_x$ junctions. *Applied Physics Letters*, 1(4):82–83, 1962. doi: 10.1063/1. 1753706. URL http://link.aip.org/link/?APL/1/82/1.

[9] T. M. Quist, R. H. Rediker, R. J. Keyes, W. E. Krag, B. Lax, A. L. McWhorter, and H. J. Zeigler. Semiconductor maser of GaAs. *Applied Physics Letters*, 1(4):91–92, 1962. doi: 10.1063/1.1753710. URL http://link.aip.org/link/?APL/1/91/1.

[10] D. Z. Garbuzov Y. V. Zhilyaev E. P. Morozov E. L. Portnoi Z. I. Alferov, V. M. Andreev and V. G. Trofim. Investigation of the influence of the AlAsGaAs heterostructure parameters on the laser threshold current and the realization of

continuous emission at the room temperature. *Fiz. Tekh. Poluprovodn*, 4:1826–1829, 1970.

[11] N. N. Ledentsov, M. Grundmann, F. Heinrichsdorff, D. Bimberg, V. M. Ustinov, A. E. Zhukov, M. V. Maximov, Zh. I. Alferov, and J. A. Lott. Quantum-dot heterostructure lasers. *Selected Topics in Quantum Electronics, IEEE Journal of*, 6(3):439–451, May/Jun 2000. ISSN 1077-260X. doi: 10.1109/2944.865099.

[12] Z. Alferov. Double heterostructure lasers: Early days and future perspectives. *Selected Topics in Quantum Electronics, IEEE Journal of*, 6(6):832–840, Nov/Dec 2000. ISSN 1077-260X. doi: 10.1109/2944.902131.

[13] C. Xing and E. A. Avrutin. Multimode spectra and active mode locking potential of quantum dot lasers. *Journal of Applied Physics*, 97(10):104301, 2005. doi: 10.1063/1.1894601. URL http://link.aip.org/link/?JAP/97/104301/1.

[14] L. A. Coldren and S. W. Corzine. *Diode Lasers and Photonic Integrated Circuits*. WileyBlackwell, 1995.

[15] K. Iga. Surface-emitting laser-its birth and generation of new optoelectronics field. *Selected Topics in Quantum Electronics, IEEE Journal of*, 6(6):1201–1215, Nov/Dec 2000. ISSN 1077-260X. doi: 10.1109/2944.902168.

[16] C. J. Chang-Hasnain. Tunable VCSEL. *Selected Topics in Quantum Electronics, IEEE Journal of*, 6(6):978–987, Nov/Dec 2000. ISSN 1077-260X. doi: 10.1109/2944.902146.

[17] M. Sargent III, M. O. Scully, and W. E. Lamb Jr. *Laser Physics*. Addison-Wesley, Massachusetts, 1974.

[18] M. T. Hill, H. J. S. Dorren, T. de Vries, X. J. M. Leijtens, J. H. den Besten, B. Smalbrugge, Y-S. Oei, H. Binsma, G-D. Khoe, and M. K. Smit. A fast low-power optical memory based on coupled micro-ring lasers. *Nature*, 432:206–209, 11 2004. doi: http://dx.doi.org/10.1038/nature03045.

[19] M. Sorel, G. Giuliani, A. Scire, R. Miglierina, S. Donati, and P. J. R. Laybourn. Operating regimes of GaAs-AlGaAs semiconductor ring lasers: Experiment and model. *Quantum Electronics, IEEE Journal of*, 39(10):1187–1195, Oct. 2003. ISSN 0018-9197. doi: 10.1109/JQE.2003.817585.

[20] M. Sorel, P. J. R. Laybourn, G. Giuliani, and S. Donati. Uni-directional bistability in semiconductor waveguide ring lasers. *Applied Physics Letters*, 80(17):3051–3053, 2002. doi: 10.1063/1.1474619. URL http://link.aip.org/link/?APL/80/3051/1.

[21] J. P. Hohimer, G. A. Vawter, and D. C. Craft. Unidirectional operation in a semiconductor ring diode laser. *Applied Physics Letters*, 62(11):1185–1187, 1993. doi: 10.1063/1.108728. URL http://link.aip.org/link/?APL/62/1185/1.

[22] J. J. Liang, S. T. Lau, M. H. Leary, and J. M. Ballantyne. Unidirectional operation of waveguide diode ring lasers. *Applied Physics Letters*, 70(10):1192–1194, 1997. doi: 10.1063/1.118527. URL http://link.aip.org/link/?APL/70/1192/1.

[23] S. Oku, M. Okayasu, and M. Ikeda. Control of unidirectional oscillation in semiconductor orbiter lasers. *Photonics Technology Letters, IEEE*, 3(12):1066–1068, Dec 1991. ISSN 1041-1135. doi: 10.1109/68.118002.

[24] T. Krauss, P. J. R. Laybourn, and J. Roberts. CW operation of semiconductor ring lasers. *Electronics Letters*, 26(25):2095–2097, Dec. 1990. ISSN 0013-5194. doi: 10.1049/el:19901349.

[25] M. F. Booth, A. Schremer, and J. M. Ballantyne. Spatial beam switching and bistability in a diode ring laser. *Applied Physics Letters*, 76(9):1095–1097, 2000. doi: 10.1063/1.125949. URL http://link.aip.org/link/?APL/76/1095/1.

[26] K. Thakulsukanant, L. Bei, I. Memon, G. Mezosi, Z. Wang, M. Sorel, and S. Yu. All-optical label swapping using bistable semiconductor ring laser in an optical switching node. *Lightwave Technology, Journal of*, 27(6):631–638, March15, 2009. ISSN 0733-8724. doi: 10.1109/JLT.2008.927755.

[27] B. Li, M. I. Memon, G. Mezosi, G. Yuan, Z. Wang, M. Sorel, and S. Yu. All-optical response of semiconductor ring laser to dual-optical injections. *Photonics Technology Letters, IEEE*, 20(10):770–772, May15, 2008. ISSN 1041-1135. doi: 10.1109/LPT.2008.921102.

[28] M. Sorel, P. J. R. Laybourn, A. Scirè, S. Balle, G. Giuliani, R. Miglierina, and S. Donati. Alternate oscillations in semiconductor ring lasers. *Optics Letters*, 27(22):1992–1994, 2002. URL http://ol.osa.org/abstract.cfm?URI=ol-27-22-1992.

[29] J. Javaloyes and S. Balle. Emission directionality of semiconductor ring lasers: a traveling-wave description. *Quantum Electronics, IEEE Journal of*, 45(5):431–438, May 2009. ISSN 0018-9197. doi: 10.1109/JQE.2009.2014079.

[30] G. Yuan and S. Yu. Analysis of dynamic switching behavior of bistable semiconductor ring lasers triggered by resonant optical pulse injection. *Selected Topics in Quantum Electronics, IEEE Journal of*, 13(5):1227–1234, Sept.-oct. 2007. ISSN 1077-260X. doi: 10.1109/JSTQE.2007.906044.

[31] G. Yuan, Z. Wang, and S. Yu. Dynamic switching response of semiconductor ring lasers to NRZ and RZ injection signals. *Photonics Technology Letters, IEEE*, 20 (10):785–787, May15, 2008. ISSN 1041-1135. doi: 10.1109/LPT.2008.921112.

[32] T. Pérez, A. Scirè, G. Van der Sande, P. Colet, and C. R. Mirasso. Bistability and all-optical switching in semiconductor ring lasers. *Optics Express*, 15(20):12941–12948, 2007. URL http://www.opticsexpress.org/abstract.cfm?URI=oe-15-20-12941.

[33] L. Gelens, S. Beri, G. Van der Sande, J. Danckaert, N. Calabretta, H. J. S. Dorren, R. Nötzel, E. A. J. M. Bente, and M. K. Smit. Optical injection in semiconductor ringlasers: backfire dynamics. *Optics Express*, 16(15):10968–10974, 2008. URL http://www.opticsexpress.org/abstract.cfm?URI=oe-16-15-10968.

[34] N. Calabretta, S. Beri, L. Gelens, R. Notzel, E. Bente, J. Danckaert, M. Smit, and H. Dorren. Experimental investigation of bistable operation of semiconductor ring lasers under optical injection. In *European Conference on Integrated Optics*, 2008.

[35] Z. Wang, G. Yuan, and S. Yu. Directional bistability in novel semiconductor ring lasers with retro-reflector microcavity. *Photonics Technology Letters, IEEE*, 20 (12):1048–1050, June15, 2008. ISSN 1041-1135. doi: 10.1109/LPT.2008.923752.

[36] Z. Wang, G. Yuan, G. Verschaffelt, J. Danckaert, and S. Yu. Injection locking and switching operations of a novel retro-reflector-cavity-based semiconductor microring laser. *Photonics Technology Letters, IEEE*, 20(20):1673–1675, Oct.15, 2008. ISSN 1041-1135. doi: 10.1109/LPT.2008.2003387.

[37] Z. Wang, G. Yuan, G. Verschaffelt, J. Danckaert, and S. Yu. Storing 2 bits of information in a novel single semiconductor microring laser memory cell. *Photonics Technology Letters, IEEE*, 20(14):1228–1230, July15, 2008. ISSN 1041-1135. doi: 10.1109/LPT.2008.926011.

[38] Z. Wang, G. Verschaffelt, S. Yi, G. Mezosi, M. Sorel, J. Danckaert, and S. Yu. Integrated small-sized semiconductor ring laser with novel retro-reflector cavity. *Photonics Technology Letters, IEEE*, 20(2):99–101, Jan.15, 2008. ISSN 1041-1135. doi: 10.1109/LPT.2007.912554.

[39] P.B. Hansen, G. Raybon, M.-D. Chien, U. Koren, B.I. Miller, M.G. Young, J.-M. Verdiell, and C.A. Burrus. A 1.54-μm monolithic semiconductor ring laser: CW and mode-locked operation. *Photonics Technology Letters, IEEE*, 4(5):411–413, May 1992. ISSN 1041-1135. doi: 10.1109/68.136469.

[40] J. P. Hohimer and G. A. Vawter. Passive mode locking of monolithic semiconductor ring lasers at 86 GHz. *Applied Physics Letters*, 63(12):1598–1600, 1993. doi: 10.1063/1.110808. URL http://link.aip.org/link/?APL/63/1598/1.

[41] T. Ohno, H. Ishii, S. Matsuo, H. Okamoto, Y. Kawaguchi, Y. Kondo, I. Furuta, H. Ito, and Y. Yoshikuni. Hybrid modelocking of semiconductor ring lasers incorporating passive deep-ridge waveguides. *Electronics Letters*, 38(16):884–886, Aug 2002. ISSN 0013-5194. doi: 10.1049/el:20020642.

[42] J. F. Martins-Filho, E. A. Avrutin, C. N. Ironside, and J. S. Roberts. Monolithic multiple colliding pulse mode-locked quantum-well lasers, experiment and theory. *Selected Topics in Quantum Electronics, IEEE Journal of*, 1(2):539–551, Jun 1995. ISSN 1077-260X. doi: 10.1109/2944.401240.

[43] A. S.-H. Liao and S. Wang. Semiconductor injection lasers with a circular resonator. *Applied Physics Letters*, 36(10):801–803, 1980. doi: 10.1063/1.91321. URL http://link.aip.org/link/?APL/36/801/1.

[44] S. Furst and M. Sorel. Cavity-enhanced four-wave mixing in semiconductor ring lasers. *Photonics Technology Letters, IEEE*, 20(5):366–368, March1, 2008. ISSN 1041-1135. doi: 10.1109/LPT.2007.915660.

[45] C. Ji, M. H. Leary, and J. M. Ballantyne. Long-wavelength triangular ring laser. *Photonics Technology Letters, IEEE*, 9(11):1469–1471, Nov 1997. ISSN 1041-1135. doi: 10.1109/68.634711.

[46] W. E. Lamb Jr. Theory of an optical maser. *Physical Review*, 134(6A):A1429–A1450, Jun 1964. doi: 10.1103/PhysRev.134.A1429.

[47] L. N. Menegozzi and W. E. Lamb Jr. Theory of a ring laser. *Physical Review A (Atomic, Molecular, and Optical Physics)*, 8(4):2103–2125, Oct 1973. doi: 10.1103/PhysRevA.8.2103.

[48] O. Hess and T. Kuhn. Maxwell-Bloch equations for spatially inhomogeneous semiconductor lasers. I. Theoretical formulation. *Physical Review A (Atomic, Molecular, and Optical Physics)*, 54(4):3347–3359, Oct 1996. doi: 10.1103/PhysRevA.54.3347.

[49] O. Hess and T. Kuhn. Maxwell-Bloch equations for spatially inhomogeneous semiconductor lasers. II. Spatiotemporal dynamics. *Physical Review A (Atomic, Molecular, and Optical Physics)*, 54(4):3360–3368, Oct 1996. doi: 10.1103/PhysRevA.54.3360.

[50] C. Henry. Theory of the linewidth of semiconductor lasers. *Quantum Electronics, IEEE Journal of*, 18(2):259–264, Feb 1982. ISSN 0018-9197.

[51] R. W. Ziolkowski, J. M. Arnold, and D. M. Gogny. Ultrafast pulse interactions with two-level atoms. *Physical Review A (Atomic, Molecular, and Optical Physics)*, 52 (4):3082–3094, Oct 1995. doi: 10.1103/PhysRevA.52.3082.

[52] G. M. Slavcheva, J. M. Arnold, and R. W. Ziolkowski. FDTD simulation of the nonlinear gain dynamics in active optical waveguides and semiconductor microcavities. *Selected Topics in Quantum Electronics, IEEE Journal of*, 10(5):1052–1062, Sept.-Oct. 2004. ISSN 1077-260X. doi: 10.1109/JSTQE.2004.836023(410)1.

[53] G.M. Slavcheva and J.M. Arnold. FDTD simulation of the nonlinear gain dynamics and modulation response of a semiconductor microcavity. In *Numerical Simulation of Semiconductor Optoelectronic Devices, 2003. NUSOD 2003. Proceedings of the IEEE/LEOS 3rd International Conference on*, pages 82–83, Oct. 2003.

[54] G.M. Slavcheva, J.M. Arnold, and R.W. Ziolkowski. FDTD simulation of the nonlinear gain and pumping dynamics of optically pumped vcsels. In *Lasers and Electro-Optics Society, 2003. LEOS 2003. The 16th Annual Meeting of the IEEE*, volume 2, pages 513–514 vol.2, Oct. 2003. doi: 10.1109/LEOS.2003.1252899.

[55] G. Slavcheva, J. M. Arnold, and R. W. Ziolkowski. Ultrashort pulse lossless propagation through a degenerate three-level medium in nonlinear optical waveguides and semiconductor microcavities. *Selected Topics in Quantum Electronics, IEEE Journal of*, 9(3):929–938, May-June 2003. ISSN 1077-260X. doi: 10.1109/JSTQE.2003.818844.

[56] M. Homar, J. V. Moloney, and M. San Miguel. Travelling wave model of a multimode Fabry-Perot laser in free running and external cavity configurations. *Quantum Electronics, IEEE Journal of*, 32(3):553–566, Mar 1996. ISSN 0018-9197. doi: 10.1109/3.485410.

[57] M. Homar, S. Balle, and M. San Miguel. Mode competition in a Fabry-Perot semiconductor laser: Travelling wave model with asymmetric dynamical gain. *Optics Communications*, 131(4-6):380 – 390, 1996. ISSN 0030-4018. doi: DOI:10.1016/0030-4018(96)00234-9.

[58] G. P. Agrawal and N. A. Olsson. Self-phase modulation and spectral broadening of optical pulses in semiconductor laser amplifiers. *Quantum Electronics, IEEE Journal of*, 25(11):2297–2306, Nov 1989. ISSN 0018-9197. doi: 10.1109/3.42059.

[59] G. P. Agrawal. Effect of gain dispersion on ultrashort pulse amplification in semi-conductor laser amplifiers. *Quantum Electronics, IEEE Journal of*, 27(6):1843–1849, Jun 1991. ISSN 0018-9197. doi: 10.1109/3.90014.

[60] V. B. Khalfin, J. M. Arnold, and J. H. Marsh. A theoretical model of synchronization of a mode-locked semiconductor laser with an external pulse stream. *Selected Topics in Quantum Electronics, IEEE Journal of*, 1(2):523–527, Jun 1995. ISSN 1077-260X. doi: 10.1109/2944.401237.

[61] H. Haus. Theory of mode locking with a slow saturable absorber. *Quantum Electronics, IEEE Journal of*, 11(9):736–746, Sep 1975. ISSN 0018-9197.

[62] R. G. M. P. Koumans and R. Van Roijen. Theory for passive mode-locking in semi-conductor laser structures including the effects of self-phase modulation, dispersion, and pulse collisions. *Quantum Electronics, IEEE Journal of*, 32(3):478–492, Mar 1996. ISSN 0018-9197. doi: 10.1109/3.485400.

[63] C. L. Tang, H. Statz, and G. deMars. Spectral output and spiking behavior of solid-state lasers. *Journal of Applied Physics*, 34(8):2289–2295, 1963. doi: 10.1063/1.1702732. URL http://link.aip.org/link/?JAP/34/2289/1.

[64] P. P. Vasil'ev, I. H. White, and J. Gowar. Fast phenomena in semicon-ductor lasers. *Reports on Progress in Physics*, 63(12):1997, 2000. URL http://stacks.iop.org/0034-4885/63/i=12/a=203.

[65] P. Mandel, C. Etrich, and K. Otsuka. Laser rate equations with phase sensitive interactions. *Quantum Electronics, IEEE Journal of*, 29(3):836–843, Mar 1993. ISSN 0018-9197. doi: 10.1109/3.206567.

[66] C. Etrich, P. Mandel, N. B. Abraham, and H. Zeghlache. Dynamics of a two-mode semiconductor laser. *Quantum Electronics, IEEE Journal of*, 28(4):811–821, Apr 1992. ISSN 0018-9197. doi: 10.1109/3.135198.

[67] E. A. Avrutin, J. M. Arnold, and J. H. Marsh. Dynamic modal analysis of monolithic mode-locked semiconductor lasers. *Selected Topics in Quantum Electronics, IEEE Journal of*, 9(3):844–856, May-June 2003. ISSN 1077-260X. doi: 10.1109/JSTQE.2003.818845.

[68] B. Tromborg, H. E. Lassen, and H. Olesen. Traveling wave analysis of semi-conductor lasers: Modulation responses, mode stability and quantum mechanical treatment of noise spectra. *Quantum Electronics, IEEE Journal of*, 30(4):939–956, Apr 1994. ISSN 0018-9197. doi: 10.1109/3.291365.

[69] K. Petermann. Calculated spontaneous emission factor for double-heterostructure injection lasers with gain-induced waveguiding. *Quantum Electronics, IEEE Journal of*, 15(7):566–570, Jul 1979. ISSN 0018-9197.

[70] A. E. Siegman. Excess spontaneous emission in non-Hermitian optical systems. I. Laser amplifiers. *Physical Review A (Atomic, Molecular, and Optical Physics)*, 39 (3):1253–1263, Feb 1989. doi: 10.1103/PhysRevA.39.1253.

[71] A. E. Siegman. Excess spontaneous emission in non-Hermitian optical systems. II. Laser oscillators. *Physical Review A (Atomic, Molecular, and Optical Physics)*, 39 (3):1264–1268, Feb 1989. doi: 10.1103/PhysRevA.39.1264.

[72] W. A. Hamel and J. P. Woerdman. Nonorthogonality of the longitudinal eigenmodes of a laser. *Physical Review A (Atomic, Molecular, and Optical Physics)*, 40 (5):2785–2787, Sep 1989. doi: 10.1103/PhysRevA.40.2785.

[73] U. Feiste. Optimization of modulation bandwidth in DBR lasers with detuned bragg reflectors. *Quantum Electronics, IEEE Journal of*, 34(12):2371–2379, Dec 1998. ISSN 0018-9197. doi: 10.1109/3.736110.

[74] H. Wenzel, U. Bandelow, H.-J. Wunsche, and J. Rehberg. Mechanisms of fast self pulsations in two-section DFB lasers. *Quantum Electronics, IEEE Journal of*, 32 (1):69–78, Jan 1996. ISSN 0018-9197. doi: 10.1109/3.481922.

[75] U. Bandelow, R. Schatz, and H.-J. Wunsche. A correct single-mode photon rate equation for multisection lasers. *Photonics Technology Letters, IEEE*, 8(5):614–616, May 1996. ISSN 1041-1135. doi: 10.1109/68.491556.

[76] J. Hader, J. V. Moloney, S. W. Koch, and W. W. Chow. Microscopic modeling of gain and luminescence in semiconductors. *Selected Topics in Quantum Electronics, IEEE Journal of*, 9(3):688–697, May-June 2003. ISSN 1077-260X. doi: 10.1109/ JSTQE.2003.818342.

[77] T. A. DeTemple and C. M. Herzinger. On the semiconductor laser logarithmic gain-current density relation. *Quantum Electronics, IEEE Journal of*, 29(5):1246–1252, May 1993. ISSN 0018-9197. doi: 10.1109/3.236138.

[78] R.S. Tucker. High-speed modulation of semiconductor lasers. *Electron Devices, IEEE Transactions on*, 32(12):2572–2584, Dec 1985. ISSN 0018-9383.

[79] C. Su and V. Lanzisera. Ultra-high-speed modulation of 1.3-μm InGaAsP diode lasers. *Quantum Electronics, IEEE Journal of*, 22(9):1568–1578, Sep 1986. ISSN 0018-9197.

[80] D. J. Channin. Effect of gain saturation on injection laser switching. *Journal of Applied Physics*, 50(6):3858–3860, 1979. doi: 10.1063/1.326510. URL http://link.aip.org/link/?JAP/50/3858/1.

[81] T. L. Koch and R. A. Linke. Effect of nonlinear gain reduction on semiconductor laser wavelength chirping. *Applied Physics Letters*, 48(10):613–615, 1986. doi: 10.1063/1.96770. URL http://link.aip.org/link/?APL/48/613/1.

[82] M. J. Adams and M. Osiṅski. Influence of spectral hole-burning on quaternary laser transients. *Electronics Letters*, 19(16):627–628, 4 1983. ISSN 0013-5194. doi: 10.1049/el:19830427.

[83] J. Bowers, B. Hemenway, A. Gnauck, and D. Wilt. High-speed InGaAsP constricted-mesa lasers. *Quantum Electronics, IEEE Journal of*, 22(6):833–844, Jun 1986. ISSN 0018-9197.

[84] G. P. Agrawal. Spectral hole-burning and gain saturation in semiconductor lasers: Strong-signal theory. *Journal of Applied Physics*, 63(4):1232–1235, 1988. doi: 10.1063/1.339990. URL http://link.aip.org/link/?JAP/63/1232/1.

[85] Y. Nambu and A. Tomita. Spectral hole burning and carrier-heating effect on the transient optical nonlinearity of highly carrier-injected semiconductors. *Quantum Electronics, IEEE Journal of*, 30(9):1981–1994, Sep 1994. ISSN 0018-9197. doi: 10.1109/3.309856.

[86] G. Agrawal. Gain nonlinearities in semiconductor lasers: Theory and application to distributed feedback lasers. *Quantum Electronics, IEEE Journal of*, 23(6):860–868, Jun 1987. ISSN 0018-9197.

[87] R. F. Kazarinov, C. H. Henry, and R. A. Logan. Longitudinal mode self-stabilization in semiconductor lasers. *Journal of Applied Physics*, 53(7):4631–4644, 1982. doi: 10.1063/1.331290. URL http://link.aip.org/link/?JAP/53/4631/1.

[88] A. Uskov, J. Mork, and J. Mark. Wave mixing in semiconductor-laser amplifiers due to carrier heating and spectral-hole burning. *Quantum Electronics, IEEE Journal of*, 30(8):1769–1781, AUG 1994. ISSN 0018-9197.

[89] M. Asada and Y. Suematsu. Density-matrix theory of semiconductor lasers with relaxation broadening model-gain and gain-suppression in semiconductor lasers. *Quantum Electronics, IEEE Journal of*, 21(5):434–442, May 1985. ISSN 0018-9197.

[90] W. W. Chow, P. M. Smowton, P. Blood, A. Girndt, F. Jahnke, and S. W. Koch. Comparison of experimental and theoretical *gainp* quantum well gain spectra. *Applied Physics Letters*, 71(2):157–159, 1997. doi: 10.1063/1.119489. URL http://link.aip.org/link/?APL/71/157/1.

[91] W. W. Chow and S. W. Koch. *Semiconductor-Laser Fundamentals: Physics of the Gain Materials.* Springe, 1999.

[92] H. Haug and S. W. Koch. Semiconductor laser theory with many-body effects. *Physical Review A (Atomic, Molecular, and Optical Physics)*, 39(4):1887–1898, Feb 1989. doi: 10.1103/PhysRevA.39.1887.

[93] H. Haug. The 1984 electron theory of the optical properties of laser-excited semiconductors revisited. What happened since? *Progress in Quantum Electronics*, 29 (6):261 – 296, 2005. ISSN 0079-6727. doi: DOI:10.1016/j.pquantelec.2005.10.001.

[94] S. Balle. Simple analytical approximations for the gain and refractive index spectra in quantum well lasers. *Physical Review A (Atomic, Molecular, and Optical Physics)*, 57:1304–1312, 1998.

[95] S. Balle. Analytical description of spectral hole-burning effects in active semiconductors. *Optics Letters*, 21:1923–1925, 2002.

[96] C. L. Tang, A. Schremer, and T. Fujita. Bistability in two-mode semiconductor lasers via gain saturation. *Applied Physics Letters*, 51(18):1392–1394, 1987. doi: 10.1063/1.98686. URL http://link.aip.org/link/?APL/51/1392/1.

[97] P.A. Khandokhin, I.V. Koryukin, Ya.I. Khanin, and P. Mandel. Dynamics of a ring laser with diffusion of active centres. *Quantum Electronics*, 25:1045–1049, 1995.

[98] R. J. C. Spreeuw, N. J. Neelen, R. C. van Druten, E. R. Eliel, and J. P. Woerdman. Mode coupling in a He-Ne ring laser with backscattering. *Physical Review A (Atomic, Molecular, and Optical Physics)*, 42(7):4315–4324, Oct 1990. doi: 10. 1103/PhysRevA.42.4315.

[99] C. Etrich, P. Mandel, R. C. Neelen, R. J. C. Spreeuw, and J. P. Woerdman. Dynamics of a ring-laser gyroscope with backscattering. *Physical Review A (Atomic, Molecular, and Optical Physics)*, 46(1):525–536, Jul 1992. doi: 10.1103/PhysRevA.46.525.

[100] F. C. Cheng. Investigation of a dye ring laser with backscattering. *Physical Review A (Atomic, Molecular, and Optical Physics)*, 45(7):5220–5227, Apr 1992. doi: 10.1103/PhysRevA.45.5220.

[101] G. Yuan, Z. Wang, B. Li, M.I. Memon, and S. Yu. Theoretical and experimental studies on bistability in semiconductor ring lasers with two optical injections. *Selected Topics in Quantum Electronics, IEEE Journal of*, 14(3):903–910, May-june 2008. ISSN 1077-260X. doi: 10.1109/JSTQE.2008.918058.

[102] G. Yuan and S. Yu. Bistability and switching properties of semiconductor ring lasers with external optical injection. *Quantum Electronics, IEEE Journal of*, 44 (1):41–48, Jan. 2008. ISSN 0018-9197. doi: 10.1109/JQE.2007.909523.

[103] R. Lang and K. Kobayashi. External optical feedback effects on semiconductor injection laser properties. *Quantum Electronics, IEEE Journal of*, 16(3):347–355, Mar 1980. ISSN 0018-9197.

[104] G. Van der Sande, L. Gelens, P. Tassin, A. Scire, and J. Danckaert. Two-dimensional phase-space analysis and bifurcation study of the dynamical behaviour of a semiconductor ring laser. *Journal of Physics B: Atomic, Molecular and Optical Physics*, 41(9):1–8, 2008. URL http://stacks.iop.org/0953-4075/41/095402.

[105] L. Gelens, S. Beri, G. Van der Sande, G. Mezosi, M. Sorel, J. Danckaert, and G. Verschaffelt. Exploring multistability in semiconductor ring lasers: Theory and experiment. *Physical Review Letters*, 102(19):193904, 2009. doi: 10.1103/PhysRevLett.102.193904. URL http://link.aps.org/abstract/PRL/v102/e193904.

[106] L. Gelens, G. Van der Sande, S. Beri, and J. Danckaert. Phase-space approach to directional switching in semiconductor ring lasers. *Physical Review E (Statistical, Nonlinear, and Soft Matter Physics)*, 79(1):016213, 2009. doi: 10.1103/PhysRevE. 79.016213. URL http://link.aps.org/abstract/PRE/v79/e016213.

[107] S. Beri, L. Gelens, M. Mestre, G. Van der Sande, G. Verschaffelt, A. Scirè, G. Mezosi, M. Sorel, and J. Danckaert. Topological insight into the non-Arrhenius mode hopping of semiconductor ring lasers. *Physical Review Letters*, 101(9):093903, 2008. doi: 10.1103/PhysRevLett.101.093903. URL http://link.aps.org/abstract/PRL/v101/e093903.

[108] S. Beri, L. Gelens, G. Van der Sande, and J. Danckaert. Asymptotic approach to the analysis of mode-hopping in semiconductor ring lasers. *Physical Review A (Atomic, Molecular, and Optical Physics)*, 80(1):013823, 2009. doi: 10.1103/ PhysRevA.80.013823. URL http://link.aps.org/abstract/PRA/v80/e013823.

[109] I. Stamataki, S. Mikroulis, A. Kapsalis, and D. Syvridis. Investigation on the multimode dynamics of InGaAsP-InP microring lasers. *Quantum Electronics, IEEE Journal of*, 42(12):1266–1273, Dec. 2006. ISSN 0018-9197. doi: 10.1109/JQE.2006.884578.

[110] M. Ahmed and M. Yamada. Influence of instantaneous mode competition on the dynamics of semiconductor lasers. *Quantum Electronics, IEEE Journal of*, 38(6): 682–693, Jun 2002. ISSN 0018-9197. doi: 10.1109/JQE.2002.1005419.

[111] H. Kanazawa, H. Saito, H. Yamada, W. Masuda, and K. Kasuya. Theoretical analysis of combustion-driven 16μm CO_2 gas dynamic lasers. *Quantum Electronics, IEEE Journal of*, 20(9):1086–1092, Sep 1984. ISSN 0018-9197.

[112] M. Yamada. Theoretical analysis of nonlinear optical phenomena taking into account the beating vibration of the electron density in semiconductor lasers. *Journal of Applied Physics*, 66(1):81–89, 1989. doi: 10.1063/1.343860. URL http://link.aip.org/link/?JAP/66/81/1.

[113] M. Yamada and Y. Suematsu. Analysis of gain suppression in undoped injection lasers. *Journal of Applied Physics*, 52(4):2653–2664, 1981. doi: 10.1063/1.329064. URL http://link.aip.org/link/?JAP/52/2653/1.

[114] C. Born, G. Yuan, Z. Wang, M. Sorel, and S. Yu. Lasing mode hysteresis characteristics in semiconductor ring lasers. *Quantum Electronics, IEEE Journal of*, 44 (12):1171–1179, Dec. 2008. ISSN 0018-9197. doi: 10.1109/JQE.2008.2003148.

[115] C. Born, M. Sorel, and Siyuan Yu. Linear and nonlinear mode interactions in a semiconductor ring laser. *Quantum Electronics, IEEE Journal of*, 41(3):261–271, March 2005. ISSN 0018-9197. doi: 10.1109/JQE.2004.841614.

[116] C. Born, G. Yuan, Z. Wang, and S. Yu. Nonlinear gain in semiconductor ring lasers. *Quantum Electronics, IEEE Journal of*, 44(11):1055–1064, Nov. 2008. ISSN 0018-9197. doi: 10.1109/JQE.2008.2003172.

[117] John Guckenheimer and Philip Holmes. *Nonlinear Oscillations, Dynamical Systems and Bifurcation of Vector Fields*. Springer, 1983.

[118] L. A. Lugiato, L. M. Narducci, E. V. Eschenazi, D. K. Bandy, and N. B. Abraham. Multimode instabilities in a homogeneously broadened ring laser. *Physical Review A (Atomic, Molecular, and Optical Physics)*, 32(3):1563–1575, Sep 1985. doi: 10.1103/PhysRevA.32.1563.

[119] Germn J. de Valcrcel, Eugenio Roldn, and Franco Prati. Generalized rate equations for multimode lasers. *Optics Communications*, 216(1-3):203 –

207, 2003. ISSN 0030-4018. doi: DOI:10.1016/S0030-4018(02)02331-3. URL http://www.sciencedirect.com/science/article/B6TVF-47HT5BM-7/2/9fb01bb58ab2cb902

[120] G. D'Alessandro, A. Politi, and F. T. Arecchi. Reduction of variables in a bidirectional ring laser. *Europhysics Letters*, 10(7):651, 1989. URL http://stacks.iop.org/0295-5075/10/i=7/a=008.

[121] D. C. Hutchings, M. Sheik-Bahae, D. J. Hagan, and E. W. Van Stryland. Kramers-krönig relations in nonlinear optics. *Optical and Quantum Electronics*, 24:1–30, 1992.

[122] C. Serrat and C. Masoller. Modeling spatial effects in multi-longitudinal-mode semiconductor lasers. *Physical Review A (Atomic, Molecular, and Optical Physics)*, 73(4):043812, 2006. doi: 10.1103/PhysRevA.73.043812. URL http://link.aps.org/abstract/PRA/v73/e043812.

[123] J. J. Sakurai. *Modern Quantum Mechanics (Revised Edition)*. Addison Wesley, 1993.

[124] H. Zeghlache and P. Mandel. Influence of detuning on the properties of laser equations. *Journal of the Optical Society of America B*, 2(1):18–22, 1985. URL http://josab.osa.org/abstract.cfm?URI=josab-2-1-18.

[125] W. W. Chow and S. W. Koch. *Semiconductor-Laser Fundamentals: Physics of the Gain Materials*. check and the year, 2001.

[126] R. Binder, D. Scott, A. E. Paul, M. Lindberg, K. Henneberger, and S. W. Koch. Carrier-carrier scattering and optical dephasing in highly excited semiconductors. *Physical Review B(Condensed Matter and Materials Physics)*, 45(3):1107–1115, Jan 1992. doi: 10.1103/PhysRevB.45.1107.

[127] M. Braun. *Differential Equations and Their Applications: An Introduction to Applied Mathematics (Texts in Applied Mathematics)*. Springer; 4th ed. edition (4 Jan 1993), 1993.

[128] W. H. Press, S. A. Teukolsky, W. T. Vetterling, and B. P. Flannery. *Numerical Recipes: The Art of Scientific Computing*. Cambridge University Press, August 2007. ISBN 0521880688.

[129] Hitoshi Kawaguchi. *Bistabilities and Nonlinearities in Laser Diodes*. Artech House, 1994.

[130] A. Pérez-Serrano, J. Javaloyes, and S. Balle. Bichromatic emission and multimode dynamics in bidirectional ring lasers. *Physical Review A (Atomic, Molecular, and Optical Physics)*, 81(4):043817, Apr 2010. doi: 10.1103/PhysRevA.81.043817.

[131] H. Risken and K. Nummedal. Self-pulsing in lasers. *Journal of Applied Physics*, 39:4662, 1968.

[132] P.A. Khandokhin, I.V. Koryukin, Ya.I. Khanin, and P. Mandel. Influence of carrier diffusion on the dynamics of a two-mode laser. *Quantum Electronics, IEEE Journal of*, 31(4):647–652, Apr 1995. ISSN 0018-9197. doi: 10.1109/3.371938.

[133] P. Ru, J. V. Moloney, R. Indik, S. W. Koch, and W. W. Chow. Microscopic modelling of bulk and quantum-well gaas-based semicondutor lasers. *Optical and Quantum Electronics*, 25:675–693, 1993.

[134] M. Osinski and J. Buus. Linewidth broadening factor in semiconductor lasers–an overview. *Quantum Electronics, IEEE Journal of*, 23(1):9–29, Jan 1987. ISSN 0018-9197.

[135] F. Stern. Calculated spectral dependence of gain in excited GaAs. *Journal of Applied Physics*, 47(12):5382–5386, 1976. doi: 10.1063/1.322565. URL http://link.aip.org/link/?JAP/47/5382/1.

[136] J. Huang and L. W. Casperson. Gain and saturation in semiconductor lasers. *Optical and Quantum Electronics*, 25:369–390, 1993.

[137] R. Lang. Injection locking properties of a semiconductor laser. *Quantum Electronics, IEEE Journal of*, 18(6):976–983, Jun 1982. ISSN 0018-9197.